Non-Relativistic Renormalization Group and Next-to-Leading Logarithm Resummation of $t\bar{t}$ near Threshold

Romy Grünhofer

Supervisor: Prof. Dr. Martin Beneke

Second Supervisor: Prof. Dr. Clara Peset

Submitted in partial fulfillment of the requirements for the degree of Master of Science in the programme *Theoretical and Mathematical Physics*, jointly awarded by Ludwig-Maximilians-Universität München and Technische Universität München in cooperation with the Elitenetwork of Bavaria.

First Examiner: Prof. Dr. Martin Beneke

Second Examiner: Prof. Dr. Gerhard Buchalla

Submitted by: Romy Grünhofer

Submission Date: 10.07.2024

Statement of authorship:

I hereby declare that this thesis is my own work and that I have not used any sources and aids other than those stated in the thesis.

Place, Date

Signature

Abstract

Top anti-top pair production near threshold in e^+e^- collisions is characterized by a hierarchy of widely separated scales. This facilitates a treatment in an effective field theory framework, specifically non-relativistic QCD (NRQCD) and potential non-relativistic QCD (PNRQCD). The fixed-order result for the cross section of this process is known up to next-to-next-to-next-to-leading order. An improvement of the fixed-order expression can be obtained by resumming large logarithms via renormalization group equations. This thesis considers the renormalization group improvement of the top anti-top pair production cross section at next-to-leading logarithm (NLL). In order to perform the resummation procedure in a way compatible with the known third-order expressions at fixed order, we transform position space expressions from the literature to momentum space. We take care to discuss the procedure consistently, alluding to possible future extensions to higher orders in the resummation of logarithms. The multi-scale nature of the heavy-quark system requires a careful analysis of the scales and leads to the renormalization group improvement being performed in multiple steps. Specifically, we consider the ultrasoft running of the potentials, the hard running of the NRQCD matching coefficients, and the potential running. The former two are written as a correction to the potentials in PNRQCD, while the latter encodes the mixing into the non-relativistic current. In addition to the analytic discussion of these individual contributions, we implement the correction obtained from renormalization group improvement numerically and discuss the effect of resummation on the cross section. Our results include the combination of NLL effects with third-order results, which has not been shown before. Compared to fixed order results, we observe a significant reduction of the scale dependence. Most noteworthy, we find that the range of scales for which perturbation theory remains valid is extended to smaller scales when NLL resummation is included.

Contents

Chapter 1

Introduction

The top quark is the heaviest known elementary particle, which gives it a unique role in the Standard Model (SM). From a combination of direct measurements at the Large Hadron Collider (LHC), its mass is determined to $(172.52 \pm 0.14\ (\text{stat.}) \pm 0.30\ (\text{syst.}))\,\text{GeV}$ [1]. There are some subtleties involved in the definition of the mass of the top quark (discussed, for example, in reference [2]), which are not relevant to this thesis. The precise measurement of the top mass, as well as its theoretical prediction, has been an ongoing endeavour for many years. Besides the general goal of determining the fundamental parameters of the SM as precisely as possible, the top mass plays an important role in the stability analysis of the SM. Together with the mass of the Higgs boson, it determines the metastability of the electroweak (EW) vacuum [3–5], which motivates the continuing effort to improve its currently known value.

A process well suited for the determination of the top mass m is a scan of the inclusive cross section of top anti-top pair production from electron-positron collisions, $e^+e^- \to t\bar{t}X$, which will be measured at the planned International Linear Collider (ILC) [6–8]. The region near threshold, where the center-of-mass energy $\sqrt{s} = 2m + E$ deviates from the production threshold of the top anti-top pair only by a small residual energy E, is of particular interest. Due to its large decay width $\Gamma \approx 1.3\,\text{GeV}$ [9], the top quark does not hadronize. Therefore, instead of distinct bound state peaks, the cross section exhibits a broad resonance around the threshold [10]. In practice, the width of the top quark is incorporated by shifting the energy parameter $E \to E + i\Gamma$.

In the threshold region, the cross section strongly depends on the top mass, which facilitates an accurate determination of its value. To achieve this, the experimental results must be combined with a precise theoretical prediction of the cross section near threshold. In this regime, one

uses that the mass m of the heavy quark (which will always refer to the top quark in this thesis) is very large. In particular, the typical velocity $v \ll 1$ of a heavy quark, defined by the small residual energy $E \equiv mv^2$, is used as a small expansion parameter. This constructs the following hierarchy of widely separated scales for a theory containing a heavy quark:

$$\begin{aligned}
&\text{hard scale:} && \mu_h \sim m && \text{(top mass)},\\
&&& \lll && \\
&\text{soft scale:} && \mu_s \sim mv && \text{(typical three momentum)},\\
&&& \lll && \\
&\text{ultrasoft scale:} && \mu_{us} \sim mv^2 && \text{(typical energy)}.
\end{aligned} \tag{1.1}$$

The hierarchy of scales defines a tower of non-relativistic effective field theories (EFTs), where, starting from Quantum Chromodynamics (QCD), heavy degrees of freedom are successively integrated out. The first step is to integrate out degrees of freedom for which both the energy k^0 and the three momentum $\mathbf{k}$ scale like the hard scale m. The resulting theory is non-relativistic QCD (NRQCD) [11–13]. Then, as a second step, also the soft scale mv and light degrees of freedom scaling as $(k^0, \mathbf{k}) \sim (mv^2, mv)$ are integrated out, constructing potential non-relativistic QCD (PNRQCD) [14–18]. This theory then contains only modes scaling like $(k^0, \mathbf{k}) \sim (mv^2, mv)$ for the heavy quarks and $(k^0, \mathbf{k}) \sim (mv^2, mv^2)$ for all light degrees of freedom. We note that there is also an alternative framework called velocitiy non-relativistic QCD (vNRQCD) [19–21] suitable for the discussion of heavy quark systems. However, in this thesis, we will only work with NRQCD and PNRQCD.

In the framework of these theories, the cross section $\sigma_{t\bar{t}X}$ is organized as an expansion in v and the strong coupling α, where we consider $v \sim \alpha$ to be of the same size. The central quantity of this thesis is the so-called R-ratio, which denotes the top anti-top cross section normalized to the high-energy limit of the cross section σ_0 of the process $e^+e^- \to \mu^+\mu^-$. At fixed order, its expansion is given by

$$R = \frac{\sigma_{t\bar{t}X}}{\sigma_0} \sim v \sum_k \left(\frac{\alpha}{v}\right)^k \times \begin{cases} 1 & \text{LO}, \\ \alpha, v & \text{NLO}, \\ \alpha^2, \alpha v, v^2 & \text{NNLO}, \\ \alpha^3, \alpha^2 v, \alpha v^2, v^3 & \text{NNNLO}, \\ \dots . & \end{cases} \tag{1.2}$$

After the initial leading order (LO) and next-to-leading order (NLO) calculations for the R-ratio [22–24], much effort has been made to determine also the next-to-next-to-leading order (NNLO) and next-to-next-to-next-to-leading order (NNNLO) results. An overview of the former is given in [25]. For the latter, the main results are discussed in [26] and a detailed account of the individual contributions can be found in [27]. We also refer to this reference for an overview of literature discussing electromagnetic and electroweak effects, as well as non-resonant contributions (cf. additionally [28–30]). The latter are related to the fact that due to the large decay width of the top quark, in practice one measures the $e^+e^- \to W^+W^-b\bar{b}$ cross section instead of direct $t\bar{t}$-production. One then also needs to account for the production of the final state through channels other than resonant $t\bar{t}$ production. In this thesis, we will, however, focus solely on QCD contributions.

The R-ratio in equation (1.2) contains a resummed factor of $\left(\frac{\alpha}{v}\right)^k \sim 1$, which corresponds to the resummation of so-called ladder diagrams. PNRQCD, where these ladder diagrams are identified with insertions of the leading-order colour Coulomb potential, provides a framework that allows for a systematic resummation of these diagrams.

However, there is another aspect of resummation that is not incorporated in the fixed-order discussion of the R-ratio. In the results of the fixed-order calculations, logarithms $\ln(v)$ containing ratios of the scales μ_h, μ_s, and μ_{us} defined in equation (1.1) appear. Due to the large scale hierarchy, these logarithms can become large. This is of particular concern if it results in $\alpha \ln(v) \sim \mathcal{O}(1)$, which causes perturbation theory to break down. In this case, the fixed-order calculations are not sufficient anymore and have to be extended by a resummation of large logarithms, which is achieved by using renormalization group equations (RGEs). The R-ratio is then organized as follows:

$$R = \frac{\sigma_{t\bar{t}X}}{\sigma_0} \sim v \sum_k \left(\frac{\alpha}{v}\right)^k \sum_l (\alpha \ln(v))^l \times \begin{cases} 1 & \text{LL}, \\ \alpha, v & \text{NLL}, \\ \alpha^2, \alpha v, v^2 & \text{NNLL}, \\ \dots . & \end{cases} \tag{1.3}$$

For the R-ratio, the leading logarithm (LL) expression is the same as the one at LO. However, the calculation at the order of next-to-leading logarithm (NLL) does give a modification of the fixed-order result, which is the main topic of this thesis. This has been discussed in PNRQCD, for example, in references [31–33], where the calculations have been performed in position space. An extensive overview can be found in [34]. There also exists a partially incomplete

resummation at the level of next-to-next-to-leading logarithm (NNLL), which is discussed, for example, in [35–37] for PNRQCD and in [38–41] in the framework of vNRQCD.

In this thesis, we will discuss in detail the NLL case, where the main objective is to provide a consistent treatment of the calculation in momentum space. We will also convert intermediate results from the literature to the conventions used in [27]. This allows us to combine the NLL results with the NNNLO expressions from that work, which has not yet been done in the literature.

The necessary renormalization group (RG) improvement will be performed in multiple steps. First, we resum large logarithms $\ln\left(\frac{\mu_s}{\mu_h}\right)$ in the matching coefficients of NRQCD, which is known as the hard running. Afterwards, logarithms $\ln\left(\frac{\mu_{us}}{\mu_s}\right)$ related to the ultrasoft calculation are considered. Finally, we determine the running of the matching coefficient of the non-relativistic current, which is called the potential running. The result of this calculation is then incorporated into the R-ratio. We discuss this last step both analytically and numerically, where we incorporate the result into the `Mathematica` code `TTbarXSection`. Eventually, this implementation will be translated to an incorporation into the `QQbar_threshold` code [42].

The structure of this thesis is as follows: We begin by reviewing the most relevant concepts of EFTs and RGEs in chapter 2. Afterwards, we introduce the setup of non-relativistic theories used in this thesis and discuss NRQCD and PNRQCD in detail in chapter 3. Chapter 4 then proceeds with an overview of the top anti-top pair production in the context of these non-relativistic theories. In chapter 5, we present the main calculations of this thesis. This entails a discussion of the hard, ultrasoft, and potential running relevant to the R-ratio at NLL. Finally, in chapter 6, we analyse the numerical implications of the analytical results.

Chapter 2

Effective Field Theories and the Renormalization Group Equation

2.1 Effective Field Theories

Whenever a physical system is characterized by a set of widely separated scales, $\Lambda_L \ll \Lambda_H$, one can simplify its description by restricting to low energies. Formally, this is achieved by constructing an EFT. An introduction to this topic can be found, for example, in references [43–45]. The effective Lagrangian $\mathcal{L}_{\text{EFT}}$ facilitates an expansion in the small parameter $\frac{\Lambda_L}{\Lambda_H}$ and is built from the effective degrees of freedom. In $d = 4 - 2\varepsilon$ dimensions, it takes the form

$$\mathcal{L}_{\text{EFT}} = \sum_{n \geq 0,\, i} c_i^{(n)}(\mu, \Lambda_H) \frac{O_i^{(n)}(\mu, \Lambda_L)}{\Lambda_H^{n-d}}, \tag{2.1}$$

where $O_i^{(n)}$ denotes operators of mass dimension n and $c_i^{(n)}$ are dimensionless coefficients. The scale μ is chosen such that $\Lambda_L \ll \mu \ll \Lambda_H$, providing a cut-off for the low-energy theory. Since μ is an arbitrary, artificially introduced quantity, physical observables cannot depend on it. The Lagrangian includes all operators $O_i^{(n)}$ built from the effective degrees of freedom consistent with the underlying symmetries. The coefficients $c_i^{(n)}$ are called matching coefficients (or Wilson coefficients) and encode the high-energy behaviour in Λ_H. They are determined by requiring the fundamental theory and the EFT to be equivalent to some order in the small expansion parameter by performing a matching procedure. In constructing the EFT, heavy degrees of freedom have been integrated out, and their effects are instead included in higher-dimensional operators, which are suppressed by the high-energy scale Λ_H.

2.2 The Renormalization Group Equation

The operators $O_i^{(n)}$ and the matching coefficients $c_i^{(n)}$ contain logarithms $\ln\left(\frac{\mu}{\Lambda_L}\right)$ and $\ln\left(\frac{\mu}{\Lambda_H}\right)$, respectively. Depending on the choice of μ, these logarithms can become large, specifically $\alpha \ln\left(\frac{\mu}{\Lambda_{L/H}}\right) \sim \mathcal{O}(1)$, where α denotes the strong coupling. When this happens, usual perturbation theory in α breaks down, and the large logarithms must be resummed to all orders. This is facilitated by the concept of RGEs, which we introduce now. A comprehensive discussion on this topic can be found, for example, in [46]. We present the parts most relevant to this thesis in the following section.

In writing the effective Lagrangian, we have explicitly introduced an arbitrary factorization scale μ separating high-energy from low-energy contributions. At the same time, this scale μ serves as the renormalization scale for the operators $O_i^{(n)}$ and coefficients $c_i^{(n)}$. For now, we are only interested in the μ-dependence of $O_i^{(n)}$ and $c_i^{(n)}$ in (2.1) and drop the additional argument of Λ_L and Λ_H, respectively.

A bare operator $O_{i,B}^{(n)}$ is renormalized by

$$O_{i,B}^{(n)} = \sum_j Z_{ij}^{(n)}(\mu) O_j^{(n)}(\mu), \tag{2.2}$$

where $Z_{ij}^{(n)}$ are the renormalization constants. Generally, the renormalization of $O_{i,B}^{(n)}$ requires counterterms containing operators $O_j^{(n)}$ with $i \neq j$, called operator mixing. Since the left-hand side is independent of the scale μ, one can derive the following RGE:

$$\begin{aligned} 0 &= \mu \frac{\mathrm{d}}{\mathrm{d}\mu} O_k^{(n)} + \sum_{i,j} \left(Z^{(n)}\right)^{-1}_{ki} \left(\mu \frac{\mathrm{d}}{\mathrm{d}\mu} Z_{ij}^{(n)}\right) O_j^{(n)} = \\ &\equiv \mu \frac{\mathrm{d}}{\mathrm{d}\mu} O_k^{(n)} + \gamma_{kj}(\mu) O_j^{(n)}, \end{aligned} \tag{2.3}$$

where the μ-dependence of the operators and the renormalization constants are implicitly understood. This defines the anomalous dimension matrix

$$\gamma(\mu) = \left(Z^{(n)}\right)^{-1} \left(\mu \frac{\mathrm{d}}{\mathrm{d}\mu} Z^{(n)}\right). \tag{2.4}$$

An observable is required to be independent of μ. We use this to obtain a similar relation for the matching coefficients $c_i^{(n)}$ at fixed n:

$$0 = \mu \frac{\mathrm{d}}{\mathrm{d}\mu} \left(\sum_i c_i^{(n)}(\mu) \langle O_i^{(n)}(\mu) \rangle \right), \tag{2.5}$$

yielding

$$0 = \mu \frac{\mathrm{d}}{\mathrm{d}\mu} c_i^{(n)}(\mu) - c_j^{(n)}(\mu) \gamma_{ji}(\mu). \tag{2.6}$$

In matrix notation, the RGEs read

$$0 = \left(\mu \frac{\mathrm{d}}{\mathrm{d}\mu} + \gamma(\mu) \right) O^{(n)}(\mu) \qquad \text{and} \qquad 0 = \left(\mu \frac{\mathrm{d}}{\mathrm{d}\mu} - \gamma^T(\mu) \right) c^{(n)}(\mu). \tag{2.7}$$

Solving these RGEs resums large logarithms, as we illustrate now with the simple example of a single Wilson coefficient without mixing. In order to obtain the solution of the differential equation at leading order, we expand the anomalous dimension in the strong coupling $\alpha(\mu)$:

$$\gamma(\mu) = \left(\frac{\alpha(\mu)}{4\pi} \right) \gamma_0 + \left(\frac{\alpha(\mu)}{4\pi} \right)^2 \gamma_1 + \mathcal{O}(\alpha^3). \tag{2.8}$$

The renormalized coupling α itself depends on the scale μ, arising through renormalization of the bare coupling α_B as

$$\alpha_B = Z_\alpha \tilde{\mu}^{2\varepsilon} \alpha(\mu), \tag{2.9}$$

where Z_α is the respective renormalization constant. We have defined $\tilde{\mu}$ through $\tilde{\mu}^2 = \mu^2 \left(\frac{e^{\gamma_E}}{4\pi} \right)$, where γ_E is the Euler-Mascheroni constant. With this definition, we implement the use of the $\overline{\text{MS}}$-scheme [47] instead of the MS-scheme when subtracting divergences. The bare coupling $\alpha_B = \frac{g_B^2}{4\pi}$ has mass dimension $[\alpha_B] = 2\varepsilon$ in dimensional regularization, while the renormalized coupling $\alpha(\mu)$ is defined to be a dimensionless quantity. Because of the scale dependence, $\alpha(\mu)$ is called the running coupling, characterized by its RGE

$$\mu \frac{\mathrm{d}}{\mathrm{d}\mu} \alpha(\mu) = -2\varepsilon \alpha(\mu) + \alpha(\mu) \beta(\alpha(\mu)), \quad \text{where} \quad \beta(\alpha) = -\frac{\alpha(\mu)}{2\pi} \sum_{n=0}^{\infty} \left(\frac{\alpha(\mu)}{4\pi} \right)^n \beta_n. \tag{2.10}$$

This defines the so-called β-function, encoding the running of the coupling. It is related to the renormalization constant via

$$\frac{1}{Z_\alpha}\left(\mu\frac{\mathrm{d}}{\mathrm{d}\mu}Z_\alpha\right) = -\beta(\alpha), \tag{2.11}$$

which, at the order relevant to this work, yields

$$Z_\alpha = 1 - \frac{\alpha(\mu)}{4\pi}\beta_0\frac{1}{\varepsilon} + \mathcal{O}\left(\alpha^2\right). \tag{2.12}$$

For one-loop running, the solution to the RGE for the running coupling is given by

$$\alpha(\mu_1) = \frac{\alpha(\mu_0)}{1 + \alpha(\mu_0)\frac{\beta_0}{4\pi}\ln\left(\frac{\mu_1^2}{\mu_0^2}\right)}. \tag{2.13}$$

This relation is exact at one-loop; subleading terms of the order $\mathcal{O}(\alpha^2\log)$ only start contributing at higher orders in the running.

Using this relation in the RGE (2.7), we deduce the following expression for the resummed Wilson coefficient in the case of no mixing:

$$c(\mu_1) \approx c(\mu_0)\left(\frac{\alpha(\mu_1)}{\alpha(\mu_0)}\right)^{-\frac{\gamma_0}{2\beta_0}}. \tag{2.14}$$

This expresses the Wilson coefficient at the scale μ_1 in terms of the coefficient at some initial scale μ_0.

We can use this result to evaluate the Lagrangian (2.1) at the low-energy scale $\mu = \Lambda_L$. In this case, the operators $O_i^{(n)}(\mu = \Lambda_L, \Lambda_L)$ do not contain large logarithms, and their matrix elements can be calculated in perturbation theory. Initially, the Wilson coefficients are determined by matching at the high-energy scale, $c_i^{(n)}(\mu = \Lambda_H, \Lambda_H)$. Using the RGE to evolve them down to Λ_L, the large logarithms have been resummed and included in $c_i^{(n)}(\mu = \Lambda_L, \Lambda_H)$. The resummation can be seen explicitly by reexpanding equation (2.14) with the one-loop running of α, yielding

$$\begin{aligned} c(\Lambda_L, \Lambda_H) = \Bigg[1 - \frac{\gamma_0}{8\pi}\alpha(\Lambda_H)\ln\left(\frac{\Lambda_H^2}{\Lambda_L^2}\right) - \frac{\gamma_0(2\beta_0 - \gamma_0)}{128\pi^2}\alpha^2(\Lambda_H)\ln^2\left(\frac{\Lambda_H^2}{\Lambda_L^2}\right) \\ + \mathcal{O}\left(\alpha^3(\Lambda_H)\ln^3\left(\frac{\Lambda_H^2}{\Lambda_L^2}\right)\right)\Bigg] c(\Lambda_H, \Lambda_H). \end{aligned} \tag{2.15}$$

In the case of large logarithms $\alpha(\Lambda_H)\ln\left(\frac{\Lambda_H^2}{\Lambda_L^2}\right) \sim \mathcal{O}(1)$, this series is not convergent. This necessitates the use of the resummed expression (2.14), which resums the tower of $\sum_n \alpha^n \log^n$, called the LL contribution. The categorization of different contributions is explained schematically in table 2.1. Note that overall factors of α are factored out, such that the counting is always done relative to the LO term.

Table 2.1: Schematic overview of the categorization of different contributions in perturbation theory. The rows indicate the possible contributions in fixed-order calculations at LO, NLO, NNLO, and NNNLO. The columns demonstrate which towers of logarithms are resummed in the LL, NLL, and NNLL calculations, respectively. This table is inspired by [44].

LO	1			
NLO	$\alpha\log$	α		
NNLO	$\alpha^2\log^2$	$\alpha^2\log$	α^2	
NNNLO	$\alpha^3\log^3$	$\alpha^3\log^2$	$\alpha^3\log$	α^3
...	...	...	...	...
	LL	NLL	NNLL	...

We conclude this section on the general aspects of RGEs by commenting in more detail on the anomalous dimension of the matching coefficient c. For simplicity, we again consider the case without mixing. Renormalizing the bare coefficient c_B directly as we did for the operators in equation (2.2),

$$c_B = Z_c c, \tag{2.16}$$

we proceed analogously to the discussion before and obtain

$$0 = \left(\mu\frac{\mathrm{d}}{\mathrm{d}\mu} + \gamma_c\right) c, \tag{2.17}$$

where the anomalous dimension γ_c is given by

$$\gamma_c = \frac{1}{Z_c}\left(\mu\frac{\mathrm{d}}{\mathrm{d}\mu} Z_c\right). \tag{2.18}$$

By comparing these expressions to equations (2.7) and (2.4), we observe that the relevant quantities for the operator O (no index) and its matching coefficient c (index c) are related by

$$\gamma_c = -\gamma \qquad \Rightarrow \qquad Z_c = \frac{1}{Z}. \tag{2.19}$$

This intuitively makes sense since it ensures that the running of the operator and its matching coefficient are opposite to each other, such that their product does not depend on the renormalization scale. The anomalous dimension γ_c can be read off from the renormalization constant Z_c. This is derived by expanding

$$Z_c = \sum_{n=0}^{\infty} Z_c^{(n)} \frac{1}{\varepsilon^n} \tag{2.20}$$

with $Z_c^{(0)} = 1$. We observe that

$$\begin{aligned}
\gamma_c Z_c &= \gamma_c \left(\sum_{n=0}^{\infty} Z_c^{(n)} \frac{1}{\varepsilon^n} \right) = \mu \frac{\mathrm{d}}{\mathrm{d}\mu} \left(\sum_{n=0}^{\infty} Z_c^{(n)} \frac{1}{\varepsilon^n} \right) = \\
&= \mu \frac{\mathrm{d}\alpha(\mu)}{\mathrm{d}\mu} \frac{\partial}{\partial \alpha(\mu)} \left(\sum_{n=0}^{\infty} Z_c^{(n)} \frac{1}{\varepsilon^n} \right) + \mu \frac{\partial}{\partial \mu} \left(\sum_{n=0}^{\infty} Z_c^{(n)} \frac{1}{\varepsilon^n} \right) = \\
&= \left(-2\varepsilon\alpha(\mu) + \alpha(\mu)\beta(\alpha(\mu)) \right) \frac{\partial}{\partial \alpha(\mu)} \left(\sum_{n=0}^{\infty} Z_c^{(n)} \frac{1}{\varepsilon^n} \right) + \mu \frac{\partial}{\partial \mu} \left(\sum_{n=0}^{\infty} Z_c^{(n)} \frac{1}{\varepsilon^n} \right) = \\
&= \sum_{n=0}^{\infty} \left\{ -2\alpha(\mu) \frac{\partial}{\partial \alpha(\mu)} Z_c^{(n+1)} + \alpha(\mu)\beta(\alpha(\mu)) \frac{\partial}{\partial \alpha(\mu)} Z_c^{(n)} + \mu \frac{\partial}{\partial \mu} Z_c^{(n)} \right\} \frac{1}{\varepsilon^n}.
\end{aligned} \tag{2.21}$$

Comparing the $\frac{1}{\varepsilon^0}$-terms on the right- and left-hand side of this equation, we deduce that

$$\gamma_c = -2\alpha(\mu) \frac{\partial}{\partial \alpha(\mu)} Z_c^{(1)}. \tag{2.22}$$

This relation allows us to determine the anomalous dimension (and RGE) of the matching coefficient from the $\frac{1}{\varepsilon}$-pole in its renormalization constant.

Chapter 3

Non-Relativistic Effective Field Theories

3.1 Effective Field Theory Setup

As discussed in the introduction, this thesis considers the production of a top anti-top pair close to threshold. In this energy region, only a small residual energy $E = \sqrt{s} - 2m \equiv mv^2$ is available to the heavy quark anti-quark pair. This naturally defines a small parameter v, the typical velocity of a heavy quark. It also provides three widely separated scales,

$$m \gg mv \gg mv^2, \tag{3.1}$$

where m is the mass of the heavy quark, mv is the size of its typical three momentum, and mv^2 is its typical energy scale. We refer to the resulting regions as

$$\begin{aligned}
&\text{hard region (h):} && k^0 \sim m, && \mathbf{k} \sim m, \\
&\text{soft region (s):} && k^0 \sim mv, && \mathbf{k} \sim mv, \\
&\text{potential region (p):} && k^0 \sim mv^2, && \mathbf{k} \sim mv, \\
&\text{ultrasoft region (us):} && k^0 \sim mv^2, && \mathbf{k} \sim mv^2
\end{aligned} \tag{3.2}$$

for a generic four-momentum $k = (k^0, \mathbf{k})$.

Taking advantage of the large hierarchy between the scales, one can use the method of regions and expand Feynman integrals at the integrand level before performing the loop integration [48, 49]. Since scaleless integrals vanish in dimensional regularization, no double counting occurs.

In practice, it is advantageous to instead turn to an EFT approach, effectively performing the expansion in v at the Lagrangian level. This constructs non-relativistic EFTs. We will proceed in two steps:

$$\begin{aligned}
&\text{QCD:} && (m < \mu) && \mathcal{L}_{\text{QCD}}[Q(h,s,p), g(h,s,p,us)], \\
& && && \downarrow \\
&\text{NRQCD:} && (mv < \mu < m) && \mathcal{L}_{\text{NRQCD}}[Q(s,p), g(s,p,us)], \\
& && && \downarrow \\
&\text{PNRQCD:} && (\mu < mv) && \mathcal{L}_{\text{PNRQCD}}[Q(p), g(us)].
\end{aligned} \tag{3.3}$$

The brackets of the Lagrangian show the content of the effective theory at the respective scale μ: Q denotes the heavy quark, which can, in general, be hard, soft, or potential; g denotes the light degrees of freedom, which can be hard, soft, potential, or ultrasoft. The light degrees of freedom are gluons, ghosts, and light quarks (all quarks apart from the heavy quark), whose mass we set to zero. This approximation is valid for the heavy quark being the top quark [27]. Starting from the full theory QCD, we first integrate out the hard scale, leading to NRQCD [11–13] (for the Quantum Electrodynamics (QED) case, see [50]). In a second step, we also integrate out the soft scale and potential light modes. This defines PNRQCD [14–18]. The theory then contains only potential heavy quarks and ultrasoft light modes. In the following sections, we will describe these theories in more detail.

When constructing PNRQCD, one needs to consider the relative size of the soft and ultrasoft scales compared to the confinement scale Λ_{QCD}, which is the scale where non-perturbative effects in QCD become relevant. In this thesis, we are exclusively going to consider the case $mv^2 \gg \Lambda_{\text{QCD}}$, where the matching procedure for the potentials can be performed perturbatively. Together with the case $mv \gg \Lambda_{\text{QCD}} \sim mv^2$ (where perturbation theory at the ultrasoft scale is not possible anymore), this is discussed in [18] and called the weak coupling regime of PNRQCD. On the other hand, the strong coupling regime is defined by $mv \sim \Lambda_{\text{QCD}}$ and discussed in [51]. An overview of the different scenarios can be found in [52]. The hierarchy $mv^2 \gg \Lambda_{\text{QCD}}$ is a good assumption for the top quark, allowing us to restrict to this case in the following.

Usual perturbation theory refers to the expansion in the strong coupling α. Phenomenologically, the relation between the small expansion parameter v of PNRQCD and the coupling α can be seen in the following way [13]: We equate the kinetic energy $\sim mv^2$ with the leading term in the potential energy, which is given by the Coulomb term $-\frac{\alpha}{r}$. Using $r \sim \frac{1}{mv}$, we obtain $v \sim \alpha$. The details of this line of argument will become clearer in the discussion of PNRQCD below (cf. section 3.3.1). The scaling implies that the non-relativistic theory is given by a simultaneous expansion in v and in α, while $\frac{\alpha}{v} \sim 1$. In this work, we will always use α to denote the strong coupling constant. If we want to refer to the electromagnetic coupling, we will use α_{em} instead.

In order to determine the scaling of the fields, we consider the scaling of the propagators in the non-relativistic region. For a non-relativistic heavy quark with four-momentum $(m + k^0, \mathbf{k})$, the propagator is

$$\frac{i(\not{k} + m)}{k^2 - m^2 + i\varepsilon} \sim \begin{cases} \dfrac{im(\gamma_0 + 1)}{2mk_0 + i\varepsilon} & \sim v^{-1} \quad \text{soft region,} \\ \dfrac{im(\gamma_0 + 1)}{2mk_0 - \mathbf{k}^2 + i\varepsilon} & \sim v^{-2} \quad \text{potential region.} \end{cases} \tag{3.4}$$

For a gluon with momentum $(k^0, \mathbf{k})$, the propagator in Feynman gauge takes the form

$$\frac{i(-g_{\mu\nu})}{k^2 + i\varepsilon} \sim \begin{cases} \dfrac{-ig_{\mu\nu}}{(k^0)^2 - \mathbf{k}^2 + i\varepsilon} & \sim v^{-2} \quad \text{soft region,} \\ \dfrac{-ig_{\mu\nu}}{-\mathbf{k}^2 + i\varepsilon} & \sim v^{-2} \quad \text{potential region,} \\ \dfrac{-ig_{\mu\nu}}{(k^0)^2 - \mathbf{k}^2 + i\varepsilon} & \sim v^{-4} \quad \text{ultrasoft region.} \end{cases} \tag{3.5}$$

The integration measure d^4k scales as v^4 in the soft region, v^5 in the potential region, and v^8 in the ultrasoft region. Using this, the heavy-quark propagator

$$\langle 0|T\{Q(x)Q(y)\}|0\rangle = \int \frac{\mathrm{d}^4k}{(2\pi)^4} \frac{i(\not{k} + m)}{k^2 - m^2 + i\varepsilon} e^{-ik\cdot(x-y)} \tag{3.6}$$

yields the following scaling for the heavy-quark field ψ (and analogously for the heavy-anti-quark field χ):

$$\psi \sim \begin{cases} v^{\frac{3}{2}} & \text{soft region,} \\ v^{\frac{3}{2}} & \text{potential region.} \end{cases} \tag{3.7}$$

In the same way, one derives the scaling of the gluon field:

$$A \sim \begin{cases} v^1 & \text{soft region,} \\ v^{\frac{3}{2}} & \text{potential region,} \\ v^2 & \text{ultrasoft region.} \end{cases} \tag{3.8}$$

3.2 Non-Relativistic Effective Field Theory

3.2.1 The NRQCD Lagrangian

We now turn to a more in-depth discussion of NRQCD [11–13]. Keeping the scaling rules given in the previous section in mind, the NRQCD Lagrangian takes the following form:

$$\mathcal{L}_{\text{NRQCD}} = \mathcal{L}_\psi + \mathcal{L}_\chi + \mathcal{L}_{\psi\chi} + \mathcal{L}_g + \mathcal{L}_{\text{light}}. \tag{3.9}$$

The general case includes two heavy quarks of potentially different masses. This is discussed, for example, in [52]. Since we want to consider heavy quark anti-quark systems, we restrict our discussion to the equal-mass case. The individual terms up to order $\mathcal{O}\left(\frac{1}{m^2}\right)$ are given by[1] [27]

$$\begin{aligned} \mathcal{L}_\psi = \psi^\dagger \Bigg(iD^0 + \frac{\mathbf{D}^2}{2m} + \frac{\mathbf{D}^4}{8m^3} - \frac{d_1}{2m} g\boldsymbol{\sigma}\cdot\mathbf{B} + \frac{d_2}{8m^2} g[D^i, E^i] + i\frac{d_3}{8m^2} g\sigma^{ij}\{D^i, E^j\} \Bigg) \psi \\ + \mathcal{O}\left(\frac{1}{m^3}\right), \end{aligned} \tag{3.10}$$

$$\mathcal{L}_\chi = -\mathcal{L}_\psi \quad \text{with} \quad \psi \to \chi,\ iD^0 \to -iD^0,\ E^i \to -E^i, \tag{3.11}$$

$$\begin{aligned} \mathcal{L}_{\psi\chi} = \frac{d_{ss}}{m^2}\psi^\dagger\psi\chi^\dagger\chi - \frac{d_{sv}}{8m^2}\psi^\dagger[\sigma^i,\sigma^j]\psi\chi^\dagger[\sigma^i,\sigma^j]\chi + \frac{d_{vs}}{m^2}\psi^\dagger T^A\psi\chi^\dagger T^A\chi \\ - \frac{d_{vv}}{8m^2}\psi^\dagger T^A[\sigma^i,\sigma^j]\psi\chi^\dagger T^A[\sigma^i,\sigma^j]\chi + \mathcal{O}\left(\frac{1}{m^3}\right), \end{aligned} \tag{3.12}$$

$$\mathcal{L}_g = -\frac{d_4}{4}G^A_{\mu\nu}G^{A\mu\nu} + \frac{d_5}{m^2}G^A_{\mu\nu}D^2G^{A\mu\nu} + \frac{d_6}{m^2}gf^{ABC}G^A_{\mu\nu}G^{B\mu}{}_\alpha G^{C\nu\alpha} + \mathcal{O}\left(\frac{1}{m^4}\right), \tag{3.13}$$

$$\mathcal{L}_{\text{light}} = \text{light-quark Lagrangian in full QCD.} \tag{3.14}$$

$\mathcal{L}_{\text{NRQCD}}$ uses the following definitions:

- Covariant derivative: $D^\mu = \partial^\mu - igA^\mu$ with $\partial^i = -\nabla^i$,

[1] In addition to the terms up to a suppression factor of $\frac{1}{m^2}$, we have included the quartic kinetic energy correction $\frac{\mathbf{D}^4}{8m^3}$, scaling like v^7 and thus contributing at NNLO. Other terms suppressed by $\frac{1}{m^3}$ are not needed for the NNNLO calculation (which we are eventually interested in), as is discussed in [27].

- Field strength tensor: $G_{\mu\nu} = \frac{i}{g}[D_\mu, D_\nu]$,
- Chromoelectric field: $E^i \equiv G^{i0} = -\nabla^i A^0 - \frac{\partial}{\partial t} A^i - ig[A^i, A^0]$,
- Chromomagnetic field: $\boldsymbol{\sigma} \cdot \mathbf{B} \equiv -\frac{1}{2}\sigma^{ij} G^{ij}$, where $\sigma^{ij} = -\frac{i}{2}[\sigma^i, \sigma^j]$ and σ^i denotes the Pauli matrices.

The Lagrangian is expressed in terms of the effective gluon field, denoted by $A^\mu = A^{A\mu} T^A$, the non-relativistic heavy quark field ψ, and the heavy-anti-quark field χ. The latter two are the two-component spinors taken directly from the four-component Dirac field. We note that there is an alternative common convention (used, for example, in [34]), where one treats the anti-particle as a particle in the anti-triplet colour representation, which results in the charge-conjugated expression of the field considered here (related by $\chi_c = -i\sigma^2 \chi^*$).

Besides this choice in the treatment of the heavy anti-quark, there are some ambiguities in the NRQCD Lagrangian related to (amongst other aspects) field redefinitions and the choice of operator basis. This affects the matching coefficients and requires special care when using results known from the literature. We adopt the Lagrangian used in [27]. We discuss these ambiguities in detail in appendix B.1 and collect the most relevant results in the following.

One could include an operator $\frac{1}{m^2} D^\mu G^A_{\mu\alpha} D_\nu G^{A\nu\alpha}$ in the gluonic Lagrangian, which has, however, not been done above. This term has also been eliminated in [33, 34, 53], which are the main references we will refer to for the RGEs of the NRQCD matching coefficients. However, these references additionally remove the operator $G^A D^2 G^A$, which is still included (multiplied by d_5 in equation (3.13)) in the operator basis we choose to use. The elimination of both of these operators is achieved by absorbing them into the Darwin operator $g\boldsymbol{\sigma} \cdot \mathbf{B}$ and a so-called heavy-light operator of the structure $\psi^\dagger T^A \psi \bar{q} \gamma^0 T^A q$ (and analogously with $\psi \to \chi$), providing an interaction between the heavy fermion and light fermions. As it is done in [53], we choose to not include the latter operator (it is not needed at NNNLO with our choice of basis, cf. [27]), which in turn modifies the coefficient d_{vs} to the four-heavy-fermion operator $\psi^\dagger T^A \psi \chi^\dagger T^A \chi$. Summarizing appendix B.1.1 and B.1.2, where we discuss these changes of basis in more detail, the coefficients in our notation are related to the ones in [33, 34, 53] by the following equations:

$$(d_2 - 16 d_5) = (c_D + c_1^{hl})_{\text{ref.[33, 34]}} = (c_D)_{\text{ref.[53]}}, \tag{3.15}$$

$$d_{vs} = (d_{vs} - \pi\alpha c_1^{hl})_{\text{ref.[33, 34]}}. \tag{3.16}$$

The Lagrangian $\mathcal{L}_{\text{NRQCD}}$ is written entirely in d dimensions. In order to deal with divergences in the non-relativistic theory, we will use dimensional regularization (setting $d = 4 - 2\varepsilon$) and subtract the divergences according to the $\overline{\text{MS}}$-scheme, like we did for the strong coupling $\alpha(\mu)$.

A particular choice in order to ensure d-dimensionality in the Lagrangian is to restrict the use of the chromomagnetic field B^i to the combination $\boldsymbol{\sigma} \cdot \mathbf{B}$ since the B^i do not represent the components of a $(d-1)$-dimensional vector and thus can't be defined in d dimensions. In the limit $d = 4$, one can use the prescription $[\sigma^i, \sigma^j] = 2i\varepsilon^{ijk}\sigma^k$ and obtains

$$\boldsymbol{\sigma} \cdot \mathbf{B} = -\frac{1}{2}\varepsilon^{ijk}\sigma^k G^{ij}. \tag{3.17}$$

An in-depth discussion of the velocity scaling of the individual terms in the Lagrangian can be found in reference [27]. Here, we only note some key aspects.

For potential heavy quarks, the leading terms in the bilinear Lagrangian $\mathcal{L}_\psi$ include the kinetic terms $\psi^\dagger i\partial^0\psi$ and $\psi^\dagger \frac{\boldsymbol{\partial}^2}{2m}\psi$, both scaling like v^5. However, $\psi^\dagger iD^0\psi$ additionally provides the interaction $\psi^\dagger gA^0\psi$. For a potential gluon field, this also scales like v^5 and is therefore not suppressed. It cannot be treated perturbatively and requires resummation. This becomes more clear once one switches to PNRQCD, as we will discuss in section 3.3.1. All other contributions are suppressed with respect to these leading terms. In the Lagrangian given above, we have included terms up to NNNLO, scaling like v^8.

For soft heavy quarks, the leading term is given by $\psi^\dagger i\partial^0\psi \sim v^4$, while all other terms are suppressed. This justifies the use of static heavy-quark propagators in the matching procedure, comparable to heavy quark effective theory (HQET) [54]. All interactions in the soft region can be treated in perturbation theory.

While NRQCD provides a way to implement the non-relativistic nature of heavy-quark bound states, the power counting is still ambiguous. As we have discussed before, the effective degrees of freedom still exist at multiple scales after integrating out the hard modes (for example, both soft and potential heavy quarks are dynamical degrees of freedom). This problem is addressed by constructing PNRQCD (cf. section 3.3.1).

3.2.2 The NRQCD Matching Coefficients at Fixed Order

The NRQCD Lagrangian (cf. equations (3.9)-(3.14)) contains the matching coefficients d_i (in the bilinear and gluonic sectors of the Lagrangian, $i = 1, \ldots, 6$) and d_{ij} (in the four-heavy-quark sector, $ij = ss, sv, vs, vv$), which are known from the literature.

The coefficients contain logarithms $\ln\left(\frac{\mu^2}{m^2}\right)$. Away from their natural scale $\mu_h \sim m$, these logarithms become large and require resummation. We will discuss this in section 5.2.

For ease of reference, we repeat the fixed-order expressions for the coefficients known from the literature in the following. We note that for this thesis, we only need the matching coefficients at the one-loop level. Two-loop results can be found in [55].

Coefficients to the Gluonic Operators

The coefficients appearing in the gluonic Lagrangian (3.13) are d_4, d_5, and d_6.

The coefficient d_4, multiplying the kinetic term of the gluon, can be set to the canonical normalization $d_4 = 1$. This defines the effective strong coupling α in the non-relativistic theory, corresponding to the coupling running with just the number of light flavours (n_f) instead of with all flavours including the heavy quark ($n_f + 1$) [43].

The first coefficient of the β-function defined in equation (2.10) then reads

$$\beta_0 = \frac{11}{3} C_A - \frac{4}{3} T_F n_f \tag{3.18}$$

in the $\overline{\text{MS}}$ scheme. This, as well as the coefficients β_1 and β_2, can be found in reference [56]. In this expression, we use the factors $C_A = N$ and $T_F = \frac{1}{2}$, where N denotes the number of colours ($N = 3$ for QCD). Later, we will additionally need $C_F = \frac{N^2-1}{2N}$ ($= \frac{4}{3}$ in QCD).

In $\mathcal{L}_{\text{NRQCD}}$, we have included terms up to NNNLO, scaling like v^8 for potential fields. The operator multiplied by d_5, $G^A_{\mu\nu} D^2 G^{A\mu\nu}$, contributes at the order v^7 for potential gluons, such that we need d_5 only up to order $\alpha \sim v^1$. The fixed-order result to this order can be found in [27] and is given by

$$d_5^{\text{FO}} = \frac{\alpha(\mu)}{\pi} \left(\frac{\mu}{m}\right)^{2\varepsilon} \frac{T_F \Gamma(1+\varepsilon) e^{\gamma_E \varepsilon}}{60} = \frac{T_F \alpha(\mu)}{60\pi} + d_5^{\varepsilon}(\varepsilon), \tag{3.19}$$

$$d_5^{\varepsilon}(\varepsilon) = \frac{\alpha(\mu)}{60\pi} T_F \ln\left(\frac{\mu^2}{m^2}\right) \varepsilon + \mathcal{O}(\varepsilon^2). \tag{3.20}$$

We have explicitly denoted the term d_5^{ε} to keep track of $\mathcal{O}(\varepsilon)$-terms. These are not relevant to the NLL calculation, however, they might lead to finite terms once one extends the calculation to NNLL order.

Lastly, the coefficient d_6 is not relevant to our calculation. It is multiplied by the operator $g f^{ABC} G^A_{\mu\nu} G^{B\mu}{}_{\alpha} G^{C\nu\alpha}$, which scales like $\sim v^{13/2}$ for soft gluons and $\sim v^8$ for potential gluons. Since d_6 starts to contribute at order $d_6 \sim \alpha$ [57], this term is beyond NNNLO.

Coefficients to the Bilinear Heavy-Quark Operators

The coefficients to the bilinear heavy-quark operators are given by d_1, d_2, and d_3. In the literature, these are commonly referred to as c_F (Fermi coefficient), c_D (Darwin coefficient), and c_S (spin-orbit coefficient), respectively.[2] We do not consider the coefficients to the kinetic operator $\frac{\mathbf{D}^2}{2m}$ and to the kinetic correction $\frac{\mathbf{D}^4}{8m^3}$ since they can be set to one by reparametrization invariance [57]. The operator multiplied by d_1, $\psi^\dagger g\boldsymbol{\sigma}\cdot\mathbf{B}\psi$, constitutes the chromomagnetic interaction and scales like v^6 for potential fields. The vertex in a single interaction of this type needs to be combined with the quark-gluon interaction in $\psi^\dagger\frac{\mathbf{D}^2}{2m}\psi$ (instead of in $\psi^\dagger iD^0\psi$), which is suppressed by an additional factor of v^1. Therefore, the chromomagnetic interaction first contributes at NNLO and d_1 is needed up to order $\alpha\sim v$ for the NNNLO calculation. The operators multiplying d_2 and d_3, $\psi^\dagger g[D^i,E^i]\psi$ and $\psi^\dagger g\sigma^{ij}\{D^i,E^i\}\psi$, respectively, both scale like v^7 for potential fields, such that d_2 and d_3 are also needed up to $\alpha\sim v$.

The fixed-order expressions for the two-fermion coefficients are given in [27] in terms of form factors. Explicitly, the coefficients read

$$\begin{aligned} d_1^{\mathrm{FO}} &= 1+\frac{\alpha(\mu)}{\pi}\left(\frac{\mu}{m}\right)^{2\varepsilon}\frac{\Gamma(\varepsilon)e^{\gamma_E\varepsilon}}{4(4\varepsilon^2-1)}\left((2\varepsilon+1)(2\varepsilon^2-1)C_A-2\varepsilon(2\varepsilon+1)^2C_F\right)= \\ &= \frac{C_A\alpha(\mu)}{4\pi}\frac{1}{\varepsilon}+\left[1+\frac{\alpha(\mu)}{2\pi}(C_A+C_F)+\frac{\alpha(\mu)}{4\pi}C_A\ln\left(\frac{\mu^2}{m^2}\right)\right]+d_1^{\varepsilon}(\varepsilon), \end{aligned} \tag{3.21}$$

$$\begin{aligned} d_2^{\mathrm{FO}} &= 1+\frac{\alpha(\mu)}{\pi}\left(\frac{\mu}{m}\right)^{2\varepsilon}\frac{\Gamma(\varepsilon)e^{\gamma_E\varepsilon}}{6(4\varepsilon^2-1)}\left((10\varepsilon^2-3\varepsilon+2)C_A+8(-4\varepsilon^2+1)C_F\right)= \\ &= -\frac{(C_A+4C_F)\alpha(\mu)}{3\pi}\frac{1}{\varepsilon}+\left[1+\frac{\alpha(\mu)}{2\pi}C_A-\frac{\alpha(\mu)}{3\pi}(C_A+4C_F)\ln\left(\frac{\mu^2}{m^2}\right)\right]+d_2^{\varepsilon}(\varepsilon). \end{aligned} \tag{3.22}$$

The last coefficient d_3 is fixed to $d_3=2d_1-1$ by reparametrization invariance [57]. The $\mathcal{O}(\varepsilon)$-terms of d_1 and d_2 are given by

$$d_1^{\varepsilon}(\varepsilon)=\frac{\alpha(\mu)}{2\pi}\left[C_A+4C_F+\frac{\pi^2}{24}C_A+(C_A+C_F)\ln\left(\frac{\mu^2}{m^2}\right)+\frac{1}{4}C_A\ln^2\left(\frac{\mu^2}{m^2}\right)\right]\varepsilon+\mathcal{O}(\varepsilon^2), \tag{3.23}$$

$$\begin{aligned} d_2^{\varepsilon}(\varepsilon) &= \frac{\alpha(\mu)}{6\pi}\left[-18C_A-\frac{\pi^2}{6}C_A-\frac{2\pi^2}{3}C_F+3C_A\ln\left(\frac{\mu^2}{m^2}\right)-(C_A+4C_F)\ln^2\left(\frac{\mu^2}{m^2}\right)\right]\varepsilon \\ &\quad+\mathcal{O}(\varepsilon^2). \end{aligned} \tag{3.24}$$

[2] As we have already mentioned in equation (3.15), there is a subtlety to relating the coefficient d_2 in our convention to c_D in other references, caused by a field redefinition in the gluonic Lagrangian. This will become apparent in section 5.2 and is commented on in appendix B.1.

Coefficients to the Four-Heavy-Quark Operators

The four-heavy-quark terms in $\mathcal{L}_{\psi\chi}$ (3.12) can be written in two different orderings: the scattering order $(\psi^\dagger\psi)(\chi^\dagger\chi)$, and the annihilation order $(\psi^\dagger\chi)(\chi^\dagger\psi)$. The resulting terms are related by a Fierz transformation, which is discussed in [58]. While the latter ordering is best suited for processes involving the annihilation of heavy quarks, the former is more natural for cases considering fermion anti-fermion bound states. At NNNLO, the annihilation contribution vanishes [27], such that the scattering ordering is the one appropriate for our scenario and has been adopted in equation (3.12).

The coefficients in the four-heavy-quark Lagrangian are denoted by d_{ss}, d_{sv}, d_{vs} and d_{vv}. We have made use of the usual notation in the literature: The indices s and v indicate the colour and spin structure of the heavy quark anti-quark term, where s in the first (second) index denotes a colour singlet (spin singlet), while v in the first (second) index refers to the colour octet (spin triplet), respectively.

Generally, the coefficients include contributions from both annihilation and scattering processes. Reference [58] discusses both of these contributions.[3] However, as we have mentioned above, only the scattering terms are relevant to our calculation. The coefficients first contain terms related to hard scattering at order $\alpha^2 \sim v^2$ since this process requires the exchange of at least two gluons. This is the order the coefficients are required to at NNNLO, since the four-fermion operators $\psi^\dagger\psi\chi^\dagger\chi$ scale like v^6.

[3]Note that the coefficients d_{sv} and d_{vv} multiplying spin-dependent operators in [58] are $(1-\varepsilon)$ times the corresponding coefficients in this work. This is related to the use of the d-dimensional expression for the spin structures in the Lagrangian (3.12).

The scattering contributions to the fixed-order expressions are taken from [27] and read

$$d_{ss}^{\mathrm{FO}} = \alpha^2(\mu) C_F(C_A - 2C_F) \left(\frac{\mu}{m}\right)^{2\varepsilon} \frac{e^{\gamma_E \varepsilon}(2\varepsilon - 3)\left(2\varepsilon^2 + \varepsilon + 1\right)\Gamma(2+\varepsilon)}{2\varepsilon\left(8\varepsilon^3 + 12\varepsilon^2 - 2\varepsilon - 3\right)} = \tag{3.25}$$

$$= \frac{(C_A - 2C_F)C_F\alpha^2(\mu)}{2\varepsilon} + \frac{\alpha^2(\mu)}{3}(C_A - 2C_F)C_F + \frac{\alpha^2(\mu)}{2}(C_A - 2C_F)C_F \ln\left(\frac{\mu^2}{m^2}\right) + d_{ss}^{\varepsilon}(\varepsilon), \tag{3.26}$$

$$d_{sv}^{\mathrm{FO}} = \alpha^2(\mu) C_F(C_A - 2C_F) \left(\frac{\mu}{m}\right)^{2\varepsilon} \frac{e^{\gamma_E \varepsilon}\Gamma(1+\varepsilon)}{2(1+2\varepsilon)} = \tag{3.27}$$

$$= \frac{\alpha^2(\mu)}{2}(C_A - 2C_F)C_F + d_{sv}^{\varepsilon}(\varepsilon), \tag{3.28}$$

$$d_{vs}^{\mathrm{FO}} = \alpha^2(\mu) \left(\frac{\mu}{m}\right)^{2\varepsilon} \frac{e^{\gamma_E \varepsilon}(3 - 2\varepsilon)\left(C_A(\varepsilon(2\varepsilon+1)(4\varepsilon+3)+5) - 8C_F(1+\varepsilon)\left(2\varepsilon^2+\varepsilon+1\right)\right)\Gamma(\varepsilon)}{4(2\varepsilon-1)(2\varepsilon+1)(2\varepsilon+3)} \tag{3.29}$$

$$= \frac{(-5C_A + 8C_F)\alpha^2(\mu)}{4\varepsilon} + \frac{\alpha^2(\mu)}{12}(11C_A + 16C_F) + \alpha^2(\mu)\left(-\frac{5}{4}C_A + 2C_F\right)\ln\left(\frac{\mu^2}{m^2}\right) + d_{vs}^{\varepsilon}(\varepsilon), \tag{3.30}$$

$$d_{vv}^{\mathrm{FO}} = \alpha^2(\mu) \left(\frac{\mu}{m}\right)^{2\varepsilon} \frac{e^{\gamma_E \varepsilon}(-C_A(1+4\varepsilon) + 8C_F\varepsilon)\Gamma(\varepsilon)}{4(1+2\varepsilon)} = \tag{3.31}$$

$$= -\frac{C_A\alpha^2(\mu)}{4\varepsilon} + \frac{\alpha^2(\mu)}{2}(-C_A + 4C_F) - \frac{\alpha^2(\mu)}{4}C_A \ln\left(\frac{\mu^2}{m^2}\right) + d_{vv}^{\varepsilon}(\varepsilon). \tag{3.32}$$

The $\mathcal{O}(\varepsilon)$-terms are given by

$$d_{ss}^{\varepsilon}(\varepsilon) = \alpha^2(\mu)(C_A - 2C_F)C_F\left[\frac{47}{18} + \frac{\pi^2}{24} + \frac{1}{3}\ln\left(\frac{\mu^2}{m^2}\right) + \frac{1}{4}\ln^2\left(\frac{\mu^2}{m^2}\right)\right]\varepsilon + \mathcal{O}(\varepsilon^2), \tag{3.33}$$

$$d_{sv}^{\varepsilon}(\varepsilon) = \alpha^2(\mu)(C_A - 2C_F)C_F\left[-1 + \frac{1}{2}\ln\left(\frac{\mu^2}{m^2}\right)\right]\varepsilon + \mathcal{O}(\varepsilon^2), \tag{3.34}$$

$$d_{vs}^{\varepsilon}(\varepsilon) = \alpha^2(\mu)\Bigg[-\frac{137}{18}C_A + \frac{94}{9}C_F - \frac{5\pi^2}{48}C_A + \frac{\pi^2}{6}C_F + \frac{1}{12}(11C_A + 16C_F)\ln\left(\frac{\mu^2}{m^2}\right) + \left(-\frac{5}{8}C_A + C_F\right)\ln^2\left(\frac{\mu^2}{m^2}\right)\Bigg]\varepsilon + \mathcal{O}(\varepsilon^2), \tag{3.35}$$

$$d_{vv}^{\varepsilon}(\varepsilon) = \alpha^2(\mu)\left[C_A - 4C_F - \frac{\pi^2}{48}C_A + \frac{1}{2}(-C_A + 4C_F)\ln\left(\frac{\mu^2}{m^2}\right) - \frac{1}{8}C_A\ln^2\left(\frac{\mu^2}{m^2}\right)\right]\varepsilon + \mathcal{O}(\varepsilon^2). \tag{3.36}$$

3.3 Potential Non-Relativistic Effective Field Theory

3.3.1 The PNRQCD Lagrangian

By integrating out all degrees of freedom except for potential heavy quarks and ultrasoft light modes from NRQCD, the power counting is made manifest: $\psi \sim v^{\frac{3}{2}}$, $\chi \sim v^{\frac{3}{2}}$, $A \sim v^2$, $\mathbf{x} \sim r \sim v^{-1}$, and derivatives acting on a heavy-quark field $\partial_0 \sim p_0 \sim v^2$ and $\boldsymbol{\partial} \sim \mathbf{p} \sim v^1$. This solves the inherent problem of non-homogenous power counting in NRQCD, which was discussed in the previous section.

As indicated in (3.3), this procedure constructs PNRQCD [14–18]. In this thesis, we will use the conventions from reference [27], where the heavy-quark sector of the Lagrangian up to NNNLO takes the form

$$\begin{aligned}\mathcal{L}_{\text{PNRQCD}} = \psi^\dagger \left(i\partial_0 + \frac{\boldsymbol{\partial}^2}{2m} + gA_0(t,\mathbf{0}) - g\mathbf{x}\cdot\mathbf{E}(t,\mathbf{0}) + \frac{\boldsymbol{\partial}^4}{8m^3} \right) \psi \\ + \chi^\dagger \left(i\partial_0 - \frac{\boldsymbol{\partial}^2}{2m} + gA_0(t,\mathbf{0}) - g\mathbf{x}\cdot\mathbf{E}(t,\mathbf{0}) - \frac{\boldsymbol{\partial}^4}{8m^3} \right) \chi \\ + \tilde{\mu}^{-2\varepsilon} \int \mathrm{d}^{d-1}\mathbf{r} \left[\psi_a^\dagger \psi_b \right](x+\mathbf{r}) V_{ab;cd}(r,\boldsymbol{\partial}) \left[\chi_c^\dagger \chi_d \right](x). \end{aligned} \tag{3.37}$$

The leading order terms scale like v^5. This includes the kinetic terms $i\partial_0 \pm \frac{\boldsymbol{\partial}^2}{2m}$ and the Coulomb potential, as we discuss below. The terms including $gA_0(t,\mathbf{0})$ can be removed by a field redefinition including a Wilson line [27, 59, 60]. The $\mathbf{x}\cdot\mathbf{E}$-term is the chromomagnetic dipole term and encodes the ultrasoft interaction. It scales like $\mathbf{x}\cdot\mathbf{E} \sim v^3$, such that the interaction is of the size $v^{\frac{13}{2}}$ (suppressed by a factor of $v^{\frac{3}{2}}$ with respect to the leading terms). Two ultrasoft vertices are required to produce a non-vanishing effect, causing the ultrasoft correction to first contribute at NNNLO. This contribution is discussed in [61, 62]. In order to make the power counting homogeneous, the ultrasoft fields have been multipole-expanded [63–65].

Unlike the NRQCD Lagrangian (3.9), the PNRQCD Lagrangian is not local. More precisely, it is still instantaneous (local in time), but non-local in space. Non-localities arise whenever one integrates out modes. However, as long as there are no modes in the effective Lagrangian that can resolve these non-localities (i.e. all effective modes only fluctuate over distances larger than the non-localities), one can perform an operator product expansion [66, 67] and render the effective theory local [60]. This is what happens for NRQCD: Integrating out the hard modes $(k^0,\mathbf{k}) \sim (m,m)$ results in non-localities of the order $\frac{1}{m}$, while all leftover effective modes are at least soft $(k^0,\mathbf{k}) \sim (mv,mv)$, fluctuating over distances $\sim \frac{1}{mv}$. Since this is significantly larger than the non-localities, they cannot be resolved and NRQCD can be rendered local.

On the other hand, for PNRQCD, we integrate out also soft heavy modes and potential light modes. This leads to non-localities of the order $\frac{1}{mv}$ in both the temporal and the spatial components. However, potential heavy modes are still contained in the effective Lagrangian, scaling like $(k^0, \mathbf{k}) \sim (mv^2, mv)$. Typical fluctuations thus are of the order $\frac{1}{mv^2}$ in the temporal component and of the order $\frac{1}{mv}$ in the spatial component. We can now see that while the temporal non-localities cannot be resolved by the effective modes (enabling an operator product expansion in this component and keeping the theory instantaneous), the spatial non-localities can be resolved and render PNRQCD spatially non-local.

The last line in (3.37) describes interactions via heavy-quark potentials

$$V_{ab;cd}(r, \boldsymbol{\partial}) = T^A_{ab} T^A_{cd} V_0(r) + \delta V_{ab;cd}(r, \boldsymbol{\partial}). \tag{3.38}$$

These are the matching coefficients of PNRQCD, encoding the high-energy behaviour of the degrees of freedom that have been integrated out. The leading term is the tree-level colour Coulomb potential

$$V_0(r) = -\frac{\alpha}{r}. \tag{3.39}$$

The scaling behaviour of the Coulomb potential is $V_0(r) \sim v^2$, such that the interaction scales like v^5. Therefore, the Coulomb potential is not suppressed with respect to the kinetic terms and has to be treated non-perturbatively. This is exactly the effect related to the exchange of potential gluons discussed above in the NRQCD setting. In practice, the non-perturbative treatment is achieved through a resummation of ladder diagrams, encoding the effect of the Coulomb potential in the use of the propagator of the heavy quark anti-quark pair instead of treating the particle and the anti-particle separately. This will be further discussed below. Since the colour Coulomb potential is contained already in the leading-order theory, PNRQCD closely resembles perturbation theory in Quantum Mechanics.

We note that this leads to a common alternative way of phrasing the PNRQCD Lagrangian, which is used, for example, in references [14, 18, 34, 52]. It relies on projecting the $Q\bar{Q}$ state onto a single field representing the heavy-quark pair and decomposing it into a singlet state $S(\mathbf{R}, \mathbf{r}, t)$ and an octet state $O(\mathbf{R}, \mathbf{r}, t)$. In this expression, $\mathbf{R}$ denotes the center-of-mass coordinate, and $\mathbf{r}$ is the relative coordinate. Details on this procedure can be found in [34]. Here, we only state the Lagrangian in this framework after multipole expanding the gluonic

fields:

$$\tilde{\mathcal{L}}_{\text{PNRQCD}} = \text{Tr}\left\{\text{S}^\dagger(i\partial_0 - h_s(r))\text{S} + \text{O}^\dagger(iD_0 - h_o(r))\text{O}\right\} + V_A(r)\,\text{Tr}\left\{\text{O}^\dagger g\mathbf{r}\cdot\mathbf{E}\text{S} + \text{S}^\dagger g\mathbf{r}\cdot\mathbf{E}\text{O}\right\} + \frac{1}{2}V_B(r)\,\text{Tr}\left\{\text{O}^\dagger\{g\mathbf{r}\cdot\mathbf{E},\text{O}\}\right\}. \quad (3.40)$$

In this expression, the ultrasoft covariant derivative is given by $iD_0\text{O} = i\partial_0\text{O} - g\,[A_0(\mathbf{R},t),\text{O}]$. The ultrasoft fields $\mathbf{E}$ are implicitly evaluated at the center-of-mass coordinate $\mathbf{R}$ and time t. The quantities h_s and h_o stand for the singlet and octet Hamiltonian, respectively, containing a kinetic term and the potentials. This Lagrangian contains two additional matching coefficients, V_A and V_B, multiplying the interaction with ultrasoft gluons. We will later use the coefficient V_A to keep track of ultrasoft contributions in the RG improvement.

Resummation of Ladder Diagrams

We now turn to the interaction terms in the non-relativistic Lagrangians that are unsuppressed relative to the leading kinetic terms.

In the case of NRQCD, these terms are given by $\psi^\dagger gA^0\psi$ and $\chi^\dagger gA^0\chi$ for potential fields, scaling like v^5. This interaction leads to diagrams that are not suppressed in the threshold region, posing a leading-order effect and thus requiring non-perturbative treatment. These diagrams are the so-called ladder diagrams, shown in figure 3.1. From the scaling properties

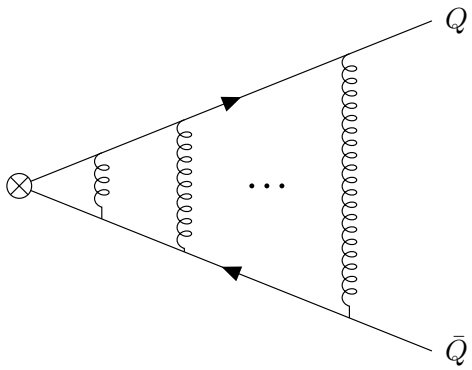

Figure 3.1: Generic ladder diagram. Each loop comes with an unsuppressed factor of order $\mathcal{O}(1)$, requiring resummation of these diagrams.

discussed in section 3.1, we deduce that each potential loop comes with a factor of

$$\underbrace{v^5}_{\text{Loop measure}} \times \underbrace{v^{-2}v^{-2}}_{\substack{\text{Heavy quark}\\ \text{propagators}}} \times \underbrace{v^{-2}}_{\substack{\text{Potential gluon}\\ \text{propagator}}} \times \underbrace{v^1}_{g^2\sim\alpha} \sim 1, \quad (3.41)$$

which is not suppressed. Therefore, these diagrams require resummation. This can be done in a systematic way in the context of PNRQCD. There, the corresponding term in the Lagrangian is given by the interaction of a heavy-quark pair via a leading-order colour Coulomb interaction, namely

$$\tilde{\mu}^{-2\varepsilon} \int \mathrm{d}^{d-1}\mathbf{r} \left[\psi_a^\dagger \psi_b\right](x+\mathbf{r}) \left(-\frac{\alpha}{r} T_{ab}^A T_{cd}^A\right) \left[\chi_c^\dagger \chi_d\right](x) \sim v^5. \tag{3.42}$$

The resummation of this interaction is achieved by phrasing the situation in terms of the propagator of the heavy quark anti-quark pair (instead of the heavy quark and anti-quark propagating separately). In momentum space, this propagator is given by

$$\frac{1}{N} \delta_{bc}\delta_{da} i G_0(\mathbf{p}, \mathbf{p}'; E) \tag{3.43}$$

for a pair in the colour-singlet state.[4] This expression contains the Green's function $G_0(\mathbf{p}, \mathbf{p}'; E)$, which satisfies the d-dimensional Lippmann-Schwinger equation:

$$(2\pi)^{d-1}\delta^{(d-1)}(\mathbf{p}-\mathbf{p}') = \left(\frac{\mathbf{p}^2}{m} - E\right) G_0(\mathbf{p}, \mathbf{p}'; E) - \tilde{\mu}^{2\varepsilon} \int \frac{\mathrm{d}^{d-1}\mathbf{k}}{(2\pi)^{d-1}} \frac{g^2 C_F}{\mathbf{k}^2} G_0(\mathbf{p}-\mathbf{k}, \mathbf{p}'; E). \tag{3.44}$$

In these expressions, $\mathbf{p}$ and $\mathbf{p}'$ denote the momentum of the incoming and outgoing quark, respectively. $E = \sqrt{s} - 2m$ denotes the energy of the heavy quark anti-quark pair. The Green's function will be discussed in more detail in section 4 .

Proceeding like in [27], we consider the scattering process $Q(p_1)\bar{Q}(p_2) \to Q(p_1')\bar{Q}(p_2')$ in the rest frame of the heavy quark anti-quark pair ($Q\bar{Q}$), that is

$$p_1 = \left(\frac{E}{2}, \mathbf{p}\right), \qquad p_1' = \left(\frac{E}{2}, \mathbf{p}'\right), \tag{3.45}$$

$$p_2 = \left(\frac{E}{2}, -\mathbf{p}\right), \qquad p_2' = \left(\frac{E}{2}, -\mathbf{p}'\right). \tag{3.46}$$

In this case, the Green's function $G_0(\mathbf{p}, \mathbf{p}'; E)$ can be written as

$$G_0(\mathbf{p}, \mathbf{p}'; E) = -\frac{(2\pi)^{d-1}\delta^{(d-1)}(\mathbf{p}-\mathbf{p}')}{E - \frac{\mathbf{p}^2}{m} + i\varepsilon} + \frac{1}{E - \frac{\mathbf{p}^2}{m} + i\varepsilon} i H(\mathbf{p}, \mathbf{p}'; E) \frac{1}{E - \frac{\mathbf{p}'^2}{m} + i\varepsilon}, \tag{3.47}$$

[4] One can consider an analogous procedure for the colour-octet Green's function, see for example [27].

where the first term represents the diagram with no insertions of the leading-order Coulomb potential and $H(\mathbf{p}, \mathbf{p}'; E)$ encodes the sum of all diagrams with one or more Coulomb exchanges. One generic example of these diagrams is depicted in figure 3.2. Explicitly, the sum of all

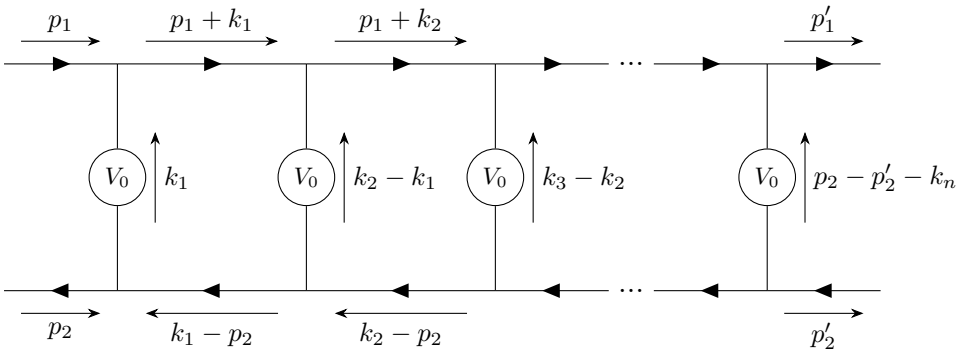

Figure 3.2: Generic ladder diagram with $n + 1$ Coulomb exchanges. These diagrams are unsuppressed and need to be resummed.

diagrams of this type is given by

$$H(\mathbf{p}, \mathbf{p}'; E) = \sum_{n=0}^{\infty} \left(\tilde{\mu}^{2\varepsilon}\right)^n \int \left[\prod_{i=1}^{n} \frac{\mathrm{d}^d k_i}{(2\pi)^d}\right] \frac{iC_F(-g^2)}{\mathbf{k}_1^2}$$
$$\times \prod_{i=1}^{n} \frac{iC_F(-g^2)}{(\mathbf{k}_{i+1} - \mathbf{k}_i)^2} \frac{i}{\frac{E}{2} + k_i^0 - \frac{(\mathbf{p}+\mathbf{k}_i)^2}{2m} + i\varepsilon} \frac{-i}{\frac{E}{2} - k_i^0 - \frac{(\mathbf{p}+\mathbf{k}_i)^2}{2m} + i\varepsilon} = \tag{3.48}$$
$$= i \sum_{n=0}^{\infty} (-g^2 C_F)^{n+1} \tilde{\mu}^{2n\varepsilon} \int \left[\prod_{i=1}^{n} \frac{\mathrm{d}^{d-1}\mathbf{k}_i}{(2\pi)^{d-1}}\right] \frac{1}{\mathbf{k}_1^2} \prod_{i=1}^{n} \frac{1}{(\mathbf{k}_{i+1} - \mathbf{k}_i)^2 \left(E - \frac{(\mathbf{p}+\mathbf{k}_i)^2}{m} + i\varepsilon\right)}, \tag{3.49}$$

where we have defined $\mathbf{k}_{n+1} = \mathbf{p}' - \mathbf{p}$. To obtain the last line, the integrations of the zero components k_i^0 have been performed by using the residue theorem and picking up the poles in the upper half plane. The factors of C_F arise when projecting the potential onto the colour singlet (cf. equation (3.53) below):

$$\frac{1}{N} \delta_{bc} \delta_{da} T_{ab}^A T_{cd}^A = C_F. \tag{3.50}$$

Reference [27] discusses multiple explicit expressions for the Green's function G_0 in both position and momentum space. For our purposes, the following one is the most relevant:

$$\begin{aligned} G_0(E) &\equiv G_0(\mathbf{r}=0,\mathbf{r}'=0;E) = \\ &= \frac{m^2 C_F \alpha}{4\pi}\left[\frac{1}{4\varepsilon} - \frac{1}{2}\ln\left(-\frac{4mE}{\mu^2}\right) + \frac{1}{2} - \frac{1}{2\lambda} - \gamma_E - \Psi(1-\lambda)\right] + \mathcal{O}(\varepsilon). \end{aligned} \tag{3.51}$$

Here, one defines the parameter

$$\lambda = \frac{\alpha C_F}{2\sqrt{-\frac{E}{m}}}. \tag{3.52}$$

For $\lambda = n$ (some positive integer), the function $\Psi(1-\lambda)$, which denotes the Euler Psi-function, exhibits poles. This characterizes the S-wave bound states of the heavy quark anti-quark pair, whose energy is denoted by E_n.

In section 4.3, we will discuss how to use this Green's function containing the resummation of the ladder diagrams in the context of the heavy-quark correlation function.

3.3.2 The PNRQCD Matching Coefficients (Potentials) at Fixed Order

We now turn to the explicit expressions for the matching coefficients of PNRQCD, namely the potentials. Since a potential insertion does not change the colour state of the heavy quark anti-quark pair, for the top anti-top pair production (where the incoming pair is in the colour singlet), only the colour-singlet projection of the potentials is necessary [27], reading

$$V = \frac{1}{N}\delta_{bc}\delta_{da}V_{ab;cd} = \frac{1}{N}\delta_{bc}\delta_{da}\left(V_1 1_{ab}1_{cd} + V_T T^A_{ab}T^A_{cd}\right) = V_1 + C_F V_T. \tag{3.53}$$

For the colour-octet potential, we refer to, for example, reference [18].

In momentum space, the colour-singlet potentials are given by [27]

$$\begin{aligned} V(\mathbf{p},\mathbf{p}') = &-\mathcal{V}_C(\alpha)\frac{4\pi C_F\alpha}{\mathbf{q}^2} + \mathcal{V}_{1/m}(\alpha)\frac{\pi^2(4\pi)C_F\alpha}{m|\mathbf{q}|} \\ &+ \mathcal{V}_\delta(\alpha)\frac{2\pi C_F\alpha}{m^2} - \mathcal{V}_p(\alpha)\frac{2\pi C_F\alpha(\mathbf{p}^2+\mathbf{p}'^2)}{m^2\mathbf{q}^2} - \mathcal{V}_s(\alpha)\frac{\pi C_F\alpha}{4m^2}[\sigma_i,\sigma_j]\otimes[\sigma_i,\sigma_j] \\ &+ \mathcal{V}_{hf}(\alpha)\frac{\pi C_F\alpha}{4m^2\mathbf{q}^2}[\sigma_i,\sigma_j]q_j\otimes[\sigma_i,\sigma_k]q_k \\ &- \mathcal{V}_{so}(\alpha)\frac{3\pi C_F\alpha}{2m^2\mathbf{q}^2}\left([\sigma_i,\sigma_j]q_ip_j\otimes 1 - 1\otimes[\sigma_i,\sigma_j]q_ip_j\right) + \ldots, \end{aligned} \tag{3.54}$$

where the momentum transfer is $\mathbf{q} = \mathbf{p} - \mathbf{p}'$. The coefficients are structured like

$$\mathcal{V}_X(\alpha) = \mathcal{V}_X^{(0)} + \frac{\alpha}{4\pi}\mathcal{V}_X^{(1)} + \left(\frac{\alpha}{4\pi}\right)^2 \mathcal{V}_X^{(2)} + \left(\frac{\alpha}{4\pi}\right)^3 \mathcal{V}_X^{(3)} + \mathcal{O}(\alpha^4) \tag{3.55}$$

and factored out such that $\mathcal{V}_X^{(0)}$ is either one or zero for all $\mathcal{V}_X$. For the rest of this thesis, we will use V_X to refer to the combination of the potential factor $\mathcal{V}_X$ and the corresponding overall constants in $V(\mathbf{p}, \mathbf{p}')$.

The leading term in (3.54) is given by the first term in the Coulomb potential ($\mathcal{V}_C^{(0)}$), scaling like $\sim v^{-1}$ in momentum space. This is the part considered non-perturbatively, while higher-order contributions to this potential ($\mathcal{V}_C^{(n)}$, $n = 1, 2, 3$) are suppressed by $\alpha^n \sim v^n$, respectively. For the NNNLO calculation, terms up to $n = 3$ are necessary. The $\frac{1}{m}$-potential scales like $\sim v^0$ for the $\mathcal{V}_{1/m}^{(0)}$-term, such that the contributions up to $\mathcal{V}_{1/m}^{(2)}$ are required at NNNLO. The potentials suppressed by $\frac{1}{m^2}$ all scale like $\sim v^1$ at leading order, first contributing at NNLO. Therefore, for these potentials, we need the coefficients $\mathcal{V}_X^{(0)}$ and $\mathcal{V}_X^{(1)}$.

Since we discuss only the S-wave case, it is enough to consider the spin-triplet projection of the potentials, for which the spin structures in equation (3.54) take the form [27]

$$[\sigma_i, \sigma_j] \otimes [\sigma_i, \sigma_j] \to (-4)(10 - 7d + d^2), \tag{3.56}$$

$$[\sigma_i, \sigma_j]q_j \otimes [\sigma_i, \sigma_k]q_k \to \frac{(10 - 7d + d^2)}{(1 - d)} 4\mathbf{q}^2, \tag{3.57}$$

$$([\sigma_i, \sigma_j]q_i p_j \otimes 1 - 1 \otimes [\sigma_i, \sigma_j]q_i p_j) \to 0. \tag{3.58}$$

The spin dependence arises first at order $\mathcal{O}\left(\frac{1}{m^2}\right)$ and allows us to cast the potentials $\mathcal{V}_s$, $\mathcal{V}_{hf}$, and $\mathcal{V}_{so}$ into the form of of $\mathcal{V}_\delta$. The spin-projected potential then takes the form

$$\begin{aligned} V(\mathbf{p}, \mathbf{p}') = &-\mathcal{V}_C(\alpha)\frac{4\pi C_F \alpha(\mu)}{\mathbf{q}^2} + \mathcal{V}_{1/m}(\alpha)\frac{\pi^2(4\pi)C_F\alpha(\mu)}{m|\mathbf{q}|} - \mathcal{V}_p(\alpha)\frac{2\pi C_F\alpha(\mu)(\mathbf{p}^2 + \mathbf{p}'^2)}{m^2\mathbf{q}^2} \\ &- \mathcal{V}_{1/m^2}(\alpha)\frac{4\pi C_F\alpha(\mu)}{m^2}, \end{aligned} \tag{3.59}$$

which is the expression we will use from now on. $\mathcal{V}_{1/m^2}$ is defined by

$$\mathcal{V}_{1/m^2}(\alpha) = -\frac{1}{2}\mathcal{V}_\delta - \frac{1}{4}(10 - 7d + d^2)\mathcal{V}_s - \frac{1}{4}\frac{(10 - 7d + d^2)}{(1 - d)}\mathcal{V}_{hf} - \frac{2\alpha(\mu)}{3\pi}\left(C_F - \frac{C_A}{2}\right)\frac{1}{\varepsilon} \tag{3.60}$$

in terms of the previous potentials.

The fixed-order expressions for these potentials have been determined in various references (see, for example, for the Coulomb potential: [68–71]; for the $\frac{1}{m}$-potential: [17, 72]; and for the $\frac{1}{m^2}$-potential: [73]). An overview (including the $\mathcal{O}(\varepsilon)$-terms necessary for some potential insertions) can be found in [27]. Note that in this reference, infrared (IR) divergences in the potentials have been removed by adding a subtraction term

$$\begin{aligned}\delta V_{sub} = \frac{\alpha(\mu)C_F}{6}\frac{1}{\varepsilon}\Bigg[C_A^3\frac{\alpha^3(\mu)}{\mathbf{q}^2} + 4(C_A^2+2C_AC_F)\frac{\pi\alpha^2(\mu)}{m|\mathbf{q}|} \\ + 16\left(C_F-\frac{C_A}{2}\right)\frac{\alpha(\mu)}{m^2} + 16C_A\frac{\alpha(\mu)}{m^2}\frac{\mathbf{p}^2+\mathbf{p}'^2}{2\mathbf{q}^2}\Bigg]\end{aligned} \tag{3.61}$$

to the potentials. This procedure moves the divergences to the calculation of the ultrasoft correction, where they cancel ultraviolet (UV) divergences in the ultrasoft contribution [61]. This has already been done explicitly for $\mathcal{V}_{1/m^2}$ in equation (3.60).

For ease of reference, we repeat the fixed-order expressions for the potentials in the following.

The Coulomb Potential

The d-dimensional Coulomb potential is given by [27]

$$\mathcal{V}_C^{(0)} = 1, \tag{3.62}$$

$$\mathcal{V}_C^{(1)} = \left[\left(\frac{\mu^2}{\mathbf{q}^2}\right)^{\varepsilon}-1\right]\frac{\beta_0}{\varepsilon} + \left(\frac{\mu^2}{\mathbf{q}^2}\right)^{\varepsilon}a_1(\varepsilon), \tag{3.63}$$

$$\mathcal{V}_C^{(2)} = a_2 + (2a_1\beta_0+\beta_1)\ln\left(\frac{\mu^2}{\mathbf{q}^2}\right) + \beta_0^2\ln^2\left(\frac{\mu^2}{\mathbf{q}^2}\right), \tag{3.64}$$

$$\begin{aligned}\mathcal{V}_C^{(3)} = a_3 + \left(2a_1\beta_1+\beta_2+3a_2\beta_0+8\pi^2C_A^3\right)\ln\left(\frac{\mu^2}{\mathbf{q}^2}\right) \\ + \left(\frac{5}{2}\beta_0\beta_1+3a_1\beta_0^2\right)\ln^2\left(\frac{\mu^2}{\mathbf{q}^2}\right) + \beta_0^3\ln^3\left(\frac{\mu^2}{\mathbf{q}^2}\right).\end{aligned} \tag{3.65}$$

For the rest of this thesis, we will use the superscript "FO" to distinguish fixed-order expressions from resummed ones when necessary. The coefficients a_i^{FO} are collected in [27].

The $\frac{1}{m}$-Potential

The d-dimensional $\frac{1}{m}$-potential reads [27]

$$\mathcal{V}^{(0)}_{1/m} = 0, \tag{3.66}$$

$$\mathcal{V}^{(1)}_{1/m} = \left(\frac{\mu^2}{\mathbf{q}^2}\right)^{\varepsilon} b_1(\varepsilon), \tag{3.67}$$

$$\begin{aligned}\mathcal{V}^{(2)}_{1/m} = &\left[\left(\frac{\mu^2}{\mathbf{q}^2}\right)^{2\varepsilon} - 1\right]\left(-\frac{8}{3\varepsilon}\right)\left(2C_F C_A + C_A^2\right) \\ &+ \left[\left(\frac{\mu^2}{\mathbf{q}^2}\right)^{2\varepsilon} - \left(\frac{\mu^2}{\mathbf{q}^2}\right)^{\varepsilon}\right]\frac{2\beta_0}{\varepsilon} b_1(\varepsilon) + \left(\frac{\mu^2}{\mathbf{q}^2}\right)^{2\varepsilon} 4b_2(\varepsilon),\end{aligned} \tag{3.68}$$

where the fixed-order coefficient functions $b_1^{\mathrm{FO}}(\varepsilon)$ and $b_2^{\mathrm{FO}}(\varepsilon)$ can again be found in reference [27]. For the calculations in this thesis, $b_1^{\mathrm{FO}}(\varepsilon = 0)$ is of particular importance and reads

$$b_1^{\mathrm{FO}}(\varepsilon = 0) = \frac{C_F}{2} - C_A. \tag{3.69}$$

The $\frac{1}{m^2}$-Potentials

The potentials contributing at order $\mathcal{O}\left(\frac{1}{m^2}\right)$ ($\mathcal{V}_{1/m^2}$, $\mathcal{V}_p$, $\mathcal{V}_s$, $\mathcal{V}_{hf}$, and $\mathcal{V}_{so}$) can be split into a hard and a soft contribution, $\mathcal{V}_X(\alpha) = \mathcal{V}_X^{(hard)}(\alpha) + \mathcal{V}_X^{(soft)}(\alpha)$, as is presented in [27]. In this reference, the spin-projected potentials are then determined with the explicit fixed-order expressions for the NRQCD matching coefficients. However, in this thesis, we eventually want to use the resummed expressions for these coefficients instead (see section 5.2.2). Therefore, we perform the spin projection again, keeping the NRQCD coefficients general in $\mathcal{V}_{1/m^2}$. The

potentials (after removing the $\frac{1}{\varepsilon}$-poles with the subtraction term δV_{sub}) read

$$\begin{aligned}
\mathcal{V}_{1/m^2}(\alpha) = &-\frac{1}{4}(1+d_2-16d_5)+\frac{1}{2}\frac{(1+\varepsilon-2\varepsilon^2)}{(-3+2\varepsilon)}d_1^2 \\
&-\frac{1}{4\pi C_F\alpha(\mu)}(d_{ss}+C_F d_{vs})+\frac{1}{4\pi C_F\alpha(\mu)}(1+\varepsilon-2\varepsilon^2)(d_{sv}+C_F d_{vv}) \\
&-\frac{2\alpha(\mu)}{3\pi}\left(C_F-\frac{C_A}{2}\right)\frac{1}{\varepsilon}+\frac{\alpha(\mu)}{4\pi}\frac{1}{2}\frac{(d_2+1)}{2}\frac{\beta_0}{\varepsilon}-\frac{\alpha(\mu)}{4\pi}\frac{1}{2}\frac{(1+\varepsilon-2\varepsilon^2)}{(-3+2\varepsilon)}d_1^2\frac{\beta_0}{\varepsilon} \\
&+\frac{\alpha(\mu)}{4\pi}\left(\frac{\mu^2}{\mathbf{q}^2}\right)^{\varepsilon}\frac{\varepsilon\Gamma(-\varepsilon)^2\Gamma(\varepsilon)e^{\gamma_E\varepsilon}}{\Gamma(-2\varepsilon)}\times \\
&\Bigg\{-\frac{1}{2}\frac{1}{12(4\varepsilon^2-8\varepsilon+3)}\Big[C_A(48\varepsilon^3-230\varepsilon^2+328\varepsilon-138-3d_1^2(4\varepsilon^2-9\varepsilon+5)) \\
&\quad -4C_F(\varepsilon-1)(16\varepsilon^2-38\varepsilon+21)-12n_fT_F(\varepsilon-1)(1+d_2)\Big] \\
&\quad +\frac{1}{2}(1+\varepsilon-2\varepsilon^2)\frac{d_1^2C_A}{(8\varepsilon-4)}+\frac{1}{2}\frac{(1+\varepsilon-2\varepsilon^2)}{(-3+2\varepsilon)}\frac{(-d_1^2)(\varepsilon-1)(C_A(4\varepsilon-5)+4n_fT_F)}{(8\varepsilon^2-16\varepsilon+6)}\Bigg\}
\end{aligned} \tag{3.70}$$

and

$$\begin{aligned}
\mathcal{V}_p(\alpha) = 1+\frac{\alpha(\mu)}{4\pi}\Bigg[&\left(\frac{\mu^2}{\mathbf{q}^2}\right)^{\varepsilon}\frac{-\varepsilon\Gamma(-\varepsilon)^2\Gamma(\varepsilon)e^{\gamma_E\varepsilon}\left(C_A(56\varepsilon^2-121\varepsilon+57)+12n_fT_F(\varepsilon-1)\right)}{6(4\varepsilon^2-8\varepsilon+3)\Gamma(-2\varepsilon)} \\
&-\frac{\beta_0}{\varepsilon}-\frac{8C_A}{3}\frac{1}{\varepsilon}\Bigg].
\end{aligned} \tag{3.71}$$

With the fixed-order NRQCD coefficients given in section 3.2.2, these potentials take the form

$$\mathcal{V}^{(0),\mathrm{FO}}_{1/m^2} \equiv v_0^{\mathrm{FO}}(\varepsilon) = -\frac{4-\varepsilon-2\varepsilon^2}{6-4\varepsilon}, \tag{3.72}$$

$$\begin{aligned}
\mathcal{V}^{(1),\mathrm{FO}}_{1/m^2} = &\left[\left(\frac{\mu^2}{\mathbf{q}^2}\right)^{\varepsilon}-1\right]\frac{1}{\varepsilon}\left(\frac{7}{3}C_F-\frac{11}{6}C_A+\beta_0 v_0^{\mathrm{FO}}(\varepsilon)\right)+\left(\frac{\mu^2}{\mathbf{q}^2}\right)^{\varepsilon}v_q^{(1),\mathrm{FO}}(\varepsilon) \\
&+\left[\left(\frac{\mu^2}{m^2}\right)^{\varepsilon}-1\right]\frac{1}{\varepsilon}\left(\frac{1}{3}C_F+\frac{1}{2}C_A\right)+\left(\frac{\mu^2}{m^2}\right)^{\varepsilon}v_m^{(1),\mathrm{FO}}(\varepsilon),
\end{aligned} \tag{3.73}$$

and

$$\mathcal{V}_p^{(0),\mathrm{FO}}(\mu) \equiv p_0^{\mathrm{FO}} = 1, \tag{3.74}$$

$$\mathcal{V}_p^{(1),\mathrm{FO}}(\mu) = \left[\left(\frac{\mu^2}{\mathbf{q}^2}\right)^{\varepsilon}-1\right]\left(\frac{8}{3}C_A+\beta_0\right)+\left(\frac{\mu^2}{\mathbf{q}^2}\right)^{\varepsilon}v_p^{(1),\mathrm{FO}}(\varepsilon), \tag{3.75}$$

as it is given in [27]. We have explicitly introduced the label p_0^{FO} for the coefficient $\mathcal{V}_p^{(0),\mathrm{FO}}(\mu) = 1$, which will allow for a consistent notation later on in the discussion of the ultrasoft running. The explicit expressions for the fixed-order coefficients $v_p^{(1),\mathrm{FO}}$, $v_q^{(1),\mathrm{FO}}$, and $v_m^{(1),\mathrm{FO}}$ are not needed here but can be found in reference [27].

The Kinetic Energy Correction

Apart from the potentials V, the PNRQCD Lagrangian (3.37) also includes the quartic correction to the kinetic energy, namely

$$\mathcal{L}_{\mathrm{PNRQCD}} \supset \psi^\dagger \frac{\boldsymbol{\partial}^4}{8m^3}\psi - \chi^\dagger \frac{\boldsymbol{\partial}^4}{8m^3}\chi. \tag{3.76}$$

It is advantageous to bring this correction into the form of a potential and treat it analogously to the ones discussed before. This is achieved by defining [27]

$$V_{kin} = -2\frac{\mathbf{p}^4}{8m^3}(2\pi)^{d-1}\delta^{(d-1)}(\mathbf{q}). \tag{3.77}$$

As mentioned before, the kinetic energy correction in the Lagrangian scales like v^7, contributing first at NNLO.

Chapter 4

Top Anti-Top Pair Production in the Non-Relativistic Limit

4.1 The Top Anti-Top Pair Production Cross Section in QCD

As discussed in the introduction, this work will focus on the inclusive cross section $\sigma_{t\bar{t}X}$ of the production of a top anti-top pair in electron-positron annihilation, $e^+e^- \to t\bar{t}X$. We normalize it with respect to the high-energy limit of the cross section of $\mu^+\mu^-$ production, which is given by $\sigma_0 = \frac{4\pi\alpha_{em}}{3s}$, where $s = q^2$ is the center-of-mass energy squared and $\alpha_{em} = \frac{e^2}{4\pi}$ is the coupling constant of QED. This defines the so-called R-ratio, $R = \frac{\sigma_{t\bar{t}X}}{\sigma_0}$. Using the optical theorem, this quantity can be expressed in terms of the imaginary part of two-point functions of the electromagnetic heavy-quark current (cf. for example [27])

$$R = 12\pi \,\mathrm{Im}\left\{ e_t^2 \Pi^{(v)}(q^2) - \frac{2q^2}{q^2 - M_Z^2} v_e v_t e_t \Pi^{(v)}(q^2) + \left(\frac{q^2}{q^2 - M_Z^2}\right)^2 (v_e^2 + a_e^2)\left(v_t^2 \Pi^{(v)}(q^2) + a_t^2 \Pi^{(a)}(q^2)\right)\right\}. \tag{4.1}$$

The constant $e_t = \frac{2}{3}$ denotes the charge of the top quark in units of the charge of the positron, and v_f (a_f) is the coupling of a Z boson to the vector current (axial-vector current) for a fermion f, respectively. In this thesis, we will not take into account the P-wave contribution from the axial-vector coupling to the Z-boson, which is small (below 1% [74]). The vector coupling to the Z-boson causes terms of the same structure as the coupling to the photon in the first term. Therefore, including these terms only changes the overall prefactor of $\Pi^{(v)}(q^2)$.

To simplify the following equations, we will only consider the coupling e_t^2 to the photon for the analytic calculations presented in this thesis. However, for the numerical analysis in chapter 6, we will also include the vector coupling to the Z-boson.

The heavy-quark correlation functions are defined by

$$\begin{aligned}\Pi_{\mu\nu}^{(v)}(q^2) &\equiv i \int \mathrm{d}^4x\, e^{iq\cdot x} \langle 0|T\left\{j_\mu^{(v)}(x) j_\nu^{(v)}(0)\right\}|0\rangle = \\ &\equiv (q_\mu q_\nu - q^2 g_{\mu\nu})\Pi^{(v)}(q^2) + q_\mu q_\nu \Pi_L^{(v)}(q^2) \end{aligned} \tag{4.2}$$

for the vector current $j_\mu^{(v)} = \bar{t}\gamma_\mu t$. Analogously, this is defined for the axial vector current $j_\mu^{(a)} = \bar{t}\gamma_\mu\gamma_5 t$ with $(v) \to (a)$, which is, however, not relevant to this thesis.

In the following sections, we will translate this setting to the context of the non-relativistic theories. This corresponds to the production of a top anti-top pair close to the threshold $s = 4m^2$.

4.2 The Non-Relativistic Current

We start by expanding the electromagnetic vector current in terms of the non-relativistic fields. Up to order $\mathcal{O}\left(\frac{1}{m^2}\right)$, the vector current $j^{(v)\mu} = \bar{t}\gamma^\mu t$ takes the form

$$j^{(v)k} = c_v \psi^\dagger \sigma^k \chi + \frac{d_v}{6m^2} \psi^\dagger \sigma^k \mathbf{D}^2 \chi + \ldots, \tag{4.3}$$

where c_v and d_v are the hard matching coefficients of the vector current. For this thesis, the matching coefficient c_v is of particular importance. Expanded in powers of α,

$$\begin{aligned} c_v &= 1 + \frac{\alpha}{4\pi} c_v^{(1)} + \left(\frac{\alpha}{4\pi}\right)^2 c_v^{(2)} + \left(\frac{\alpha}{4\pi}\right)^3 c_v^{(3)} + \mathcal{O}(\alpha^4) = \\ &\equiv 1 + c_{v,1} + c_{v,2} + c_{v,3} + \mathcal{O}(\alpha^4), \end{aligned} \tag{4.4}$$

it reads at fixed-order:[1] [27, 75, 76]

$$c_v^{(1),\mathrm{FO}}(\mu) = -8C_F, \tag{4.5}$$

$$c_v^{(2),\mathrm{FO}}(\mu) = \beta_0 c_v^{(1),\mathrm{FO}}(m) \ln\left(\frac{\mu^2}{m^2}\right) + C_F\pi^2\left(-4C_A - \frac{8}{3}C_F\right)\ln\left(\frac{\mu^2}{m^2}\right) + c_v^{(2),\mathrm{FO}}(m), \tag{4.6}$$

$$\begin{aligned} c_v^{(3),\mathrm{FO}}(\mu) = {} & \left(\beta_0^2 \ln^2\left(\frac{\mu^2}{m^2}\right) + \beta_1 \ln\left(\frac{\mu^2}{m^2}\right)\right) c_v^{(1),\mathrm{FO}}(m) \\ & + \beta_0 \ln^2\left(\frac{\mu^2}{m^2}\right) C_F\pi^2\left(-4C_A - \frac{8}{3}C_F\right) + 2\beta_0 \ln\left(\frac{\mu^2}{m^2}\right) c_v^{(2),\mathrm{FO}}(m) \\ & + \ln^2\left(\frac{\mu^2}{m^2}\right) C_F\pi^2\left(-4C_A^2 - 15C_AC_F - 10C_F^2\right) \\ & + \ln\left(\frac{\mu^2}{m^2}\right) C_F\pi^2\Bigg[(-36 + 96\ln(2))C_F^2 + \left(-\frac{944}{27} - 48\ln(2)\right)C_FC_A \\ & \qquad + \left(-\frac{128}{9} - 48\ln(2)\right)C_A^2 + \frac{400}{27}C_FT_Fn_f + \frac{148}{9}C_AT_Fn_f - \frac{16}{5}C_FT_F\Bigg] \\ & + c_v^{(3),\mathrm{FO}}(m). \end{aligned} \tag{4.7}$$

This expanded expression for the current will be used to determine the heavy-quark correlation function $\Pi^{(v)}(q^2)$ in the non-relativistic setting. This will consequently lead to an expression for the R-ratio, which is the quantity we are eventually interested in.

4.3 The Heavy-Quark Correlation Function in NRQCD and PNRQCD

For the pair production close to threshold, we consider the frame where $q^\mu = (2m + E, \mathbf{0})$, such that the small parameter E encodes the residual energy of the quark pair as we discussed in the setup of the EFTs in section 3.1. In this reference frame, the transverse part of the heavy-quark correlation function (4.2) can be expressed as

$$\Pi^{(v)}(q^2) = \frac{1}{q^2(d-1)}\Pi_{ii}^{(v)}. \tag{4.8}$$

[1] The third-order coefficient has been slightly restructured in the double logarithmic terms compared to reference [27], reexpressing T_Fn_f-terms as β_0.

Inserting the expansion of the vector current from equation (4.3), we finally obtain

$$\Pi^{(v)}(q^2) = \frac{N}{2m^2}\left(c_v^2 - \frac{E}{m}c_v\left(c_v + \frac{d_v}{3}\right)\right)G(E) + \ldots, \tag{4.9}$$

where we have defined an essential quantity in the context of non-relativistic heavy-quark pair production, the two-point function of the non-relativistic currents (also called the non-relativistic correlation function):

$$G(E) = \frac{i}{2N(d-1)}\tilde{\mu}^{-2\varepsilon}\int \mathrm{d}^d x\, e^{iEx^0}\langle 0|T\left\{[\chi^\dagger\sigma^i\psi](x)[\psi^\dagger\sigma^i\chi](0)\right\}|0\rangle\big|_{\mathrm{NRQCD}}. \tag{4.10}$$

This Green's function has already been partially introduced in equation (3.43) in the context of the resummation of ladder diagrams in PNRQCD.

The dots in equation (4.9) denote terms beyond NNNLO as well as some terms not relevant to the R-ratio [27]. The terms proportional to the energy E (recall for the counting that the energy scales like $E \sim v^2$) arise in two ways: The c_v^2-term is multiplied by a factor of E coming from the expansion of the prefactor $\frac{1}{q^2}$, while the $c_v d_v$-term arises from applying an equation of motion (EOM) to the $\mathbf{D}^2$-structure in $j^{(v)}$.

From equation (4.1), this allows us to give an expression for the R-ratio in NRQCD (focusing on the coupling to the photon):

$$R = \frac{6\pi N e_t^2}{m^2}\left(c_v^2 - \frac{E}{m}c_v\left(c_v + \frac{d_v}{3}\right)\right)\mathrm{Im}\{G(E)\} + \ldots, \tag{4.11}$$

where the dots denote the same structure of terms as in equation (4.9).

Proceeding from NRQCD to PNRQCD, no major adjustments are necessary. As is discussed in detail in [27], the non-relativistic vector current (4.3) requires no further matching from NRQCD to PNRQCD at the order we are considering. Therefore, completely analogous to (4.10), the non-relativistic correlation function is given by

$$G(E) = \frac{i}{2N(d-1)}\tilde{\mu}^{-2\varepsilon}\int \mathrm{d}^d x\, e^{iEx^0}\langle 0|T\left\{[\chi^\dagger\sigma^i\psi](x)[\psi^\dagger\sigma^i\chi](0)\right\}|0\rangle\big|_{\mathrm{PNRQCD}} \tag{4.12}$$

in the framework of PNRQCD. The matrix element is now evaluated in perturbation theory in PNRQCD. This is the expression we will use for the remainder of this thesis.

In perturbation theory, the correlation function is expanded in the form

$$G(E) = G_0(E) + \delta_1 G(E) + \delta_2 G(E) + \delta_3 G(E) + \ldots, \tag{4.13}$$

where $G_0(E) \equiv G_0(\mathbf{r} = 0, \mathbf{r}' = 0; E)$ as it is given in (3.51). The corrections $\delta_i G(E)$ are composed of this leading-order Green's function $G_0(E)$ and insertions of the potentials, as well as the ultrasoft correction first contributing at third order. Using operator notation, we write

$$G_0(E) = \langle \mathbf{0}|\hat{G}_0(E)|\mathbf{0}\rangle, \tag{4.14}$$

$$\delta_1 G(E) = \langle \mathbf{0}|\hat{G}_0(E) i\delta V_1 i\hat{G}_0(E)|\mathbf{0}\rangle, \tag{4.15}$$

$$\delta_2 G(E) = \langle \mathbf{0}|\hat{G}_0(E) i\delta V_2 i\hat{G}_0(E)|\mathbf{0}\rangle + \langle \mathbf{0}|\hat{G}_0(E) i\delta V_1 i\hat{G}_0(E) i\delta V_1 i\hat{G}_0(E)|\mathbf{0}\rangle, \tag{4.16}$$

$$\begin{aligned}\delta_3 G(E) = {} & \langle \mathbf{0}|\hat{G}_0(E) i\delta V_3 i\hat{G}_0(E)|\mathbf{0}\rangle + 2\langle \mathbf{0}|\hat{G}_0(E) i\delta V_1 i\hat{G}_0(E) i\delta V_2 i\hat{G}_0(E)|\mathbf{0}\rangle \\ & + \langle \mathbf{0}|\hat{G}_0(E) i\delta V_1 i\hat{G}_0(E) i\delta V_1 i\hat{G}_0(E) i\delta V_1 i\hat{G}_0(E)|\mathbf{0}\rangle + \delta_3^{us} G(E).\end{aligned} \tag{4.17}$$

Each δV_n stands for one of the perturbation potentials in equation (3.38) after the colour-singlet projection has been performed, suppressed by v^n with respect to the leading-order Coulomb potential.

In momentum space, the Green's function is given by

$$\begin{aligned}G(E) = {} & (\tilde{\mu}^{2\varepsilon})^2 \int \frac{\mathrm{d}^{d-1}\mathbf{p}_1}{(2\pi)^{d-1}} \frac{\mathrm{d}^{d-1}\mathbf{p}_2}{(2\pi)^{d-1}} G_0(\mathbf{p}_1, \mathbf{p}_2; E) \\ & + (\tilde{\mu}^{2\varepsilon})^4 \int \prod_{i=1}^{4} \left[\frac{\mathrm{d}^{d-1}\mathbf{p}_i}{(2\pi)^{d-1}}\right] G_0(\mathbf{p}_1, \mathbf{p}_2; E) i\delta V_i(\mathbf{p}_2, \mathbf{p}_3) i G_0(\mathbf{p}_3, \mathbf{p}_4; E) + \ldots,\end{aligned} \tag{4.18}$$

where the dots denote insertions of more than one potential. This is the form that is used in [77] to determine the NNNLO calculation of the top anti-top pair production near threshold.

Apart from the R-ratio, another important quantity related to the Green's function is the wave function at the origin $|\psi_n(0)|^2$ (some exemplary references discussing this quantity in the framework of PNRQCD at fixed order are [61, 78, 79]). It is defined by the poles

$$\lim_{E \to E_n} G_0(E) = \frac{|\psi_n(0)|^2}{E_n - E - i\varepsilon} + \text{regular}. \tag{4.19}$$

While we will not discuss this further in this thesis, we note that the calculations performed below for the R-ratio can analogously be done for the wave function at the origin.

4.4 The R-Ratio up to NNNLO in PNRQCD

Finally, we end this chapter by explicitly discussing the R-ratio in PNRQCD. Putting together equation (4.11) with the expansions of c_v and $G(E)$ (cf. equations (4.4) and (4.13), respectively),

we obtain order by order:

$$R_{\mathrm{LO}} = \frac{6\pi N e_t^2}{m^2} \operatorname{Im}\{G_0(E)\}, \tag{4.20}$$

$$R_{\mathrm{NLO}} = \frac{6\pi N e_t^2}{m^2} \left[\operatorname{Im}\left\{\delta_1 G(E)\right\} + 2c_{v,1} \operatorname{Im}\left\{G_0(E)\right\}\right], \tag{4.21}$$

$$\begin{aligned} R_{\mathrm{NNLO}} = \frac{6\pi N e_t^2}{m^2} \Bigg[& \operatorname{Im}\left\{\delta_2 G(E)\right\} + 2c_{v,1} \operatorname{Im}\left\{\delta_1 G(E)\right\} + \left(2c_{v,2} + c_{v,1}^2\right) \operatorname{Im}\left\{G_0(E)\right\} \\ & - \frac{1}{m}\frac{4}{3} \operatorname{Im}\left\{E G_0(E)\right\} \Bigg], \end{aligned} \tag{4.22}$$

$$\begin{aligned} R_{\mathrm{NNNLO}} = \frac{6\pi N e_t^2}{m^2} \Bigg[& \operatorname{Im}\left\{\delta_3 G(E)\right\} + 2c_{v,1} \operatorname{Im}\left\{\delta_2 G(E)\right\} + \left(2c_{v,2} + c_{v,1}^2\right) \operatorname{Im}\left\{\delta_1 G(E)\right\} \\ & - \frac{1}{m}\frac{4}{3} \operatorname{Im}\left\{E\delta_1 G(E)\right\} + \left(2c_{v,3} + 2c_{v,2}c_{v,1}\right) \operatorname{Im}\left\{G_0(E)\right\} \\ & - \frac{1}{m}\left(c_{v,1} + \frac{1}{3}d_{v,1}\right) \operatorname{Im}\left\{E G_0(E)\right\} \Bigg]. \end{aligned} \tag{4.23}$$

In the next chapter, we proceed with the main calculation of this thesis, which is the renormalization group improvement of this R-ratio.

Chapter 5

Renormalization Group Improvement of NRQCD and PNRQCD

5.1 Renormalization Group Setup

After discussing the setup of the effective field theories used for top anti-top pair production near threshold at fixed order, we now turn to its improvement obtained through the resummation of large logarithms.

As we have discussed in detail when setting up the non-relativistic theories in section 3.1, we consider the three widely separated scales μ_h (mass of the heavy quark), μ_s (three-momentum of the heavy quark), and μ_{us} (energy of the heavy quark). Together with the renormalization scale μ, these scales appear as ratios in logarithms in the fixed-order calculation, scaling like $\ln\left(\frac{\mu^2}{\mu_h^2}\right)$, $\ln\left(\frac{\mu^2}{\mu_s^2}\right)$, and $\ln\left(\frac{\mu^2}{\mu_{us}^2}\right)$, respectively. Depending on the value of μ, these logarithms can become large and require resummation. Specifically, this is the case when

$$\alpha \times \ln\left(\frac{\mu^2}{\mu_0^2}\right) \sim \mathcal{O}(1), \tag{5.1}$$

which causes perturbation theory to break down.

There is a freedom of choice for the common scale μ, which is depicted schematically in figure 5.1. In this work, we choose to work at the soft scale $\mu = \mu_s$, which is the natural scale of the potentials. With this choice, the logarithms $\ln\left(\frac{\mu^2}{\mathbf{q}^2}\right) \sim \ln\left(\frac{\mu^2}{\mu_s^2}\right)$ in the potentials $\mathcal{V}_X$ are small and do not require resummation. However, the logarithms of the form $\ln\left(\frac{\mu^2}{\mu_h^2}\right)$ and

$\ln\left(\frac{\mu^2}{\mu_{us}^2}\right)$ are large. They are resummed by evolving the corresponding contribution from its respective natural scale μ_h and μ_{us} to the common scale $\mu = \mu_s$ via RGEs. Note that while we will still denote the common scale by μ, it is from now on understood to denote the chosen scale $\mu = \mu_s$ instead of an arbitrary regularization scale as in [27].

One could also choose another common scale μ different from μ_s. In that case, also the potentials would need to be evolved to this scale μ. This complication is avoided by choosing the common scale as the natural scale of the potentials, μ_s. In the full result, the scale dependence on $\mu = \mu_s$ has to cancel between the different contributions.

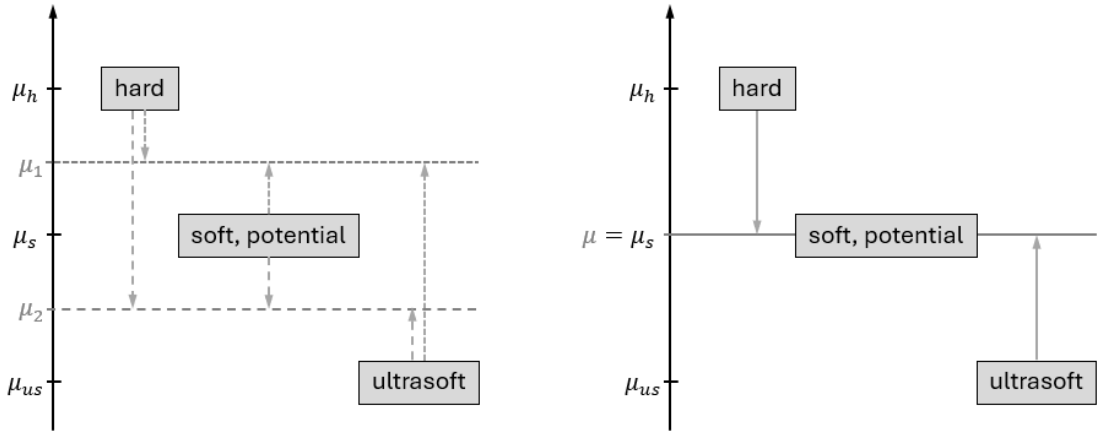

Figure 5.1: Choice of the common scale μ all contributions are evolved to. While the left-hand side shows two possible generic choices for μ, the diagram on the right-hand side illustrates the choice we make: $\mu = \mu_s$, the natural scale of the potentials.

In the following, we will refer to the resummation of large logarithms related to divergences from ultrasoft loops as the "ultrasoft running" and analogously for the "hard" and "potential running" related to divergent hard and potential loops, respectively. In the next sections, we will proceed in the following way:

Large logarithms $\ln\left(\frac{\mu^2}{\mu_h^2}\right)$ related to divergent hard loops are contained in the hard NRQCD matching coefficients d_i and d_{ij}, which were introduced at fixed order in section 3.2.2. In section 5.2, this contribution is evolved down from its natural initial condition μ_h to the common scale μ. We assume the hard scale to be $\mu_h \sim m$; however, we do not set them exactly equal. We will write the effect of this resummation as a correction to the fixed-order potential. More precisely, we absorb it into $\mathcal{V}_{1/m^2}$ (cf. equation (3.70)), which is the only potential that depends on the NRQCD matching coefficients.

The ultrasoft running is discussed in section 5.3. We will evolve the respective contribution from its natural initial condition μ_{us} up to the common scale μ and again write it as a correction to the fixed-order potentials. This contribution resums logarithms like $\ln\left(\frac{\mu^2}{\mu_{us}^2}\right)$.

As a last step, we will use the RG improved potentials to determine the potential running of the hard matching coefficient c_v of the non-relativistic current, which was defined in equation (4.3). This is discussed in section 5.4.

5.2 Hard Running of the NRQCD Matching Coefficients

After discussing the NRQCD matching coefficients at fixed order in section 3.2.2, we now turn to the RG improvement of these quantities.

As we have noted before, the fixed-order matching coefficients d_i $(i = 1, \ldots, 6)$ and d_{ij} $(ij = ss, sv, vs, vv)$ contain logarithms $\ln\left(\frac{\mu^2}{m^2}\right)$. These logarithms are small at their natural scale, the hard scale $\mu_h \sim m$. However, at the common scale $\mu = \mu_s$, these logarithms become large and must be resummed. Specifically, one splits

$$\ln\left(\frac{\mu^2}{m^2}\right) = \underbrace{\ln\left(\frac{\mu_h^2}{m^2}\right)}_{\text{small}} + \underbrace{\ln\left(\frac{\mu^2}{\mu_h^2}\right)}_{\text{large, resum}} . \tag{5.2}$$

The first term can be considered in perturbation theory. Most references (for example [33, 34, 53]) choose $\mu_h = m$, such that these logarithms appearing at the matching conditions can directly be set to zero. However, since other choices are also possible, we choose to keep μ_h not necessarily equal to m (physically, it has to be similar, $\mu_h \sim m$). Literature results can be recovered by setting $\mu_h = m$. The second term, which represents the large logarithms, is resummed using the RGEs for the matching coefficients.

5.2.1 RGEs for the NRQCD Matching Coefficients and their Solution

The RGEs are discussed in various references, where the results used in this thesis are mainly taken from [33, 53]. We have used these equations and converted them to the conventions and notations used in [27]. Solving them, our results agree with the expressions for the resummed matching coefficients from the literature.

RGEs for the Bilinear Coefficients

The RGEs for the bilinear NRQCD matching coefficients can be found in [53]. As we have mentioned before in equation (3.15) (and in detail in appendix B.1), the RGE given for c_D in

that reference is actually the RGE for the combination $(d_2 - 16d_5)$ in our notation due to the different choice of operator basis in the Lagrangian. The equations are

$$\mu\frac{\mathrm{d}}{\mathrm{d}\mu}d_1 = \frac{\alpha}{4\pi}2C_A d_1, \tag{5.3}$$

$$\mu\frac{\mathrm{d}}{\mathrm{d}\mu}(d_2 - 16d_5) = \frac{\alpha}{4\pi}\left[\frac{13}{3}C_A(d_2 - 16d_5) - \left(\frac{20}{3}C_A + \frac{32}{3}C_F\right) - \frac{1}{3}C_A d_1^2\right], \tag{5.4}$$

where the μ-dependence of α and the coefficients d_i is implicitly understood. The equations are solved by

$$d_1(\mu) = d_1(\mu_h) - \left[1 - z^{-C_A}\right], \tag{5.5}$$

$$(d_2 - 16d_5)(\mu) = (d_2 - 16d_5)(\mu_h) + \left(\frac{20}{13} + \frac{32}{13}\frac{C_F}{C_A}\right)\left[1 - z^{-\frac{13}{6}C_A}\right] - \left[1 - z^{-2C_A}\right], \tag{5.6}$$

where we have defined $z \equiv \left(\frac{\alpha(\mu)}{\alpha(\mu_h)}\right)^{\frac{1}{\beta_0}}$. These expressions resum the LL series $\sum_n \alpha^n \log^n$ for the bilinear matching coefficients. Note that we use "LL" here only in the context of considering the matching coefficients isolated from the rest of the calculation. The overall counting will be different when we integrate them into other quantities later.

The matching conditions at the scale $\mu = \mu_h$ can be read off from equations (3.19), (3.21) and (3.22) above. At the level of the LL resummation, we only need the leading term, which is given by

$$d_1(\mu_h) = 1 + \mathcal{O}(\alpha(\mu_h)), \tag{5.7}$$

$$(d_2 - 16d_5)(\mu_h) = 1 + \mathcal{O}(\alpha(\mu_h)). \tag{5.8}$$

While the $\mathcal{O}(\alpha(\mu_h))$-terms still contain logarithms, they only include $\ln\left(\frac{\mu_h^2}{m^2}\right)$, which is small (unlike $\ln\left(\frac{\mu^2}{m^2}\right)$, which appears when the fixed-order expressions are evaluated at the scale $\mu = \mu_s$). Therefore, these terms really are suppressed and can be neglected here. In section 5.2.2, we will comment on the effect that using higher-order terms in $d_i(\mu_h)$ would have, specifically how they would only contribute at higher order in the resummation of logarithms.

RGEs for the Four-Fermion Coefficients

The RGEs for the four-fermion coefficients d_{ij} $(ij = ss, sv, vs, vv)$ can be taken from [33]. However, we are using a different operator basis compared to this reference since we have eliminated the heavy-light operator $\psi^\dagger T^A \psi \bar{q}\gamma^0 T^A q$ multiplied by the coefficient c_1^{hl}. This

changes the RGE for d_{vs} when written in our conventions.[1] The RGEs in our choice of operator basis are

$$\mu\frac{\mathrm{d}}{\mathrm{d}\mu}d_{ss} = -2C_F\left(C_F - \frac{C_A}{2}\right)\alpha^2, \tag{5.9}$$

$$\mu\frac{\mathrm{d}}{\mathrm{d}\mu}d_{sv} = 0, \tag{5.10}$$

$$\mu\frac{\mathrm{d}}{\mathrm{d}\mu}d_{vs} = \left(4C_F - \frac{5}{2}C_A\right)\alpha^2 - \frac{3}{4}C_A\alpha^2 d_1^2 + \frac{3}{4}C_A\alpha^2(d_2 - 16d_5), \tag{5.11}$$

$$\mu\frac{\mathrm{d}}{\mathrm{d}\mu}d_{vv} = -\frac{C_A}{2}\alpha^2 d_1^2. \tag{5.12}$$

They are solved by

$$d_{ss}(\mu) = d_{ss}(\mu_h) + 4C_F\left(-C_F + \frac{C_A}{2}\right)\frac{\pi}{\beta_0}\alpha(\mu_h)\left[1 - z^{\beta_0}\right], \tag{5.13}$$

$$d_{sv}(\mu) = d_{sv}(\mu_h), \tag{5.14}$$

$$\begin{aligned} d_{vs}(\mu) = d_{vs}(\mu_h) &+ \left(-\frac{35}{13}C_A + \frac{152}{13}C_F\right)\frac{\pi}{\beta_0}\alpha(\mu_h)\left[1 - z^{\beta_0}\right] \\ &- \left(\frac{30}{13}C_A + \frac{48}{13}C_F\right)\frac{\pi}{\beta_0 - \frac{13}{6}C_A}\alpha(\mu_h)\left[1 - z^{\beta_0 - \frac{13}{6}C_A}\right], \end{aligned} \tag{5.15}$$

$$d_{vv}(\mu) = d_{vv}(\mu_h) + C_A\frac{\pi}{2C_A - \beta_0}\alpha(\mu_h)\left[1 - z^{\beta_0 - 2C_A}\right]. \tag{5.16}$$

This resums terms like $\sum_n \alpha^{n+1}\log^n$. As we will show below, the four-fermion coefficients are multiplied by a factor of $\frac{1}{\alpha}$ in the potentials, which brings the resummation again to the level of $\sum_n \alpha^n \log^n$. At the matching scale $\mu = \mu_h$, the coefficients $d_{ij}(\mu_h)$ do not contain large logarithms and are of the order $\mathcal{O}\left(\alpha^2(\mu_h)\right)$ (cf. equations (3.25)-(3.32)), which is beyond the order we are considering for the resummation of large logarithms in these coefficients. Therefore, we set $d_{ij}(\mu_h) = 0$ for the purpose of this work. In the next section, we briefly comment on the effect of keeping the $\mathcal{O}\left(\alpha^2(\mu_h)\right)$-terms in the potential.

[1] When converting the RGE for d_{vs} to our conventions, we use equation (3.16), $d_{vs} = (d_{vs} - \pi\alpha c_1^{hl})_{\text{ref.[33]}}$, and the individual RGEs

$$\mu\frac{\mathrm{d}}{\mathrm{d}\mu}(d_{vs})_{\text{ref.[33]}} = 4(C_F - C_A)\alpha^2 + \frac{3}{2}\alpha^2(c_D)_{\text{ref.[33]}},$$

$$\mu\frac{\mathrm{d}}{\mathrm{d}\mu}\left(c_1^{hl}\right)_{\text{ref.[33]}} = \frac{\alpha}{4\pi}\left[3C_A(c_D)_{\text{ref.[33]}} - 6C_A + 3C_A d_1^2 + (-3C_A + 2\beta_0)(c_1^{hl})_{\text{ref.[33]}}\right].$$

The RGE for c_1^{hl} has been determined from reference [53]. Recalling equation (3.15), $(d_2 - 16d_5) = (c_D + c_1^{hl})_{\text{ref.[33]}}$, we obtain the RGE given above.

5.2.2 Incorporating the Resummed NRQCD Matching Coefficients into the Potentials

As we have discussed in section 3.3.2, the NRQCD matching coefficients are contained in the spin-projected potential $\mathcal{V}_{1/m^2}$, which is given in equation (3.70). Instead of using the fixed-order expressions for these coefficients (as it was done in [27]), we now incorporate the resummed results given above.

We want to keep track of the $\mathcal{O}(\varepsilon)$-terms in order to simplify a possible extension to higher log-orders. Also, when the fixed-order Wilson coefficients are incorporated into the potential in [27], the $\frac{1}{\varepsilon}$-pole is still explicit. On the other hand, when solving the RGE, we only considered the four-dimensional expressions, essentially losing this information contained in the fully d-dimensional results. We mitigate this by keeping the $\mathcal{O}\left(\frac{1}{\varepsilon}\right)$- and $\mathcal{O}(\varepsilon)$-terms from the fixed-order results. That is, we take the full fixed-order expression for the coefficients and only substitute the large logarithm with the RG improved expression that resums the whole tower of logarithms. In practice, this is achieved by setting

$$d_i \to d_i^{\mathrm{FO}} + \left[d_i^{\mathrm{RGI}} - \bar{d}_i^{\mathrm{FO}}\right] \equiv d_i^{\mathrm{FO}} + d_i^{\mathrm{RG}}. \tag{5.17}$$

We use superscripts to distinguish between renormalization group improved (RGI) coefficients and the corresponding fixed order (FO) expressions. While d_i^{FO} is the fully d-dimensional fixed-order expression including $\mathcal{O}\left(\frac{1}{\varepsilon}\right)$- and $\mathcal{O}(\varepsilon)$-terms, $\bar{d}_i^{\mathrm{FO}}$ denotes just the terms reproduced by reexpanding the resummed results (where the d-dimensional nature of the expression has been lost). We demonstrate this for d_1:

$$d_1^{\mathrm{FO}} = \frac{C_A\alpha(\mu)}{4\pi}\frac{1}{\varepsilon} + \left[1 + \frac{\alpha(\mu)}{2\pi}\left(C_A + C_F\right) + \frac{\alpha(\mu)}{4\pi}C_A \ln\left(\frac{\mu^2}{m^2}\right)\right] + d_1^{\varepsilon}(\varepsilon)$$
$$\text{as defined in (3.21)}, \tag{5.18}$$

$$d_1^{\mathrm{RGI}} = 1 - \left[1 - z^{-C_A}\right] \quad \text{as given in (5.5)}, \tag{5.19}$$

$$\bar{d}_1^{\mathrm{FO}} = 1 + \frac{\alpha(\mu)}{4\pi}C_A \ln\left(\frac{\mu^2}{\mu_h^2}\right). \tag{5.20}$$

The last line was obtained by reexpanding d_1^{RGI} in α, where we have used

$$z^x = \left(\frac{\alpha(\mu)}{\alpha(\mu_h)}\right)^{\frac{x}{\beta_0}} = 1 - \frac{\alpha(\mu)}{4\pi}x \ln\left(\frac{\mu^2}{\mu_h^2}\right) + \mathcal{O}(\alpha^2 \log), \tag{5.21}$$

where log stands for a large logarithm. This expression holds for one-loop running of the strong coupling α, which we discussed in section 2.2 (cf. equation (2.13)). The procedure

presented here for d_1 is used analogously for all NRQCD matching coefficients appearing in the $\mathcal{V}_{1/m^2}$-potential (3.70).

Before actually incorporating the resummed coefficients into the potential, we comment on the structure these coefficients obtain through the resummation procedure.

Comparing d_1^{FO} (5.18) and $\bar{d}_1^{\mathrm{FO}}$ (5.20), the obvious difference is the loss of d-dimensionality in $\bar{d}_1^{\mathrm{FO}}$, which is caused by solving the RGE only in four dimensions. Considering the rest of the fixed-order expression, reexpanding the RG improved result reproduces the terms counted like order $\mathcal{O}(1)$ in d_1^{FO}, that is

$$d_1^{\mathrm{FO}} \supset \bar{d}_1^{\mathrm{FO}} = 1 + \frac{\alpha(\mu)}{4\pi} C_A \ln\left(\frac{\mu^2}{\mu_h^2}\right). \tag{5.22}$$

Note that this only contains the large part of the logarithm $\ln\left(\frac{\mu^2}{m^2}\right)$, which we split into two parts in equation (5.2). What is, however, not reproduced are the terms actually suppressed in α, namely

$$d_1^{\mathrm{FO}} \supset \frac{\alpha(\mu)}{2\pi}\left(C_A + C_F\right) + \frac{\alpha(\mu)}{4\pi} C_A \ln\left(\frac{\mu_h^2}{m^2}\right), \tag{5.23}$$

which includes the small part of the logarithm.

We recall that d_1^{RGI} was given by

$$d_1^{\mathrm{RGI}} = d_1(\mu_h) - \left[1 - z^{-C_A}\right], \tag{5.24}$$

where we have set $d_1(\mu_h) = 1$. We now briefly comment on the effect of also using subleading terms in the matching condition, that is, setting

$$d_1(\mu_h) = 1 + \frac{\alpha(\mu_h)}{2\pi}(C_A + C_F) + \frac{\alpha(\mu_h)}{4\pi} C_A \ln\left(\frac{\mu_h^2}{m^2}\right). \tag{5.25}$$

In that case, the terms that should be reproduced in the fixed-order expression, denoted by $\bar{d}_1^{\mathrm{FO}}$, would change to

$$\bar{d}_1^{\mathrm{FO}} = 1 + \frac{\alpha(\mu)}{2\pi}(C_A + C_F) + \frac{\alpha(\mu)}{4\pi} C_A \ln\left(\frac{\mu^2}{m^2}\right). \tag{5.26}$$

There is now a difference between the two expressions, reading

$$d_1^{\mathrm{RGI}} - \bar{d}_1^{\mathrm{FO}} = -\left[1 - z^{-C_A}\right] - \frac{\alpha(\mu)}{4\pi} C_A \ln\left(\frac{\mu^2}{\mu_h^2}\right) + (\alpha(\mu_h) - \alpha(\mu))\left[\frac{1}{2\pi}(C_A + C_F) + \frac{1}{4\pi} C_A \ln\left(\frac{\mu_h^2}{m^2}\right)\right]. \tag{5.27}$$

The second line is the contribution caused by using higher-order terms in the coefficient at the matching scale. However, we note that this term contains

$$\alpha(\mu_h) - \alpha(\mu) = \alpha(\mu)\left[z^{-\beta_0} - 1\right], \tag{5.28}$$

which accounts for the running of α from the matching scale μ_h to the general scale μ used in the potentials. This contributes only at subleading order of resummed logarithms (NLL) and is therefore not relevant to our calculation. The first line of equation (5.27) also illustrates what we achieve by writing the RG improved coefficients in the form $d_i \to d_i^{\mathrm{FO}} + \left[d_i^{\mathrm{RGI}} - \bar{d}_i^{\mathrm{FO}}\right]$: Starting from the fixed-order expression used in [27], the square bracket subtracts the large logarithm contained in the fixed-order coefficient and replaces it by the whole resummed tower of logarithms at LL.

In the same way, we treat the analogous terms appearing in the four-fermion coefficients d_{ij}. The higher order matching condition, in this case, contains factors of $\alpha^2(\mu_h)$ and the coefficients are multiplied by an overall factor of $\frac{1}{\alpha(\mu)}$ in $\mathcal{V}_{1/m^2}$. The difference in scales of α would appear in the form

$$\frac{1}{\alpha(\mu)}\left(d_{ij}^{\mathrm{RGI}} - \bar{d}_{ij}^{\mathrm{FO}}\right) \supset \left[\frac{\alpha^2(\mu_h)}{\alpha(\mu)} - \alpha(\mu)\right](\dots) = \alpha(\mu)\left[z^{-2\beta_0} - 1\right](\dots), \tag{5.29}$$

where the dots denote terms analogous to the square bracket in (5.27). This again contributes only at higher order in the resummation of logarithms. In the following, we will therefore not consider the higher order terms in the matching condition and stick to $d_1(\mu_h) = (d_2 - 16d_5)(\mu_h) = 1$, $d_{ij}(\mu_h) = 0$ at the order of interest.

We now explicitly use the resummed coefficients in the potential $\mathcal{V}_{1/m^2}$, which is given in (3.70). In the soft contributions (and the counterterms) contained in this equation, all NRQCD coefficients are multiplied by an additional factor of $\alpha(\mu)$, such that the resummed parts of the coefficients correspond to higher logarithmic orders. Therefore, it is enough use the (tree-level) fixed-order expressions $d_1 = d_2 = d_3 = 1$ in this part.[2] The only modification of the potential

[2]Note that it is not a problem that d_2 appears without the additional term of $-16d_5$ that we used before, since d_5 only starts at $\mathcal{O}(\alpha)$, not contributing to the tree-level expression.

caused by the running of the matching coefficients at LL order comes from the terms not multiplied by an overall factor of $\alpha(\mu)$. These terms read

$$\mathcal{V}_{1/m^2} \supset -\frac{1}{4}(d_2 - 16d_5) - \frac{1}{4\pi C_F \alpha(\mu)}(d_{ss} + C_F d_{vs}) + \frac{1}{4\pi C_F \alpha(\mu)}(d_{sv} + C_F d_{vv}) - \frac{1}{6}d_1^2, \tag{5.30}$$

where we have set $\varepsilon = 0$ since the RGE only considers the four-dimensional case.

Plugging in the resummed coefficients, we obtain

$$\begin{aligned}
\mathcal{V}^{\text{RGI}}_{1/m^2} - \bar{\mathcal{V}}^{\text{FO}}_{1/m^2} = &-\left(\frac{5}{13} + \frac{8}{13}\frac{C_F}{C_A}\right)\left[1 - z^{-\frac{13}{6}C_A}\right] + \frac{5}{12}\left[1 - z^{-2C_A}\right] \\
&+ \left(\frac{9}{52}C_A - \frac{25}{13}C_F\right)\frac{1}{\beta_0}z^{-\beta_0}\left[1 - z^{\beta_0}\right] \\
&+ \left(\frac{15}{26}C_A + \frac{12}{13}C_F\right)\frac{1}{\beta_0 - \frac{13}{6}C_A}z^{-\beta_0}\left[1 - z^{\beta_0 - \frac{13}{6}C_A}\right] \\
&- \frac{1}{4}C_A\frac{1}{\beta_0 - 2C_A}z^{-\beta_0}\left[1 - z^{\beta_0 - 2C_A}\right] \\
&+ \frac{\alpha(\mu)}{4\pi}\ln\left(\frac{\mu^2}{\mu_h^2}\right)\left(-\frac{1}{2}C_A - \frac{1}{3}C_F\right).
\end{aligned} \tag{5.31}$$

The first line corresponds to the resummed contributions of d_1^2 and $d_2 - 16d_5$. The second, third, and fourth lines correspond to the four-fermion coefficients. All contributions are zero at the matching scale $\mu = \mu_h$, as they should be, and encode the full tower of resummed logarithms. Reexpanding them, the logarithm at order $\mathcal{O}(\alpha)$ exactly cancels the one subtracted in the last line. This must be the case to avoid double counting since the fixed order expression given in equation (3.73) already includes the first logarithm, coming from the term $\left[\left(\frac{\mu^2}{m^2}\right)^{\varepsilon} - 1\right]\frac{1}{\varepsilon}$. Essentially, as already discussed for the matching coefficients themselves, we subtract the large logarithm contained in the fixed-order calculation and replace it with the full tower of resummed logarithms.

Lastly, we write the correction to $\mathcal{V}^{(0)}_{1/m^2}$ from the hard running as a modification of the coefficient v_0^{FO}, which was defined in equation (3.72):

$$v_0^{\mathrm{RGI},h} \equiv v_0^{\mathrm{FO}} + v_0^{\mathrm{RG},h} = \tag{5.32}$$

$$\begin{aligned} &= v_0^{\mathrm{FO}} - \left(\frac{5}{13} + \frac{8}{13}\frac{C_F}{C_A}\right)\left[1 - z^{-\frac{13}{6}C_A}\right] + \frac{5}{12}\left[1 - z^{-2C_A}\right] \\ &\quad + \left(\frac{9}{52}C_A - \frac{25}{13}C_F\right)\frac{1}{\beta_0} z^{-\beta_0}\left[1 - z^{\beta_0}\right] \\ &\quad + \left(\frac{15}{26}C_A + \frac{12}{13}C_F\right)\frac{1}{\beta_0 - \frac{13}{6}C_A} z^{-\beta_0}\left[1 - z^{\beta_0 - \frac{13}{6}C_A}\right] \\ &\quad - \frac{1}{4}C_A \frac{1}{\beta_0 - 2C_A} z^{-\beta_0}\left[1 - z^{\beta_0 - 2C_A}\right]. \end{aligned} \tag{5.33}$$

The subtraction of the otherwise double counted logarithm in the last line of (5.31) is understood to be done separately whenever this expression for v_0^{RGI} is used and therefore not included explicitly.

This concludes the discussion of the hard running of the NRQCD matching coefficients d_i and d_{ij}. In the next section, we turn to the ultrasoft running. We will eventually incorporate it into the potential coefficients $\mathcal{V}_X$ in a similar procedure to the one we used here.

5.3 Ultrasoft Running of the Potentials

We now consider the resummation of logarithms related to the ultrasoft scale. In PNRQCD, the $g\mathbf{x}\cdot\mathbf{E}$-term in equation (3.37) provides an interaction between the heavy quark anti-quark pair and an ultrasoft gluon. When radiating off an ultrasoft gluon, the heavy quark anti-quark state changes from the colour singlet to the colour octet configuration. Figure 5.2 shows the relevant diagram, which includes a divergent ultrasoft loop.

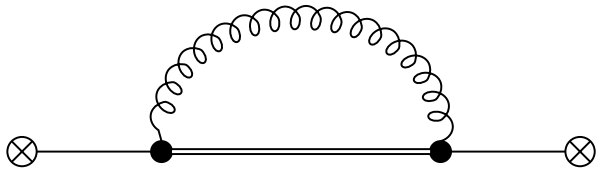

Figure 5.2: Divergent ultrasoft one-loop diagram in the framework of PNRQCD. The curly line denotes the ultrasoft gluon, which interacts with the heavy quark anti-quark pair via the $g\mathbf{x}\cdot\mathbf{E}$-vertex. This is denoted by the black dot. The single line denotes the Green's function for the heavy quark anti-quark pair in the singlet state, while the double line corresponds to its octet state. The crossed dots stand for the non-relativistic current.

These UV divergences in the ultrasoft correction are related to IR divergences in the potential coefficients. Therefore, it is advantageous to remove these divergences from the potentials and add them to the ultrasoft calculation [61, 62], as it is done in [27] via the subtraction term δV_{sub} (cf. equation (3.61)). This also means that the effect of ultrasoft running can be written as a correction to the potentials, which we will do in the following. We will refer to the term used to remove the divergences from the potentials as the ultrasoft counterterm.

When performing the calculations for this thesis, we have considered this counterterm up to $\mathcal{O}(\alpha^2(\mu_{(us)}))$. While this will be needed for an extension to higher orders in log-resummation, it is not strictly within the scope of this thesis, where we are interested in the NLL corrections to the R-ratio, for which the one-loop ultrasoft counterterm is sufficient. Therefore, we will only present the $\mathcal{O}(\alpha(\mu_{(us)}))$-terms of the calculation in the main body of this work. However, we will provide the analogous two-loop expressions in appendix C in order to facilitate an easier extension of the calculation in the future.

We use the following procedure: First, we closely follow [34] in the derivation of the ultrasoft counterterm in position space, providing additional details in the calculation and converting to the conventions used in [27]. Secondly, we express this counterterm in momentum space via a fully d-dimensional Fourier transform. Lastly, we determine the resulting RGE and its solution.

5.3.1 Derivation of the Ultrasoft Counterterm in Position Space

The ultrasoft counterterm δV to the potentials is written such that the renormalized potential

$$V = V_B + \delta V_{us} \tag{5.34}$$

is free of divergences, where V_B denotes the divergent bare potential. Note the difference in signs in the definition of the counterterm compared to [34], which arises because we are adopting the conventions of [27].

The counterterm can be conveniently written as[3]

$$\delta V_{us} = \sum_{n=1}^{\infty} Z_V^{(n)} \frac{1}{\varepsilon^n}. \tag{5.35}$$

[3]Note again a difference in conventions: In this work, the dimension in dimensional regularization is defined as $d = 4 - 2\varepsilon$, while in [34] it is denoted by $D = d + 1 = 4 + 2\varepsilon$. This changes the sign of $Z_V^{(n)}$ depending on the power of ε.

An insertion of the bare potential V_B also includes an insertion of the counterterm $(-\delta V_{us})$, which leads to the following contribution to the Green's function:

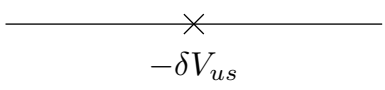

$$= -G_0(E)(-\delta V_{us})G_0(E) + \dots \,. \tag{5.36}$$

This also demonstrates why the divergences in

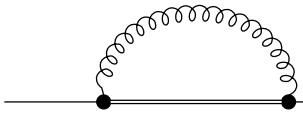

$$= -G_0(E)\Sigma_B^{1-\text{loop}}G_0(E) + \dots \tag{5.37}$$

can be absorbed into the counterterm to the potential as

$$\delta V_{us}\big|_{\text{divergent}} = \Sigma_B\big|_{\text{divergent}}. \tag{5.38}$$

In this expression, $\Sigma_B^{1-\text{loop}}$ denotes the one-loop contribution to the bare Euclidean chromomagnetic correlator [34]

$$\Sigma_B(E) = V_A^2 \frac{T_F}{N(d-1)} \int_0^\infty \mathrm{d}t\, \mathbf{r} e^{-t(h_o^B - E)} \mathbf{r} \left\langle 0 \middle| g_B \mathbf{E}^A(t) \phi_{\text{adj}}^{AB}(t,0) g_B \mathbf{E}^B(0) \middle| 0 \right\rangle, \tag{5.39}$$

where $\phi_{\text{adj}}^{AB}(t,0)$ is the Wilson line

$$\phi_{\text{adj}}^{AB}(t,0) = P e^{-ig_B \int_0^t \mathrm{d}t' A_0(t')} \tag{5.40}$$

in the adjoint representation and bare quantities are marked with an index B. The individual quantities are defined as in the alternative formulation of the PNRQCD Lagrangian given in (3.40). We especially note the use of the coefficient V_A^2 multiplying the ultrasoft expression. This quantity arises as a matching coefficient when decomposing the heavy-quark pair field into its colour-singlet and colour-octet components, as we briefly discussed in section 3.3.1. It reads [80]

$$V_A = 1 + \mathcal{O}(\alpha^2), \tag{5.41}$$

such that we could set it to one at the order of interest to this work. However, this factor later on provides a way of tracking the ultrasoft contribution when taken together with other parts of the calculation, which is why we choose to keep this factor unevaluated. Nevertheless, we stress already here that we can consider it as a constant in the context of the renormalization

group equation for the one-loop ultrasoft correction since[4] [81]

$$\mu\frac{\mathrm{d}}{\mathrm{d}\mu}V_A = \mathcal{O}(\alpha^2). \tag{5.42}$$

The one-loop correlator $\Sigma_B^{\text{1-loop}}$ reads [34, 80]

$$\begin{aligned}\Sigma_B^{\text{1-loop}} &= -g_B^2 C_F V_A^2 (1-\varepsilon)\frac{\Gamma(2-\varepsilon)\Gamma(-3+2\varepsilon)}{\pi^{2-\varepsilon}}\mathbf{r}(h_o^B - E)^{3-2\varepsilon}\mathbf{r} = \\ &\equiv c_{\text{1-loop}}\tilde{\mu}^{2\varepsilon}\mathbf{r}(h_o^B - E)^{3-2\varepsilon}\mathbf{r},\end{aligned} \tag{5.43}$$

where h_o^B denotes the bare octet Hamiltonian. We have defined a dimensionless prefactor $c_{\text{1-loop}}$, which contains terms divergent in ε, given by (including terms up to order $\mathcal{O}(\alpha)$)

$$c_{\text{1-loop}} = \frac{C_F V_A^2}{3\pi}\alpha\frac{1}{\varepsilon} + \mathcal{O}(\varepsilon^0), \tag{5.44}$$

where we have expressed g_B in terms of the renormalized coupling α (cf. equation (2.9)).

In $\Sigma_B^{\text{1-loop}}$, this coefficient multiplies an operator structure of the form

$$\tilde{\mu}^{2\varepsilon}\mathbf{r}(h_o^B - E)^{3-2\varepsilon}\mathbf{r} = \mathbf{r}(h_o^B - E)^3\mathbf{r} - 2\mathbf{r}(h_o^B - E)^3 \ln\left(\frac{h_o^B - E}{\tilde{\mu}}\right)\mathbf{r}\varepsilon + \mathcal{O}(\varepsilon^2). \tag{5.45}$$

The $\mathcal{O}(\varepsilon)$-term produces a term finite in ε when multiplying the $\frac{1}{\varepsilon}$-pole and does not contribute to the counterterm. Therefore, it is enough to consider the leading-order term $\mathbf{r}(h_o^B - E)^3\mathbf{r}$ in the expansion (5.45) of the operator structure in $\Sigma_B^{\text{1-loop}}$ when determining the divergent part, which is relevant to the counterterm δV_{us}. Explicitly, the divergence is given by

$$\Sigma_B^{\text{1-loop}} = C_F V_A^2 \frac{\alpha}{3\pi}\frac{1}{\varepsilon}\mathbf{r}(h_o - E)^3\mathbf{r} + \mathcal{O}(\varepsilon^0), \tag{5.46}$$

where we now consider the renormalized octet Hamiltonian. From equation (5.38), we finally read off the one-loop counterterm to the potentials related to ultrasoft running, expressed in

[4] In reference [34], the even stronger claim

$$\mu\frac{\mathrm{d}}{\mathrm{d}\mu}V_A = \mathcal{O}(\alpha^3)$$

is made, which we could not confirm by other references. Since this statement is only relevant when discussing the two-loop ultrasoft running (which we will not do in this work), we consider this issue beyond the scope of this thesis and will not discuss it further.

position space (PS):

$$\delta V_{us}^{\rm PS} = C_F V_A^2 \frac{\alpha}{3\pi}\frac{1}{\varepsilon}\mathbf{r}(h_o - E)^3\mathbf{r}. \tag{5.47}$$

In order to Fourier transform the operator structure $\mathbf{r}(h_o - E)^3\mathbf{r}$ to momentum space, we first express it in terms of the singlet and octet static potentials. The relevant relation is given in [34, 82] and reads (again converted to our conventions)

$$\begin{aligned}\mathbf{r}(h_o - E)^3\mathbf{r} = \mathbf{r}^2(\Delta V)^3 + \frac{1}{m}\Bigg[&4\Delta V\left(r\frac{\rm d}{{\rm d}r}V_s^{(0)}\right) + (\Delta V)^2(3d-8)\\ &+ 4\Delta V\left(\left(r\frac{\rm d}{{\rm d}r}\Delta V\right) + \Delta V\right) + \left(\left(r\frac{\rm d}{{\rm d}r}\Delta V\right) + \Delta V\right)^2\Bigg]\\ &+ \frac{1}{m^2}\Big[-2[\mathbf{p},[\mathbf{p},V_o^{(0)}]] + 2\{\mathbf{p}^2,\Delta V\}\Big] + \mathcal{O}((h_s - E)).\end{aligned} \tag{5.48}$$

This expression uses the approximations

$$h_s = \frac{\mathbf{p}^2}{m} + V_s^{(0)} \quad \text{and} \quad h_o = \frac{\mathbf{p}^2}{m} + V_o^{(0)}, \tag{5.49}$$

dropping higher-order potentials. This defines $h_o - h_s = V_o^{(0)} - V_s^{(0)} \equiv \Delta V$. Terms containing external factors[5] of positive powers of $(h_s - E)$ can be neglected since they are irrelevant in physical observables, where one takes expectation values with states containing the Green's function. The Green's function contains powers of $\frac{1}{(h_s - E)}$, which are cancelled by the $\mathcal{O}((h_s - E))$-terms. Neglecting these terms leads to ambiguities in the identity given in (5.48). Different choices of organizing the terms would lead to different expressions, which can be related by field redefinitions. Further discussion on this topic can be found in [82–84]. The reason why the expression given above is particularly convenient is that the $\frac{1}{m}$-contribution is phrased in terms of the combination $\left(\left(r\frac{\rm d}{{\rm d}r}\Delta V\right) + \Delta V\right)$, which is suppressed in ε and therefore drops out if one neglects $\mathcal{O}(\varepsilon)$-terms. While this suppression is not obvious at this stage, it will become clear for the Fourier-transformed terms in the next section. We present the derivation of identity (5.48) in detail in appendix C.2. In the following, the irrelevant $\mathcal{O}((h_s - E))$-terms are not denoted explicitly anymore.

[5] *External* in this context means that there are no further factors to either the left or the right of a factor of $(h_s - E)$.

Before turning to the Fourier transform of the rewritten counterterm

$$\begin{aligned}\delta V_{us}^{\mathrm{PS}} = C_F V_A^2 \frac{\alpha}{3\pi}\frac{1}{\varepsilon}\Bigg\{&\mathbf{r}^2(\Delta V)^3 + \frac{1}{m}\Bigg[4\Delta V\left(r\frac{\mathrm{d}}{\mathrm{d}r}V_s^{(0)}\right) + (\Delta V)^2(3d-8)\\ &+ 4\Delta V\left(\left(r\frac{\mathrm{d}}{\mathrm{d}r}\Delta V\right)+\Delta V\right) + \left(\left(r\frac{\mathrm{d}}{\mathrm{d}r}\Delta V\right)+\Delta V\right)^2\Bigg]\\ &+ \frac{1}{m^2}\left[-2[\mathbf{p},[\mathbf{p},V_o^{(0)}]] + 2\{\mathbf{p}^2,\Delta V\}\right]\Bigg\},\end{aligned} \tag{5.50}$$

we discuss the static singlet and octet potentials $V_s^{(0)}$ and $V_o^{(0)}$, respectively. In position space, the (bare) static potentials can be written in the form (cf. e.g. [82, 85, 86])

$$V_{s/o,B}^{(0),\mathrm{PS}} = C_{s/o} g_B^2 \sum_{n=0}^{\infty} g_B^{2n} c_n^{(s/o)} r^{-1+2(n+1)\varepsilon}. \tag{5.51}$$

The important thing to note is that the constants $c_n^{(s/o)}$ are the same for the singlet and octet static potentials for $n=0$ and $n=1$. Since we do not need the potentials beyond that order, $V_s^{(0)}$, $V_o^{(0)}$, and $V_\Delta^{(0)} \equiv \Delta V$ only differ in their constant prefactors

$$C_s = -C_F, \quad C_o = \frac{C_A}{2} - C_F, \quad \text{and} \quad C_\Delta = \frac{C_A}{2}. \tag{5.52}$$

From section 3.3.2, we quote the Coulomb potential

$$V_{s/o/\Delta}^{(0)} = C_{s/o/\Delta} \times \frac{4\pi\alpha}{\mathbf{q}^2}\left\{1 + \frac{\alpha}{4\pi}\left(\left[\left(\frac{\mu^2}{\mathbf{q}^2}\right)^{\varepsilon} - 1\right]\frac{\beta_0}{\varepsilon} + \left(\frac{\mu^2}{\mathbf{q}^2}\right)^{\varepsilon} a_1(\varepsilon)\right) + \mathcal{O}(\alpha^2)\right\} \tag{5.53}$$

in momentum space up to the one-loop coefficient. We have substituted the singlet coefficient $-C_F$ by $C_{s/o/\Delta}$ to account also for the octet potential and ΔV. In the counterterm (5.50), we need these potentials in position space, where they are given by

$$\begin{aligned}V_{s/o/\Delta}^{(0),\mathrm{PS}} &= C_{s/o/\Delta}\alpha 4\pi \mathcal{F}_2(r)\\ &\quad + C_{s/o/\Delta}\alpha^2\left[\mu^{2\varepsilon}\mathcal{F}_{2+2\varepsilon}(r)\left(\frac{\beta_0}{\varepsilon} + a_1(\varepsilon)\right) - \mathcal{F}_2(r)\frac{\beta_0}{\varepsilon}\right] + \mathcal{O}(\alpha^3).\end{aligned} \tag{5.54}$$

Here, analogously to reference [86], we have introduced the functions

$$\mathcal{F}_n(r) = \tilde{\mu}^{2\varepsilon}\int \frac{\mathrm{d}^{d-1}\mathbf{q}}{(2\pi)^{d-1}}\frac{e^{-i\mathbf{q}\cdot\mathbf{r}}}{|\mathbf{q}|^n} = \tilde{\mu}^{2\varepsilon}\frac{2^{-n}\pi^{-\frac{d-1}{2}}}{r^{d-1-n}}\frac{\Gamma\left(\frac{d-1}{2}-\frac{n}{2}\right)}{\Gamma\left(\frac{n}{2}\right)} \equiv f(n)\tilde{\mu}^{2\varepsilon}r^{-d+1+n}, \tag{5.55}$$

which denote the d-dimensional Fourier transform of $\frac{1}{|\mathbf{q}|^n}$. We recall that d was defined as $d = 4 - 2\varepsilon$. To shorten the notation in the following calculation, we rewrite (5.54) as

$$V_{s/o/\Delta}^{(0),\mathrm{PS}} = \alpha c_1^{s/o/\Delta} \mathcal{F}_2(r) + \alpha^2 \left[c_{21}^{s/o/\Delta} \mathcal{F}_{2+2\varepsilon}(r) + c_{22}^{s/o/\Delta} \mathcal{F}_2(r) \right] + \mathcal{O}(\alpha^3), \tag{5.56}$$

where the constants are defined as

$$c_1^{s/o/\Delta} = C_{s/o/\Delta} 4\pi, \tag{5.57}$$

$$c_{21}^{s/o/\Delta} = C_{s/o/\Delta} \mu^{2\varepsilon} \left(\frac{\beta_0}{\varepsilon} + a_1(\varepsilon) \right), \tag{5.58}$$

$$c_{22}^{s/o/\Delta} = C_{s/o/\Delta} \left(-\frac{\beta_0}{\varepsilon} \right). \tag{5.59}$$

Since the second part in $V_{s/o/\Delta}^{(0),\mathrm{PS}}$ is suppressed in α, it is sufficient to consider only the first term in the one-loop case. In the next section, we will comment more on the systematics of the Fourier transforms in this context.

5.3.2 d-Dimensional Fourier Transform of the Ultrasoft Counterterm

The counterterm given in equation (5.50) was derived in position space (denoted by the superscript "PS") and represents an operator. We find it more convenient to instead consider its momentum space equivalent, where it is not operator-valued anymore. The relation between the two is given by the matrix element

$$V = \left\langle \mathbf{p}' \middle| V^{\mathrm{PS}} \middle| \mathbf{p} \right\rangle. \tag{5.60}$$

Since (apart from the previous section) we rarely consider position space expressions in this work, we will not introduce additional indices for momentum space quantities. Instead, we understand momentum space as the default choice.

In this section, we perform the fully d-dimensional Fourier transform of the counterterm (5.50) to momentum space. We start by plugging the explicit expression (5.56) for the static potentials into the counterterm (5.50) and expand in α. At leading order in α, the terms obtained by

this procedure are given by

$$\mathbf{r}^2(\Delta V)^3 = \alpha^3 \left(c_1^\Delta\right)^3 r^2 \mathcal{F}_2(r)^3 + \mathcal{O}(\alpha^4), \tag{5.61}$$

$$\Delta V \left(r\frac{\mathrm{d}}{\mathrm{d}r} V_s^{(0)}\right) = \alpha^2 \left(c_1^\Delta\right)\left(c_1^s\right) \mathcal{F}_2(r) \left(r\frac{\mathrm{d}}{\mathrm{d}r}\mathcal{F}_2(r)\right) + \mathcal{O}(\alpha^3), \tag{5.62}$$

$$(\Delta V)^2 = \alpha^2 \left(c_1^\Delta\right)^2 \mathcal{F}_2(r)^2 + \mathcal{O}\left(\alpha^3\right), \tag{5.63}$$

$$(\Delta V)\left(r\frac{\mathrm{d}}{\mathrm{d}r}\Delta V + \Delta V\right) = \alpha^2 \left(c_1^\Delta\right)^2 \left[\mathcal{F}_2(r)\left(r\frac{\mathrm{d}}{\mathrm{d}r}\mathcal{F}_2(r)\right) + \mathcal{F}_2(r)^2\right] + \mathcal{O}\left(\alpha^3\right), \tag{5.64}$$

$$\left(r\frac{\mathrm{d}}{\mathrm{d}r}\Delta V + \Delta V\right)^2 = \alpha^2 \left(c_1^\Delta\right)^2 \left[\left(r\frac{\mathrm{d}}{\mathrm{d}r}\mathcal{F}_2(r)\right)^2 + 2\mathcal{F}_2(r)\left(r\frac{\mathrm{d}}{\mathrm{d}r}\mathcal{F}_2(r)\right) + \mathcal{F}_2(r)^2\right] + \mathcal{O}\left(\alpha^3\right), \tag{5.65}$$

$$[\mathbf{p},[\mathbf{p},V_o^{(0)}]] = \alpha\left(c_1^o\right)[\mathbf{p},[\mathbf{p},\mathcal{F}_2(r)]] + \mathcal{O}(\alpha^2), \tag{5.66}$$

$$\{\mathbf{p}^2,\Delta V\} = \alpha\left(c_1^\Delta\right)\{\mathbf{p}^2,\mathcal{F}_2(r)\} + \mathcal{O}(\alpha^2). \tag{5.67}$$

In appendix C.3, we list these results extended to next-to-leading order in α. Using these expressions, we Fourier transform the individual position space structures to momentum space via the matrix element given above. Some relevant relations are given in table 5.1.

Table 5.1: Important relations between some operators in position space and the corresponding quantities in momentum space.

Position Space	Momentum Space
$\mathcal{F}_n(r)$	$\frac{1}{\lvert\mathbf{q}\rvert^n}$
r^x	$\tilde{\mu}^{-2\varepsilon}\frac{1}{f(3-2\varepsilon+x)}\frac{1}{\lvert\mathbf{q}\rvert^{3-2\varepsilon+x}}$
$[\mathbf{p},[\mathbf{p},\mathcal{F}_n(r)]]$	$\frac{1}{\lvert\mathbf{q}\rvert^{n-2}}$
$\{\mathbf{p}^2,\mathcal{F}_n(r)\}$	$\frac{\mathbf{p}^2+\mathbf{p}'^2}{\lvert\mathbf{q}\rvert^n}$

The explicit Fourier transforms of the individual structures (also for the two-loop case) are listed in appendix C.4. Here, we give these Fourier transformed expressions appearing in the counterterm (5.50) at leading order in α.

For the term $\mathbf{r}^2(\Delta V)^3$, corresponding to the Coulomb potential, we obtain

$$\mathbf{r}^2(\Delta V)^3 \longrightarrow \alpha^3 C_\Delta^3 (4\pi)^3 \frac{f(2)^3}{f(2+4\varepsilon)}\tilde{\mu}^{4\varepsilon}\frac{1}{|\mathbf{q}|^{2+4\varepsilon}} + \mathcal{O}(\alpha^4). \tag{5.68}$$

The $\frac{1}{m}$-potential includes multiple terms, which lead to

$$\Delta V\left(r\frac{\mathrm{d}}{\mathrm{d}r}V_s^{(0)}\right) \longrightarrow \alpha^2 C_\Delta C_S (4\pi)^2(-1+2\varepsilon)\frac{f(2)^2}{f(1+2\varepsilon)}\tilde{\mu}^{2\varepsilon}\frac{1}{|\mathbf{q}|^{1+2\varepsilon}} + \mathcal{O}(\alpha^3), \quad (5.69)$$

$$(\Delta V)^2 \longrightarrow \alpha^2 C_\Delta^2 (4\pi)^2\frac{f(2)^2}{f(1+2\varepsilon)}\tilde{\mu}^{2\varepsilon}\frac{1}{|\mathbf{q}|^{1+2\varepsilon}}\mathcal{O}(\alpha^3), \quad (5.70)$$

$$(\Delta V)\left(r\frac{\mathrm{d}}{\mathrm{d}r}\Delta V + \Delta V\right) \longrightarrow \alpha^2 C_\Delta^2 (4\pi)^2(2\varepsilon)\frac{f(2)^2}{f(1+2\varepsilon)}\tilde{\mu}^{2\varepsilon}\frac{1}{|\mathbf{q}|^{1+2\varepsilon}} + \mathcal{O}(\alpha^3), \quad (5.71)$$

$$\left(r\frac{\mathrm{d}}{\mathrm{d}r}\Delta V + \Delta V\right)^2 \longrightarrow \alpha^2 C_\Delta^2 (4\pi)^2(4\varepsilon^2)\frac{f(2)^2}{f(1+2\varepsilon)}\tilde{\mu}^{2\varepsilon}\frac{1}{|\mathbf{q}|^{1+2\varepsilon}} + \mathcal{O}(\alpha^3). \quad (5.72)$$

Note that one can explicitly see the $\mathcal{O}(\varepsilon)$-suppression of the term $\left(r\frac{\mathrm{d}}{\mathrm{d}r}\Delta V + \Delta V\right)$ in the last two expressions. We add up all of these $\frac{1}{m}$-terms in the way that they appear in the counterterm and obtain

$$\begin{aligned}&\frac{1}{m}\left[4\Delta V\left(r\frac{\mathrm{d}}{\mathrm{d}r}V_s^{(0)}\right) + (\Delta V)^2(3d-8) + 4\Delta V\left(\left(r\frac{\mathrm{d}}{\mathrm{d}r}\Delta V\right) + \Delta V\right) + \left(\left(r\frac{\mathrm{d}}{\mathrm{d}r}\Delta V\right) + \Delta V\right)^2\right] \\ &\longrightarrow \frac{1}{m}\left[\alpha^2(4\pi)^2\left(C_A C_F(2-4\varepsilon) + C_A^2\left(1+\frac{1}{2}\varepsilon+\varepsilon^2\right)\right)\frac{f(2)^2}{f(1+2\varepsilon)}\tilde{\mu}^{2\varepsilon}\frac{1}{|\mathbf{q}|^{1+2\varepsilon}} + \mathcal{O}(\alpha^3)\right].\end{aligned} \quad (5.73)$$

The $\frac{1}{m^2}$-potentials lead to the following expressions:

$$[\mathbf{p},[\mathbf{p},V_o^{(0)}]] \longrightarrow \alpha C_o(4\pi) + \mathcal{O}(\alpha^2), \quad (5.74)$$

$$\{\mathbf{p}^2,\Delta V\} \longrightarrow \alpha C_\Delta(4\pi)\frac{(\mathbf{p}^2+\mathbf{p}'^2)}{|\mathbf{q}|^2} + \mathcal{O}(\alpha^2). \quad (5.75)$$

We again group these two terms together as they appear in the counterterm, obtaining

$$\frac{1}{m^2}\left[-2[\mathbf{p},[\mathbf{p},V_o^{(0)}]] + 2\{\mathbf{p}^2,\Delta V\}\right] \longrightarrow \frac{1}{m^2}\left[\alpha(4\pi)\left(-C_A + 2C_F + C_A\frac{(\mathbf{p}^2+\mathbf{p}'^2)}{|\mathbf{q}|^2}\right) + \mathcal{O}(\alpha^2)\right]. \quad (5.76)$$

We have now Fourier transformed all terms in the ultrasoft counterterm (5.50) to momentum space in d dimensions. Putting everything together, we obtain the following expression for the

one-loop counterterm in momentum space:

$$\begin{aligned}\delta V_{us} = \frac{1}{\varepsilon} C_F V_A^2 \frac{\alpha(\mu_{(us)})}{3\pi} \Bigg\{ & \alpha^3(\mu_{(s)}) \frac{C_A^3}{8} (4\pi)^3 \frac{f(2)^3}{f(2+4\varepsilon)} \tilde{\mu}_{(s)}^{4\varepsilon} \frac{1}{|\mathbf{q}|^{2+4\varepsilon}} \\ & + \frac{1}{m} \alpha^2(\mu_{(s)}) (4\pi)^2 \left(C_A C_F (2-4\varepsilon) + C_A^2 \left(1 + \frac{1}{2}\varepsilon + \varepsilon^2 \right) \right) \frac{f(2)^2}{f(1+2\varepsilon)} \tilde{\mu}_{(s)}^{2\varepsilon} \frac{1}{|\mathbf{q}|^{1+2\varepsilon}} \\ & + \frac{1}{m^2} \alpha(\mu_{(s)}) (4\pi) \left(-C_A + 2C_F + C_A \frac{(\mathbf{p}^2 + \mathbf{p}'^2)}{|\mathbf{q}|^2} \right) \Bigg\} + \text{higher order terms.} \end{aligned} \tag{5.77}$$

In this expression, we have introduced additional indices (us) and (s) for the scales μ to indicate their origin. Since the counterterm is determined in the fixed-order calculation, all scales represent, in principle, the generic renormalization scale μ. However, divergences arise from different regions. Here, we are considering the divergences coming from ultrasoft loops, which provide one overall power of α. Besides this, additional factors of α are contained in the potentials. These are the ones we have expanded in when performing the Fourier transform, and they are not related to the ultrasoft divergence. We have indicated this fact by using explicit indices $\mu_{(us)}$ and $\mu_{(s)}$. This only denotes the origin of the factors of α and not the actual scale where they are evaluated (those we will use later and denote by μ_{us} and μ_s). In particular, distinguishing between these factors of α will become relevant in the next section, where we consider the ultrasoft RGE, which only acts on $\alpha(\mu_{(us)})$. For ease of notation, we continue to use the functions $f(n)$ defined in equation (5.55).

At this point, we recall the subtraction term δV_{sub} from equation (3.61) that was used in reference [27] to remove divergences from the potentials and relate them to the ultrasoft contribution. Setting $\varepsilon \to 0$ in the term δV_{us} we discussed now, we observe that the two expressions exactly agree. The difference is just a choice of conventions: In [27], the subtraction term was chosen such that it only subtracts the pole parts in ε, while here we have decided to include terms finite in ε. The latter corresponds to the conventions from [34], in whose framework the ultrasoft calculation has been extended to the two-loop result.

The two-loop generalization of the fully d-dimensional counterterm in momentum space has also been determined during the course of this thesis. It is given in equation (C.54) in appendix C.4.

5.3.3 RGE and Ultrasoft Running

Since the bare potential $V_B = V - \delta V_{us}$ is independent of the renormalization scale μ, we derive the following RGE for the renormalized potential in terms of the ultrasoft counterterm:

$$0 = \mu_{(us)} \frac{\mathrm{d}}{\mathrm{d}\mu_{(us)}} V_B \quad \Longrightarrow \quad \mu_{(us)} \frac{\mathrm{d}}{\mathrm{d}\mu_{(us)}} V = \mu_{(us)} \frac{\mathrm{d}}{\mathrm{d}\mu_{(us)}} \delta V_{us}. \tag{5.78}$$

Here, we explicitly use the index (us) on the scale μ to symbolize that we are considering divergences from ultrasoft loops. Rewriting δV_{us} as defined in (5.35), we obtain

$$\begin{aligned} \mu_{(us)} \frac{\mathrm{d}}{\mathrm{d}\mu_{(us)}} V &= \mu_{(us)} \frac{\mathrm{d}}{\mathrm{d}\mu_{(us)}} \left(\sum_{n=1}^{\infty} Z_V^{(n)} \frac{1}{\varepsilon^n} \right) = \\ &= \mu_{(us)} \frac{\mathrm{d}\alpha(\mu_{(us)})}{\mathrm{d}\mu_{(us)}} \frac{\partial}{\partial \alpha(\mu_{(us)})} \left(\sum_{n=1}^{\infty} Z_V^{(n)} \frac{1}{\varepsilon^n} \right) + \mu_{(us)} \frac{\mathrm{d}\mathcal{O}_V}{\mathrm{d}\mu_{(us)}} \frac{\partial}{\partial \mathcal{O}_V} \left(\sum_{n=1}^{\infty} Z_V^{(n)} \frac{1}{\varepsilon^n} \right), \end{aligned} \tag{5.79}$$

where we have introduced the shorthand notation

$$\mathcal{O}_V \equiv \mathbf{r}(h_o - E)^3 \mathbf{r}. \tag{5.80}$$

In deriving the second line of the differential equation, we have used that the counterterm (5.50) depends on $\mu_{(us)}$ through $\alpha(\mu_{(us)})$ and the operator $\mathcal{O}_V$ (or its momentum space equivalent), which encodes the potentials.

In equation (2.21), we derived the relation between the $\frac{1}{\varepsilon}$-poles of a general matching coefficient and its anomalous dimension. We now use a similar argument for the ultrasoft counterterm, first recalling that

$$\mu_{(us)} \frac{\mathrm{d}\alpha(\mu_{(us)})}{\mathrm{d}\mu_{(us)}} = -2\varepsilon\alpha(\mu_{(us)}) + \alpha(\mu_{(us)})\beta\left(\alpha(\mu_{(us)})\right), \tag{5.81}$$

as it was defined in equation (2.10). This allows us to rewrite

$$\begin{aligned} \mu_{(us)} \frac{\mathrm{d}}{\mathrm{d}\mu_{(us)}} V = -2\alpha(\mu_{(us)}) \frac{\partial}{\partial \alpha(\mu_{(us)})} Z_V^{(1)} + \sum_{n=1}^{\infty} \Bigg\{ &- 2\alpha(\mu_{(us)}) \frac{\partial}{\partial \alpha(\mu_{(us)})} Z_V^{(n+1)} \\ &+ \alpha(\mu_{(us)})\beta\left(\alpha(\mu_{(us)})\right) Z_V^{(n)} + \mu_{(us)} \frac{\mathrm{d}\mathcal{O}_V}{\mathrm{d}\mu_{(us)}} \frac{\partial}{\partial \mathcal{O}_V} Z_V^{(n)} \Bigg\} \frac{1}{\varepsilon^n}. \end{aligned} \tag{5.82}$$

Since the left-hand side describes the derivative of the renormalized potential, it cannot contain poles in ε. Therefore, all poles on the right-hand side have to cancel. We choose the counterterm

such that the curly bracket is zero for all n and the RGE reduces to

$$\mu_{(us)}\frac{\mathrm{d}}{\mathrm{d}\mu_{(us)}}V = -2\alpha(\mu_{(us)})\frac{\partial}{\partial\alpha(\mu_{(us)})}Z_V^{(1)}. \tag{5.83}$$

Note that the coefficients $Z_V^{(n)}$ can contain terms proportional to positive powers of ε. The vanishing curly bracket in (5.82) is really only a choice for the counterterm and not a naturally following requirement.[6] For $n = 1$, the constraint reads

$$0 = -2\alpha(\mu_{(us)})\frac{\partial}{\partial\alpha(\mu_{(us)})}Z_V^{(2)} + \alpha(\mu_{(us)})\beta\left(\alpha(\mu_{(us)})\right)Z_V^{(1)} + \mu_{(us)}\frac{\mathrm{d}\mathcal{O}_V}{\mathrm{d}\mu_{(us)}}\frac{\partial}{\partial\mathcal{O}_V}Z_V^{(1)}. \tag{5.84}$$

In appendix C.5, we briefly show that the two-loop counterterm determined in the appendix satisfies this condition.

While it was convenient to briefly go back to the position space expressions for this discussion on our choice for the counterterm, we now come back to the RGE given in equation (5.83) and its implications in momentum space. There, we read off $Z_V^{(1)}$ from equation (5.77) and derive the explicit RGE as

$$\begin{aligned}\mu_{(us)}\frac{\mathrm{d}}{\mathrm{d}\mu_{(us)}}V = -2\alpha(\mu_{(us)})C_F V_A^2\frac{1}{3\pi}\Bigg\{&\alpha^3(\mu_{(s)})\frac{C_A^3}{8}(4\pi)^3\frac{f(2)^3}{f(2+4\varepsilon)}\tilde{\mu}_{(s)}^{4\varepsilon}\frac{1}{|\mathbf{q}|^{2+4\varepsilon}}\\ &+\frac{1}{m}\alpha^2(\mu_{(s)})(4\pi)^2\left(C_A C_F(2-4\varepsilon)+C_A^2\left(1+\frac{1}{2}\varepsilon+\varepsilon^2\right)\right)\frac{f(2)^2}{f(1+2\varepsilon)}\tilde{\mu}_{(s)}^{2\varepsilon}\frac{1}{|\mathbf{q}|^{1+2\varepsilon}}\\ &+\frac{1}{m^2}\alpha(\mu_{(s)})(4\pi)\left(-C_A+2C_F+C_A\frac{(\mathbf{p}^2+\mathbf{p}'^2)}{|\mathbf{q}|^2}\right)\Bigg\},\end{aligned} \tag{5.85}$$

where we recall that we treat $V_A = 1$ as a constant (cf. equation (5.42)).

Integrating the left-hand side of the equation, we obtain

$$\int_{\mu_1}^{\mu_2}\mathrm{d}\mu_{(us)}\,\frac{\mathrm{d}}{\mathrm{d}\mu_{(us)}}V = V(\mu_2) - V(\mu_1). \tag{5.86}$$

Since we want to resum logarithms associated with the ultrasoft running, we take the initial scale μ_1 to be μ_{us}, the natural scale of the ultrasoft contribution. As discussed in section 5.1, we evolve all contributions to the common scale $\mu_2 = \mu = \mu_s$, associating the arbitrary renormalization scale μ with the soft scale μ_s. In this case, the logarithms $\ln\left(\frac{\mu^2}{\mathbf{q}^2}\right)$ contained in the fixed-order potentials (cf. section 3.3.2) are small, as should be the case at the matching

[6] More precisely, an $\mathcal{O}(\varepsilon)$-term in the curly bracket gives a finite term when multiplying the $\frac{1}{\varepsilon}$-pole. This finite term *can* be contained on the left-hand side of the equation, but we require also the finite terms to cancel inside of the curly bracket.

scale. Integrating the RGE leads to

$$\int_{\mu_{us}}^{\mu} \mathrm{d}\mu_{(us)} \, \frac{\mathrm{d}}{\mathrm{d}\mu_{(us)}} V = V(\mu) - V(\mu, \mu_{us}) = \\ = -\frac{2C_F V_A^2}{3\pi} \Big\{ \dots \Big\} \int_{\mu_{us}}^{\mu} \mathrm{d}\mu_{(us)} \, \frac{\alpha(\mu_{(us)})}{\mu_{(us)}} = \frac{4C_F V_A^2}{3\beta_0} \ln\left(\frac{\alpha(\mu)}{\alpha(\mu_{us})}\right) \Big\{ \dots \Big\}, \tag{5.87}$$

where the curly bracket $\{\dots\}$ remains the same as in (5.85). The fixed-order potential $V(\mu)$ only depends on the scale μ. The ultrasoft running replaces some (but not all) of these scale dependencies by μ_{us}, which we have indicated by using the notation $V(\mu, \mu_{us})$.

Therefore, the solution to the RGE is given by

$$\begin{aligned} V(\mu, \mu_{us}) = &-\frac{4\pi\alpha(\mu) C_F}{\mathbf{q}^2} \\ &\times \Bigg\{ \Bigg[\mathcal{V}_C(\mu) + \alpha(\mu)^2 \ln\left(\frac{\alpha(\mu)}{\alpha(\mu_{us})}\right) \frac{2^{-1+4\varepsilon} \pi^{-1+2\varepsilon} \Gamma\left(\frac{1}{2} - \varepsilon\right)^3 \Gamma(1+2\varepsilon)}{3\beta_0 \Gamma\left(\frac{1}{2} - 3\varepsilon\right)} V_A^2 C_A^3 \left(\frac{\tilde{\mu}^2}{\mathbf{q}^2}\right)^{2\varepsilon} \Bigg] \\ &\quad - \frac{\pi^2 |\mathbf{q}|}{m} \Bigg[\mathcal{V}_{1/m}(\mu) - \alpha(\mu) \ln\left(\frac{\alpha(\mu)}{\alpha(\mu_{us})}\right) \frac{2^{1+2\varepsilon} \pi^{-\frac{5}{2}+\varepsilon} \Gamma\left(\frac{1}{2} - \varepsilon\right)^2 \Gamma\left(\frac{1}{2} + \varepsilon\right)}{3\beta_0 \Gamma(1-2\varepsilon)} \\ &\qquad\qquad \times V_A^2 \left(C_A C_F (2 - 4\varepsilon) + C_A^2 \left(1 + \frac{1}{2}\varepsilon + \varepsilon^2\right) \right) \left(\frac{\tilde{\mu}^2}{\mathbf{q}^2}\right)^{\varepsilon} \Bigg] \\ &\quad + \frac{\mathbf{q}^2}{m^2} \Bigg[\mathcal{V}_{1/m^2}(\mu) + \ln\left(\frac{\alpha(\mu)}{\alpha(\mu_{us})}\right) \frac{4}{3\beta_0} V_A^2 (-C_A + 2C_F) \Bigg] \\ &\quad + \frac{\mathbf{p}^2 + \mathbf{p}'^2}{2m^2} \Bigg[\mathcal{V}_p(\mu) + \ln\left(\frac{\alpha(\mu)}{\alpha(\mu_{us})}\right) \frac{8}{3\beta_0} V_A^2 C_A \Bigg] \Bigg\}. \end{aligned} \tag{5.88}$$

When writing the corrections from the ultrasoft running in this way, we adopt the same structure as for the fixed-order potentials $\mathcal{V}_X(\mu)$ in equation (3.59). We will denote the correction terms added to each $\mathcal{V}_X(\mu)$ in the square brackets by $\delta\mathcal{V}_X(\mu, \mu_{us})$.

Equation (5.88) contains the full $\mathcal{O}(\varepsilon)$-dependence in the terms encoding the ultrasoft resummation. This ε-dependence comes from the d-dimensional curly bracket in (5.77). However, since we have solved the ultrasoft RGE in 4 dimensions, this is not actually relevant to our

calculation. Expanding these factors, we obtain:

$$\delta\mathcal{V}_C(\mu,\mu_{us}) = \alpha(\mu)^2 \ln\left(\frac{\alpha(\mu)}{\alpha(\mu_{us})}\right)\left(\frac{\mu^2}{\mathbf{q}^2}\right)^{2\varepsilon} V_A^2 \frac{C_A^3}{6\beta_0} + \mathcal{O}(\varepsilon^2), \tag{5.89}$$

$$\delta\mathcal{V}_{1/m}(\mu,\mu_{us}) = -\alpha(\mu)\ln\left(\frac{\alpha(\mu)}{\alpha(\mu_{us})}\right)\left(\frac{\mu^2}{\mathbf{q}^2}\right)^{\varepsilon} V_A^2\Bigg[\frac{2C_A(C_A+2C_F)}{3\pi\beta_0} + \frac{1}{3\beta_0\pi}C_A\left(C_A - 8C_F + 2(C_A+2C_F)\ln(4)\right)\varepsilon\Bigg] + \mathcal{O}(\varepsilon^2), \tag{5.90}$$

$$\delta\mathcal{V}_{1/m^2}(\mu,\mu_{us}) = \ln\left(\frac{\alpha(\mu)}{\alpha(\mu_{us})}\right)\frac{4}{3\beta_0}V_A^2(-C_A+2C_F), \tag{5.91}$$

$$\delta\mathcal{V}_p(\mu,\mu_{us}) = \ln\left(\frac{\alpha(\mu)}{\alpha(\mu_{us})}\right)\frac{8}{3\beta_0}V_A^2 C_A. \tag{5.92}$$

The factor $\left(\frac{e^{\gamma_E}}{4\pi}\right)$ contained in $\tilde{\mu}^2 = \mu^2\left(\frac{e^{\gamma_E}}{4\pi}\right)$ has cancelled terms proportional to γ_E in the usual manner of the $\overline{\text{MS}}$-scheme.

To conclude the discussion of the ultrasoft running of the potentials, we note that the corrections obtained above can be encoded in a modification of appropriate constants in the potential coefficients $\mathcal{V}_X$, where we factor out $\left(\frac{\alpha(\mu)}{4\pi}\right)^n$ as necessary. The relevant constants are:

- a_2 in $\mathcal{V}_C^{(2)}$ (cf. equation (3.64)),
- b_1 in $\mathcal{V}_{1/m}^{(1)}$ (cf. equation (3.67)),
- v_0 in $\mathcal{V}_{1/m^2}^{(0)}$ (cf. equation (3.72)),
- and p_0 in $\mathcal{V}_p^{(0)}$ (cf. equation (3.74)).

Introducing the coefficient $p_0 = 1$ explicitly at fixed order allows us to write all corrections from the ultrasoft running in the same way. While the ultrasoft running is the only modification contributing to the RG improvement of a_2, b_1, and p_0, this is not the case for v_0: The hard running of the NRQCD matching coefficients, which was discussed in section 5.2, also contributed to v_0^{RGI}. This is the reason why we have introduced the additional superscript "h" in equation (5.32).

In the following, we give the full RG improvement of the relevant coefficients in the potentials. We continue to denote the fixed-order expressions for these coefficients with a superscript "FO" while introducing the superscripts "RG" for the additive correction obtained from ultrasoft

and hard running and "RGI" for the RG improved expressions.

$$a_2^{\mathrm{RGI}} \equiv a_2^{\mathrm{FO}} + a_2^{\mathrm{RG},us} = a_2^{\mathrm{FO}} + \ln\left(\frac{\alpha(\mu)}{\alpha(\mu_{us})}\right) V_A^2 \frac{8\pi^2 C_A^3}{3\beta_0}, \tag{5.93}$$

$$b_1^{\mathrm{RGI}} \equiv b_1^{\mathrm{FO}} + b_1^{\mathrm{RG},us} = b_1^{\mathrm{FO}} - \ln\left(\frac{\alpha(\mu)}{\alpha(\mu_{us})}\right) V_A^2 \frac{8C_A(C_A+2C_F)}{3\beta_0}, \tag{5.94}$$

$$\begin{aligned} v_0^{\mathrm{RGI}} &\equiv v_0^{\mathrm{FO}} + v_0^{\mathrm{RG},us} + v_0^{\mathrm{RG},h} = \\ &= v_0^{\mathrm{FO}} + \ln\left(\frac{\alpha(\mu)}{\alpha(\mu_{us})}\right) V_A^2 \frac{4(-C_A+2C_F)}{3\beta_0} \\ &\quad - \left(\frac{5}{13} + \frac{8}{13}\frac{C_F}{C_A}\right)\left[1 - z^{-\frac{13}{6}C_A}\right] + \frac{5}{12}\left[1 - z^{-2C_A}\right] \\ &\quad + \left(\frac{9}{52}C_A - \frac{25}{13}C_F\right)\frac{1}{\beta_0} z^{-\beta_0}\left[1 - z^{\beta_0}\right] \\ &\quad + \left(\frac{15}{26}C_A + \frac{12}{13}C_F\right)\frac{1}{\beta_0 - \frac{13}{6}C_A} z^{-\beta_0}\left[1 - z^{\beta_0 - \frac{13}{6}C_A}\right] \\ &\quad - \frac{1}{4}C_A \frac{1}{\beta_0 - 2C_A} z^{-\beta_0}\left[1 - z^{\beta_0 - 2C_A}\right], \end{aligned} \tag{5.95}$$

$$p_0^{\mathrm{RGI}} \equiv p_0^{\mathrm{FO}} + p_0^{\mathrm{RG},us} = p_0^{\mathrm{FO}} + \ln\left(\frac{\alpha(\mu)}{\alpha(\mu_{us})}\right) V_A^2 \frac{8C_A}{3\beta_0}. \tag{5.96}$$

Here, we have only inlcuded the $\mathcal{O}(\varepsilon^0)$-terms, which are the ones relevant to the calculations in this work. Corrections to a_2 and b_1 of higher order in ε can be read off from equations (5.89) and (5.90).

5.4 Potential Running - Mixing into the Current

In the last two sections, we have presented a way to include RG improvements related to the hard and ultrasoft running in the PNRQCD potentials $\mathcal{V}_X$. We will now use these results in the last element of the RG improvement considered in this work, namely the potential running. It is encoded in the hard matching coefficient c_v of the non-relativistic vector current $j^{(v),i} = c_v \psi^\dagger \sigma^i \chi + \mathcal{O}\left(\frac{1}{m^2}\right)$, which we have introduced in section 4.3.

5.4.1 Schematic Structure of the Calculation

We begin this section by noting some aspects of the general structure of the calculation used to determine the running of c_v.

In equation (4.11), we have defined the normalized cross section (R-ratio) in NRQCD, which is an observable and thus has to be finite for $\varepsilon \to 0$. For the leading terms, this reduces to

$$R \sim c_v^2 \,\mathrm{Im}\,\{G(E)\} \stackrel{!}{=} \text{ finite for } \varepsilon \to 0. \tag{5.97}$$

This condition can be used to express the divergences in c_v in terms of the divergences in $\mathrm{Im}\{G(E)\}$. While the latter will be determined in the following, we will eventually use the former to determine the running of c_v according to equation (2.22). Schematically, we write

$$c_v = 1 + c_v^{\left(\frac{1}{\varepsilon}\right)} \frac{1}{\varepsilon} + \ldots, \tag{5.98}$$

$$\mathrm{Im}\{G(E)\} = \mathrm{Im}\{G_0(E)\} + g^{\left(\frac{1}{\varepsilon}\right)} \frac{1}{\varepsilon} \,\mathrm{Im}\{G_0(E)\} + \ldots, \tag{5.99}$$

where the prefactors of the divergent terms are understood to be suppressed in α. The dots denote terms of order $\mathcal{O}(\alpha)$, which are not divergent in ε, as well as higher order terms. Requiring condition (5.97) to hold, we obtain the relation

$$c_v^{\left(\frac{1}{\varepsilon}\right)} = -\frac{1}{2} g^{\left(\frac{1}{\varepsilon}\right)}. \tag{5.100}$$

Therefore, we can determine the divergence in the coefficient c_v from the divergence in the imaginary part of the Green's function. These divergences in $\mathrm{Im}\{G(E)\}$ are written as a divergent factor multiplying the imaginary part of the leading-order Green's function $\mathrm{Im}\{G_0(E)\}$.

The divergences in the Green's function $G(E)$ arise in corrections to the leading-order Green's function $G_0(E)$ containing insertions of the potentials, where we use the expressions introduced in equations (4.13)ff. The divergent diagrams are given in figure 5.3.

These diagrams implicitly contain gluon exchanges to the left and right of the potential insertion. They are contained in the heavy-quark-pair Green's function since we have resummed ladder diagrams in section 3.3.1. For the running of c_v, we are only interested in the divergent parts of the vertex graphs in these diagrams. We consider the following configurations:

- An insertion of the $\frac{1}{m}$-potential as depicted in figure 5.3a leads to a divergence when no additional gluon is exchanged in one vertex graph. The insertion then leads to a potential loop contributing a factor of $\frac{m}{\mathbf{p}^2 - mE}$, cancelling the factor of $\frac{1}{m}$. The specific configurations leading to a divergence are shown below in figure 5.4.
- Inserting the potentials suppressed by $\frac{1}{m^2}$ (containing $\mathcal{V}_{1/m}$ and $\mathcal{V}_p$, cf. figure 5.3b and 5.3c, respectively) also yields a divergence. Without additional gluon exchanges in one

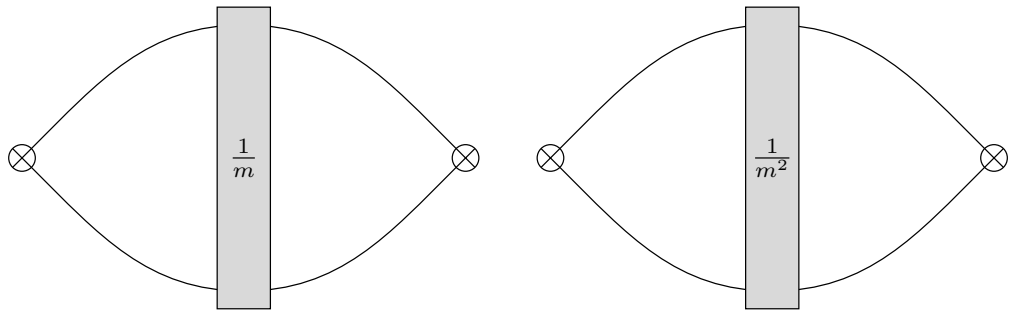

(a) $\frac{1}{m}$-potential. (b) $\frac{1}{m^2}$-potential.

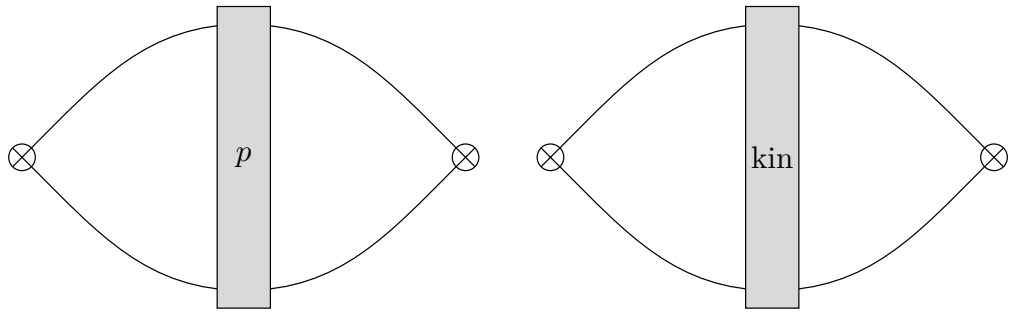

(c) p-potential. (d) Kinetic energy correction.

Figure 5.3: Insertions of the potentials and the quartic kinetic energy correction contributing to the divergence in the Green's function. To the left and right of the insertions, the full Green's function contains any number of gluon exchanges since it includes the resummation of ladder diagrams. However, only specific configurations of gluon exchanges lead to divergences. For the insertion of the $\frac{1}{m}$-potential, this is discussed in more detail in figure 5.4.

vertex graph, the diagram is linearly divergent, not leading to a $\frac{1}{\varepsilon}$-pole in dimensional regularization. However, we do obtain a logarithmic divergence and, thus, a pole when considering the potential insertion with one gluon exchange in the vertex graph. In this scenario, there are two potential loops in the vertex graph, exactly cancelling the factor of $\frac{1}{m^2}$ in the potentials. Diagrams with multiple gluon exchanges between the vertex and the potential insertion are not divergent.

- In addition to the potential insertions discussed above, the quartic kinetic energy correction in figure 5.3d also contributes to the divergence.
- Inserting the Coulomb potential into the Green's function does not lead to a divergence relevant to the potential running, which is why it wasn't included in figure 5.3.

In the following, we explicitly extract the divergences.

5.4.2 Divergences in Potential Loops in the Green's Functions

Reference [77] discusses in detail how to calculate potential insertions, including the ones shown in figure 5.3. The insertion of the $\frac{1}{m}$-potential is also discussed explicitly in [87]. While we do not need the full expressions for the analytical calculation in this thesis, we will rely on the divergences determined in [77]. We first define the so-called insertion functions used in these references:

$$I[x+a\varepsilon] = (\tilde{\mu}^{2\varepsilon})^4 \int \prod_{i=1}^{4} \left[\frac{\mathrm{d}^{d-1}\mathbf{p}_i}{(2\pi)^{d-1}}\right] G_0(\mathbf{p}_1,\mathbf{p}_2;E) \frac{1}{(\mathbf{q}_{23}^2)^x} \left(\frac{\mu^2}{\mathbf{q}_{23}^2}\right)^{a\varepsilon} G_0(\mathbf{p}_3,\mathbf{p}_4;E), \tag{5.101}$$

where $\mathbf{q}_{23} = \mathbf{p}_2 - \mathbf{p}_3$. They provide a compact notation for the insertion of a single potential $\delta V_i(\mathbf{p}_2,\mathbf{p}_3)$ as presented in equation (4.18). Note, however, that the definition of $I[x+a\varepsilon]$ does not include the factor of $i^2 = (-1)$, which arises in the insertion of a single potential and has to be accounted for separately. Generally, the PNRQCD potentials take the following form in momentum space:

$$\delta V_i(\mathbf{p}_2,\mathbf{p}_3) = \frac{1}{(\mathbf{q}_{23}^2)^x} \left(\frac{\mu^2}{\mathbf{q}_{23}^2}\right)^{a\varepsilon} \times w(\varepsilon), \tag{5.102}$$

which justifies the expression used in (5.101) and defines the constants x and a (both integers). The function

$$w(\varepsilon) = w^{\left(\frac{1}{\varepsilon}\right)} \frac{1}{\varepsilon} + w + w^{(\varepsilon)}\varepsilon + \mathcal{O}(\varepsilon^2) \tag{5.103}$$

is a coefficient function which has not been included in the definition of $I[x+a\varepsilon]$. In general, $w(\varepsilon)$ can be divergent, in which case a careful analysis of the counterterm structure is necessary. However, in this thesis, all relevant expressions fulfil $w^{\left(\frac{1}{\varepsilon}\right)} = 0$ such that this complication does not arise.[7]

For the resummation of logarithms at NLL in the R-ratio, it is enough to consider the $\frac{1}{m}$-potential up to $\mathcal{V}_{1/m}^{(1)}$ and the two potentials of order $\mathcal{O}\left(\frac{1}{m^2}\right)$ up to $\mathcal{V}_{1/m^2}^{(0)}$ and $\mathcal{V}_{p}^{(0)}$. We will drop terms in the potentials that are of higher order in α. In all three cases, the considered terms are the leading non-zero ones in the respective potentials. They all contribute to the potential δV_2 as defined in equation (4.16). These terms contain the coefficients b_1^{RGI}, v_0^{RGI},

[7] In reference [77], a counterterm-including insertion function $J[x+a\varepsilon;w(\varepsilon)]$ is defined. When reading off the results used in this thesis, it is enough to note that for non-divergent $w(\varepsilon)$, the expressions

$$w(\varepsilon) I[x+a\varepsilon] = J[x+a\varepsilon;w(\varepsilon)]$$

are equal.

and p_0^{RGI} that absorb the corrections from hard and ultrasoft running. In the following, we will use the expressions for these coefficients given in equations (5.94)-(5.96).

Since we are eventually interested in the divergences of c_v, we use equation (5.100) and first extract the divergences in $\mathrm{Im}\{G(E)\}$, which are contained in the imaginary part of the diagrams in figure 5.3. To do this, we relate the potential insertions in the diagrams with the corresponding insertion functions and use the expressions derived in [77]. Note that we are interested in divergences from the vertex graphs which multiply $\mathrm{Im}\{G_0(E)\}$, not in overall divergences contained in $\mathrm{Im}\{G_0(E)\}$ itself (cf. equation (3.51)). Not all insertion functions contain this kind of divergence. For ease of reference, we quote the ones that do and are relevant to the following calculation from [77] and collect them here:

$$\mathrm{Im}\left\{I[\frac{1}{2}+a\varepsilon]\right\} = \frac{m}{2\pi^2(a+1)\varepsilon}\,\mathrm{Im}\{G_0(E)\} + \mathcal{O}(\varepsilon^0), \tag{5.104}$$

$$\mathrm{Im}\left\{I[0]\right\} = \frac{m^2 C_F \alpha(\mu)}{8\pi\varepsilon}\,\mathrm{Im}\{G_0(E)\} + \mathcal{O}(\varepsilon^0). \tag{5.105}$$

In the following discussion, we will comment on these expressions in more detail.

Divergence in the Insertion of the $\frac{1}{m}$-Potential

We start by considering an insertion of the $\frac{1}{m}$-potential as it is shown in figure 5.3a. As explained above, we consider the leading non-zero term in the RG improved $\frac{1}{m}$-potential, which reads

$$V_{1/m} = b_1^{\mathrm{RGI}} \frac{\alpha^2(\mu)\pi^2 C_F}{m|\mathbf{q}|}\left(\frac{\mu^2}{\mathbf{q}^2}\right)^{\varepsilon} + \mathcal{O}(\alpha^3), \tag{5.106}$$

including the overall factor of $\frac{\alpha}{4\pi}$. This expression can be read off from equation (3.59) together with (3.67). We note that while b_1^{RGI} depends on μ and μ_{us}, it is independent of $\mathbf{q}$. Therefore, replacing b_1^{FO} with b_1^{RGI} only modifies the coefficient function $w(\varepsilon)$ and not the insertion function itself, which is $I[\frac{1}{2}+\varepsilon]$. The divergent part of its imaginary part was given in (5.104). Before explicitly extracting the divergence of diagram 5.3a, we briefly comment on the overall factor of $G_0(E)$ contained in $I[\frac{1}{2}+\varepsilon]$:

As explained in [77], the divergence comes from diagrams with no gluon exchange in a subgraph. These are shown in figure 5.4. While the first diagram 5.4a gives a divergence proportional to the Green's function with zero gluon exchanges, diagram 5.4b yields a divergence multiplying the Green's function with one gluon exchange, and so on. In total, this exactly reconstructs

the full leading-order Green's function $G_0(E)$ containing the resummation of ladder diagrams, which was discussed in section 3.3.1.

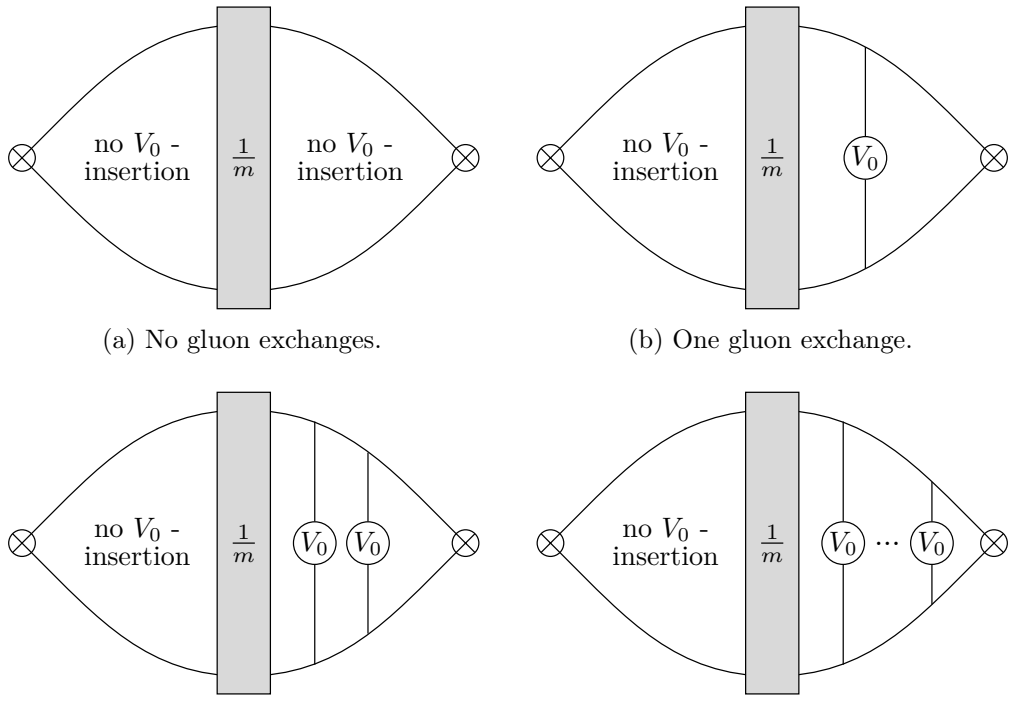

(a) No gluon exchanges.

(b) One gluon exchange.

(c) Two gluon exchanges.

(d) More than two gluon exchanges.

Figure 5.4: Insertion of the $\frac{1}{m}$-potential with gluon exchanges made explicit. Only configurations leading to a divergence in the vertex graph are depicted. Mirrored diagrams of (b)-(d) are also relevant but not depicted explicitly in this figure.

Therefore, the divergence of diagram 5.3a relevant to the running of c_v is given by

$$\begin{aligned}\mathrm{Im}\left\{\frac{1}{m}\text{-insertion}\right\} &= \mathrm{Im}\left\{-b_1^{\mathrm{RGI}}\frac{\alpha^2(\mu)\pi^2 C_F}{m} I[\frac{1}{2}+\varepsilon]\right\} = \\ &= -b_1^{\mathrm{RGI}}\alpha^2(\mu)C_F\frac{1}{4\varepsilon}\,\mathrm{Im}\left\{G_0(E)\right\} + \mathcal{O}(\varepsilon^0). \end{aligned} \tag{5.107}$$

We have used the divergence given in (5.104) and have accounted for the additional minus sign arising from the single insertion of a potential, as we have discussed at the beginning of this section. It is enough to use b_1^{RGI} in the limit $\varepsilon \to 0$ since terms involving positive powers of ε do not contribute to the divergence. We have already hinted at this when giving the explicit expression for b_1^{RGI} in equation (5.94), where we have only included $\mathcal{O}(\varepsilon^0)$-terms.

Divergence in the Insertion of the $\frac{1}{m^2}$-Potential

Turning to the $\frac{1}{m^2}$-potential inserted in figure 5.3b, the relevant term is

$$V_{1/m^2} = -v_0^{\mathrm{RGI}} \frac{\alpha(\mu) 4\pi C_F}{m^2}. \tag{5.108}$$

Thus, the divergence of the imaginary part of this insertion is given by

$$\begin{aligned} \mathrm{Im}\left\{ \frac{1}{m^2}\text{-insertion} \right\} &= \mathrm{Im}\left\{ v_0^{\mathrm{RGI}} \frac{\alpha(\mu) 4\pi C_F}{m^2} I[0] \right\} = \\ &= v_0^{\mathrm{RGI}} \alpha^2(\mu) C_F^2 \frac{1}{2\varepsilon} \,\mathrm{Im}\left\{ G_0(E) \right\} + \mathcal{O}(\varepsilon^0). \end{aligned} \tag{5.109}$$

The insertion of V_{1/m^2} has no momentum dependence and contains no divergences. Therefore, according to its definition (5.101), $I[0]$ factorizes and yields $I[0] = G_0(E)^2$. This implies $\mathrm{Im}\left\{I[0]\right\} = 2\,\mathrm{Re}\left\{G_0(E)\right\}\mathrm{Im}\left\{G_0(E)\right\}$, which has been used when extracting the divergence given in equation (5.105). The real part of the Green's function contains the divergent part

$$G_0(E) = \frac{\alpha(\mu) C_F m^2}{4\pi} \frac{1}{4\varepsilon} + \mathcal{O}(\varepsilon^0), \tag{5.110}$$

which can be directly seen from its full expression in (3.51).

Divergence in the Insertion of the p-Potential

The RG improved p-potential inserted figure 5.3c is given by

$$V_p = -p_0^{\mathrm{RGI}} \alpha(\mu) 4\pi C_F \frac{\mathbf{p}^2 + \mathbf{p}'^2}{2m^2 \mathbf{q}^2}. \tag{5.111}$$

In order to treat this potential in terms of the insertion functions from [77] as defined in equation (5.101), we employ an EOM identity:

$$\begin{aligned} &(\tilde{\mu}^{2\varepsilon})^4 \int \prod_{i=1}^{4} \left[\frac{\mathrm{d}^{d-1}\mathbf{p}_i}{(2\pi)^{d-1}} \right] G_0(\mathbf{p}_1, \mathbf{p}_2; E) \frac{\mathbf{p}_2^2 + \mathbf{p}_3^2}{2m^2 \mathbf{q}_{23}^2} G_0(\mathbf{p}_3, \mathbf{p}_4; E) = \\ &= \frac{E}{m} (\tilde{\mu}^{2\varepsilon})^4 \int \prod_{i=1}^{4} \left[\frac{\mathrm{d}^{d-1}\mathbf{p}_i}{(2\pi)^{d-1}} \right] G_0(\mathbf{p}_1, \mathbf{p}_2; E) \frac{1}{\mathbf{q}_{23}^2} G_0(\mathbf{p}_3, \mathbf{p}_4; E) \\ &\quad + \frac{\alpha(\mu)\pi C_F}{2m} (\tilde{\mu}^{2\varepsilon})^4 \int \prod_{i=1}^{4} \left[\frac{\mathrm{d}^{d-1}\mathbf{p}_i}{(2\pi)^{d-1}} \right] G_0(\mathbf{p}_1, \mathbf{p}_2; E) k(0) \frac{1}{(\mathbf{q}_{23}^2)^{\frac{1}{2}}} \left(\frac{\mu^2}{\mathbf{q}_{23}^2} \right)^{\varepsilon} G_0(\mathbf{p}_3, \mathbf{p}_4; E), \end{aligned} \tag{5.112}$$

where[8]

$$k(u) = \frac{e^{\gamma_E \varepsilon}\Gamma\left(\frac{1}{2}+u+\varepsilon\right)\Gamma\left(\frac{1}{2}-u-\varepsilon\right)\Gamma\left(\frac{1}{2}-\varepsilon\right)}{\pi^{\frac{3}{2}}\Gamma(1+u)\Gamma(1-u-2\varepsilon)}. \tag{5.113}$$

This relation has been taken from [27], where an in-depth discussion on EOM identities can be found. We are interested in the divergence of

$$\begin{aligned}\mathrm{Im}\left\{p\text{-insertion}\right\} &= \mathrm{Im}\left\{p_0^{\mathrm{RGI}}\alpha(\mu)4\pi C_F\left(\frac{E}{m}I[1]+\frac{\alpha(\mu)\pi C_F}{2m}k(0)I[\frac{1}{2}+\varepsilon]\right)\right\} = \\ &= p_0^{\mathrm{RGI}}\alpha^2(\mu)C_F^2\frac{1}{2\varepsilon}\,\mathrm{Im}\left\{G_0(E)\right\}+\mathcal{O}(\varepsilon^0).\end{aligned} \tag{5.114}$$

While the first term proportional to $I[1]$ does involve a divergence, this is the overall divergence contained in $G_0(E)$, which is not what we are interested in. It does not lead to a divergence of the type $\frac{1}{\varepsilon}\,\mathrm{Im}\{G_0(E)\}$, such that we do not consider this term further. From the second term, we obtain the second line of equation (5.114), where we employ $k(0) = 1+\mathcal{O}(\varepsilon)$ and use the divergence in $I[\frac{1}{2}+\varepsilon]$ given in equation (5.104).

Divergence in the Insertion of the Quartic Correction to the Kinetic Energy

In addition to the potential insertions discussed above, we also need to consider the quartic correction to the kinetic energy discussed in section 3.3.2. We recall that it can be treated analogously to a potential insertion by defining

$$V_{\mathrm{kin}} = -\frac{\mathbf{p}^4}{4m^3}(2\pi)^{d-1}\delta^{(d-1)}(\mathbf{q}). \tag{5.115}$$

[8] Unlike in reference [27], we have chosen to move a factor of $\mu^{2\varepsilon}$ outside of $k(u)$ to render it a dimensionless constant. This makes the formation of $\left(\frac{\mu^2}{\mathbf{q}^2}\right)^{\varepsilon}$-terms more visible.

We proceed like for the V_p-potential and again employ an EOM identity, namely [27]

$$
\begin{aligned}
&(\tilde{\mu}^{2\varepsilon})^4 \int \prod_{i=1}^{4} \left[\frac{\mathrm{d}^{d-1}\mathbf{p}_i}{(2\pi)^{d-1}}\right] G_0(\mathbf{p}_1,\mathbf{p}_2;E)(2\pi)^{d-1}\delta^{(d-1)}(\mathbf{q}_{23})\frac{\mathbf{p}_2^4}{m^3}G_0(\mathbf{p}_3,\mathbf{p}_4;E) = \\
&= \frac{E^2}{m}(\tilde{\mu}^{2\varepsilon})^3 \int \prod_{i=1}^{3} \left[\frac{\mathrm{d}^{d-1}\mathbf{p}_i}{(2\pi)^{d-1}}\right] G_0(\mathbf{p}_1,\mathbf{p}_2;E)G_0(\mathbf{p}_2,\mathbf{p}_3;E) \\
&\quad + \frac{2E}{m}(\tilde{\mu}^{2\varepsilon})^2 \int \prod_{i=1}^{2} \left[\frac{\mathrm{d}^{d-1}\mathbf{p}_i}{(2\pi)^{d-1}}\right] G_0(\mathbf{p}_1,\mathbf{p}_2;E) \\
&\quad + \frac{\alpha(\mu)8\pi C_F E}{m}(\tilde{\mu}^{2\varepsilon})^4 \int \prod_{i=1}^{4} \left[\frac{\mathrm{d}^{d-1}\mathbf{p}_i}{(2\pi)^{d-1}}\right] G_0(\mathbf{p}_1,\mathbf{p}_2;E)\frac{1}{\mathbf{q}_{23}^2}G_0(\mathbf{p}_3,\mathbf{p}_4;E) \\
&\quad + \frac{(\alpha(\mu)4\pi C_F)^2}{m}(\tilde{\mu}^{2\varepsilon})^4 \int \prod_{i=1}^{4} \left[\frac{\mathrm{d}^{d-1}\mathbf{p}_i}{(2\pi)^{d-1}}\right] G_0(\mathbf{p}_1,\mathbf{p}_2;E)\frac{k(0)}{8}\frac{1}{(\mathbf{q}_{23}^2)^{\frac{1}{2}}}\left(\frac{\mu^2}{\mathbf{q}_{23}^2}\right)^{\varepsilon} G_0(\mathbf{p}_3,\mathbf{p}_4;E).
\end{aligned}
\tag{5.116}
$$

Using this relation, we obtain

$$
\begin{aligned}
&\mathrm{Im}\{\text{kinetic correction}\} = \\
&\quad = \mathrm{Im}\left\{\frac{1}{4}\left(\frac{E^2}{m}I[\delta] + \frac{2E}{m}G_0(E) + \frac{\alpha(\mu)8\pi C_F E}{m}I[1] + \frac{(\alpha(\mu)4\pi C_F)^2}{m}\frac{k(0)}{8}I[\frac{1}{2}+\varepsilon]\right)\right\} = \\
&\quad = \alpha^2(\mu)C_F^2\frac{1}{8\varepsilon}\,\mathrm{Im}\left\{G_0(E)\right\} + \mathcal{O}(\varepsilon^0).
\end{aligned}
\tag{5.117}
$$

The first three terms do not contribute to the divergence. $I[\delta]$ denotes the contact potential

$$
I[\delta] = (\tilde{\mu}^{2\varepsilon})^3 \int \prod_{i=1}^{3} \left[\frac{\mathrm{d}^{d-1}\mathbf{p}_i}{(2\pi)^{d-1}}\right] G_0(\mathbf{p}_1,\mathbf{p}_2;E)G_0(\mathbf{p}_2,\mathbf{p}_3;E) \tag{5.118}
$$

and is finite. The second term directly contains $G_0(E)$ without an additional divergence from the vertex graph. For the third term, the same discussion as for the analogous term in diagram 5.3c holds: While these terms do contain a divergence, it is only an overall divergence from $G_0(E)$, not one related to the vertex graph, as would be relevant to us. Therefore, only the last term actually yields a divergence of the form we are interested in, which is read off from equation (5.104) and given in the second line.

This concludes the extraction of the divergences in the diagrams in figure 5.3. From these results, we now determine the divergence in c_v, which eventually leads to the running of this coefficient.

5.4.3 Full RGE for c_v

Putting all the expressions obtained above together, the full divergence of the imaginary part of the Green's function is given by

$$\mathrm{Im}\left\{G(E)\right\} = \alpha^2(\mu) C_F \left[-\frac{1}{4} b_1^{\mathrm{RGI}} + \frac{1}{2} C_F v_0^{\mathrm{RGI}} + \frac{1}{2} C_F p_0^{\mathrm{RGI}} + \frac{1}{8} C_F\right] \frac{1}{\varepsilon} \mathrm{Im}\left\{G_0(E)\right\} + \mathcal{O}\left(\varepsilon^0\right) = \tag{5.119}$$

$$\equiv g^{\left(\frac{1}{\varepsilon}\right)} \frac{1}{\varepsilon} \mathrm{Im}\left\{G_0(E)\right\} + \mathcal{O}\left(\varepsilon^0\right), \tag{5.120}$$

where the divergences are the ones contained in $\delta_2 G$. We note that at fixed order (where all scales are set equal), this divergence reduces to

$$\mathrm{Im}\left\{G(E)\right\}\Big|_{\mathrm{FO}} = \alpha^2(\mu) C_F \left[\frac{1}{4} C_A + \frac{1}{6} C_F\right] \frac{1}{\varepsilon} \mathrm{Im}\left\{G_0(E)\right\} + \mathcal{O}\left(\varepsilon^0\right). \tag{5.121}$$

As we discussed above (cf. equation (5.100)), the divergence in $\mathrm{Im}\{G(E)\}$ also provides the divergences in the matching coefficient c_v of the non-relativistic current:

$$c_v = -\frac{1}{2} g^{\left(\frac{1}{\varepsilon}\right)} \frac{1}{\varepsilon} = \tag{5.122}$$

$$= \alpha^2(\mu) C_F \left[\frac{1}{8} b_1^{\mathrm{RGI}} - \frac{1}{4} C_F v_0^{\mathrm{RGI}} - \frac{1}{4} C_F p_0^{\mathrm{RGI}} - \frac{1}{16} C_F\right]\Big|_{\varepsilon\to 0} \frac{1}{\varepsilon} + \mathcal{O}(\varepsilon^0) = \tag{5.123}$$

$$\equiv c^{\left(\frac{1}{\varepsilon}\right)} \frac{1}{\varepsilon} + \mathcal{O}(\varepsilon^0). \tag{5.124}$$

We note again that terms in the RG improved coefficients involving positive powers of ε are not included in $c_v^{\left(\frac{1}{\varepsilon}\right)}$. This has now been explicitly denoted by setting ε to zero in these terms.

From the divergence, we can now directly read off the RGE for c_v. We recall that equation (2.22) relates the coefficient of the $\frac{1}{\varepsilon}$-pole in the renormalization constant of c_v with its anomalous dimension. Using the notation introduced in that chapter, we have $Z_c^{(1)} = c^{\left(\frac{1}{\varepsilon}\right)}$. Therefore, the RGE for c_v reads

$$\mu \frac{\mathrm{d}}{\mathrm{d}\mu} c_v = -\gamma_c c_v = \left(2\alpha \frac{\partial}{\partial \alpha} c^{\left(\frac{1}{\varepsilon}\right)}\right) c_v. \tag{5.125}$$

This yields

$$\mu \frac{\mathrm{d}}{\mathrm{d}\mu} c_v = \alpha^2 C_F \left[\frac{1}{2} b_1^{\mathrm{RGI}} - C_F v_0^{\mathrm{RGI}} - C_F p_0^{\mathrm{RGI}} - \frac{1}{4} C_F\right]\Big|_{\varepsilon\to 0} c_v. \tag{5.126}$$

In this equation, c_v and α as well as the coefficients b_1^{RGI}, v_0^{RGI}, and p_0^{RGI} depend on the scale μ, which needs to be considered in the differential equation. We have explicitly checked that this RGE agrees with the one given in [34]. Some helpful relations between our notation and the one used in that work are listed in appendix B.2.

Plugging in the RG improved coefficients b_1^{RGI}, v_0^{RGI}, and p_0^{RGI} given in equations (5.94)-(5.96), the RGE for c_v takes the explicit form

$$\begin{aligned}
\mu\frac{\mathrm{d}}{\mathrm{d}\mu}c_v(\mu) = \Bigg[& -\alpha^2(\mu)C_F\left(\frac{1}{2}C_A+\frac{1}{3}C_F\right) \\
& -\alpha^2(\mu)\ln\left(\frac{\alpha(\mu)}{\alpha(\mu_{us})}\right)V_A^2\frac{4}{3\beta_0}C_F\left(C_A^2+3C_AC_F+2C_F^2\right) \\
& -\alpha^2(\mu)C_F^2\Bigg\{-\left(\frac{5}{13}+\frac{8}{13}\frac{C_F}{C_A}\right)\left[1-z^{-\frac{13}{6}C_A}\right]+\frac{5}{12}\left[1-z^{-2C_A}\right] \\
& \qquad +\left(\frac{9}{52}C_A-\frac{25}{13}C_F\right)\frac{1}{\beta_0}z^{-\beta_0}\left[1-z^{\beta_0}\right] \\
& \qquad +\left(\frac{15}{26}C_A+\frac{12}{13}C_F\right)\frac{1}{\beta_0-\frac{13}{6}C_A}z^{-\beta_0}\left[1-z^{\beta_0-\frac{13}{6}C_A}\right] \\
& \qquad -\frac{1}{4}C_A\frac{1}{\beta_0-2C_A}z^{-\beta_0}\left[1-z^{\beta_0-2C_A}\right]\Bigg\}\Bigg]c_v(\mu). \qquad (5.127)
\end{aligned}$$

We recall that z was defined as $z=\left(\frac{\alpha(\mu)}{\alpha(\mu_h)}\right)^{\frac{1}{\beta_0}}$. This RGE agrees with the one obtained by using the results of [34] together with [33].

The first line in (5.127) collects the terms already appearing in the fixed-order calculation. It agrees with the RGE given for example in [19] and corresponds to the μ-dependence of the terms not multiplied by β_0 in the fixed-order expression of $c_v^{(2)}$, namely (cf. equation (4.6))

$$c_v^{(2),\mathrm{FO}} \supset C_F\pi^2\left(-4C_A-\frac{8}{3}C_F\right)\ln\left(\frac{\mu^2}{m^2}\right). \qquad (5.128)$$

Including the ultrasoft and hard running provides additional terms to this RGE. The terms caused by the ultrasoft running are gathered in the second line, while the term starting from the third line collects the effect of the hard running.

We have now determined the full RGE for the potential running encoded in the coefficient c_v, taking into account the hard and ultrasoft running discussed in sections 5.2 and 5.3, respectively. What remains to be done is to solve this RGE, which we will do in the next section.

5.4.4 Solving the RGE for c_v

When solving the RGE (5.127), we evolve the hard matching coefficient c_v of the non-relativistic current from the hard scale μ_h to the common scale μ, analogously to the procedure performed for the hard matching coefficients d_i and d_{ij} in the Lagrangian. However, now an additional complication arises compared to the previous discussion. The right-hand side of the differential equation contains the strong coupling α evaluated at the hard and ultrasoft scale μ_h and μ_{us}, respectively. Naively, these are just the initial conditions of the hard and ultrasoft running, which can be seen as constant. However, when performing the evolution of c_v, we need to ensure that the ultrasoft scale μ_{us} stays below the soft scale μ at all times, since otherwise, the hierarchy of scales defining the EFT would no longer be fulfilled. The scales are implicitly related by $\mu_{us} \sim mv^2$ and $\mu \sim mv$, such that we can correlate them like $\mu_{us} = \frac{\mu^2}{\mu_h}$ (where $\mu_h \sim m$), as suggested in [19]. This procedure is also adopted in [34]. We can loosen the correlation constraint slightly by introducing a variable factor $k \sim \mathcal{O}(1)$, such that the correlation reads

$$\mu_{us} = k\frac{\mu^2}{\mu_h}. \tag{5.129}$$

Correlating the scales in this manner also yields a correlation between the coupling constant α at different scales. We eliminate $\alpha(\mu_{us})$ from the RGE for c_v using the following relation:

$$\begin{aligned}\frac{\alpha(\mu)}{\alpha(\mu_{us})} &= 1 + \alpha(\mu)\frac{\beta_0}{4\pi}\ln\left(\frac{\mu_{us}^2}{\mu^2}\right) + \mathcal{O}(\alpha^2\log) = \\ &= 1 + \alpha(\mu)\frac{\beta_0}{4\pi}\ln\left(\frac{\mu^2}{\mu_h^2}\right) + \alpha(\mu)\frac{\beta_0}{4\pi}\ln\left(k^2\right) + \mathcal{O}(\alpha^2\log).\end{aligned} \tag{5.130}$$

Here, we have used the one-loop running of α defined in equation (2.13) and explicitly denoted subleading terms scaling like $\mathcal{O}(\alpha^2\log)$, where log stands for a large logarithm involving a large ratio of scales. Since $\alpha^2\log$ is counted as $\mathcal{O}(\alpha)$, these neglected terms are of the same order as $\alpha(\mu)\ln\left(k^2\right)$, where the logarithm is not large. Therefore, we can safely neglect the effect of the factor k in the correlation when we are only interested in considering the correlation at one-loop running of α. Lastly, we use that

$$z^{\beta_0} = \frac{\alpha(\mu)}{\alpha(\mu_h)} = 1 - \alpha(\mu)\frac{\beta_0}{4\pi}\ln\left(\frac{\mu^2}{\mu_h^2}\right) + \mathcal{O}(\alpha^2\log) \tag{5.131}$$

and rewrite

$$\frac{\alpha(\mu)}{\alpha(\mu_{us})} = 2 - z^{\beta_0} + \mathcal{O}(\alpha^2\log). \tag{5.132}$$

This replaces $\alpha(\mu_{us})$ by an expression in terms of $\alpha(\mu)$ and $\alpha(\mu_h)$. Using this in the RGE (5.127) yields a differential equation in μ where the only μ-dependence is contained in $\alpha(\mu)$. We can therefore replace

$$\mu\frac{\mathrm{d}}{\mathrm{d}\mu}c_v(\mu) = \mu\frac{\mathrm{d}\alpha(\mu)}{\mathrm{d}\mu}\frac{\partial}{\partial\alpha(\mu)}c_v\left(\alpha(\mu)\right) = -\alpha^2(\mu)\frac{\beta_0}{2\pi}\frac{\partial}{\partial\alpha(\mu)}c_v\left(\alpha(\mu)\right) \tag{5.133}$$

and solve the RGE in terms of $\alpha(\mu)$. We obtain the following expression for the resummed coefficient c_v:

$$\begin{aligned}
c_v(\mu) &= c_v(\mu_h) \\
&\quad\times\exp\Bigg\{\alpha(\mu_h)\left[1-z^{\beta_0}\right]\frac{\pi C_F\left(C_AC_F(9C_A-100C_F)+\beta_0(-26C_A^2-19C_AC_F+32C_F^2)\right)}{26C_A\beta_0^2} \\
&\quad+\alpha(\mu_h)\left[1-z^{\beta_0}\right]V_A^2\frac{8\pi C_F(C_A+C_F)(C_A+2C_F)}{3\beta_0^2} \\
&\quad+\alpha(\mu_h)\left[2-z^{\beta_0}\right]\ln\left(\frac{1}{2-z^{\beta_0}}\right)V_A^2\frac{8\pi C_F(C_A+C_F)(C_A+2C_F)}{3\beta_0^2} \\
&\quad+\alpha(\mu_h)\left[1-z^{\beta_0-\frac{13}{6}C_A}\right]\frac{24\pi C_F^2(5C_A+8C_F)(11C_A-3\beta_0)}{13C_A(13C_A-6\beta_0)^2} \\
&\quad+\alpha(\mu_h)\left[1-z^{\beta_0-2C_A}\right]\frac{\pi C_F^2(-13C_A+5\beta_0)}{6(2C_A-\beta_0)^2} \\
&\quad+\alpha(\mu_h)\ln\left(z^{\beta_0}\right) \\
&\qquad\times\frac{\pi C_F^2\left(C_A^2(9C_A-100C_F)+2C_A\beta_0(-8C_A+37C_F)+6\beta_0^2(C_A-2C_F)\right)}{\beta_0^2(13C_A-6\beta_0)(2C_A-\beta_0)}\Bigg\}.
\end{aligned} \tag{5.134}$$

The expressions in the third and fourth lines are multiplied by $V_A^2 = 1$. As mentioned before, this coefficient tracks the contribution from the ultrasoft running.

Instead of using this exponentiated form of the resummed c_v, it is more convenient for further considerations in this work (especially for the numerical implementation of the resummation effects) to only use terms up to $\mathcal{O}(\alpha)$. That is, we expand the exponential in $\alpha(\mu_h)$ while

keeping the terms involving z, which encode the resummation. We obtain

$$\begin{aligned}
c_v(\mu) = &\left(1 + \frac{\alpha(\mu_h)}{4\pi} c_v^{(1),\mathrm{FO}}(\mu_h)\right) \\
&+ \alpha(\mu_h)\left[1 - z^{\beta_0}\right] \frac{\pi C_F \left(C_A C_F (9C_A - 100C_F) + \beta_0(-26C_A^2 - 19C_A C_F + 32C_F^2)\right)}{26 C_A \beta_0^2} \\
&+ \alpha(\mu_h)\left[1 - z^{\beta_0}\right] V_A^2 \frac{8\pi C_F (C_A + C_F)(C_A + 2C_F)}{3\beta_0^2} \\
&+ \alpha(\mu_h)\left[2 - z^{\beta_0}\right] \ln\left(\frac{1}{2 - z^{\beta_0}}\right) V_A^2 \frac{8\pi C_F (C_A + C_F)(C_A + 2C_F)}{3\beta_0^2} \\
&+ \alpha(\mu_h)\left[1 - z^{\beta_0 - \frac{13}{6} C_A}\right] \frac{24\pi C_F^2 (5C_A + 8C_F)(11C_A - 3\beta_0)}{13 C_A (13C_A - 6\beta_0)^2} \\
&+ \alpha(\mu_h)\left[1 - z^{\beta_0 - 2C_A}\right] \frac{\pi C_F^2 (-13C_A + 5\beta_0)}{6(2C_A - \beta_0)^2} \\
&+ \alpha(\mu_h) \ln\left(z^{\beta_0}\right) \frac{\pi C_F^2 \left(C_A^2 (9C_A - 100C_F) + 2C_A \beta_0 (-8C_A + 37C_F) + 6\beta_0^2 (C_A - 2C_F)\right)}{\beta_0^2 (13C_A - 6\beta_0)(2C_A - \beta_0)} \\
&+ \mathcal{O}(\alpha^2),
\end{aligned} \tag{5.135}$$

which agrees with the result given in references [32, 34].

The reason for using this expression is that it only encodes the resummation of NLL logarithms but no subleading logarithms. While the exponentiated version (5.134) has the advantage of also providing partial resummation of some subleading logarithms, this would complicate the structure of the calculation. Especially the subtraction of otherwise double-counted logarithms, which we will discuss in the next section, would be a lot less clear. Since in this work we are only interested in the effect of NLL resummation, we prefer to drop any additional information obtained from partial resummation of subleading logarithms and work with the expression where the exponential has been expanded.

Similar to the hard and ultrasoft running, we write this correction obtained from the potential running as an additive modification of the fixed-order result, this time to the one-loop matching coefficient $c_v^{(1),\mathrm{FO}}$:

$$\begin{aligned}
c_v^{(1),\mathrm{RGI}} &= c_v^{(1),\mathrm{FO}} + c_v^{(1),\mathrm{RGI}} - c_v^{(1),\mathrm{FO}} = \\
&\equiv c_v^{(1),\mathrm{FO}} + c_v^{(1),\mathrm{RG}}.
\end{aligned} \tag{5.136}$$

To achieve this, we subtract the fixed-order expression

$$1 + \frac{\alpha(\mu)}{4\pi} c_v^{(1),\mathrm{FO}}(\mu) \tag{5.137}$$

up to $\mathcal{O}(\alpha)$, such that the first line in (5.135) and the subtraction term combine to

$$\left(1 + \frac{\alpha(\mu_h)}{4\pi} c_v^{(1),\mathrm{FO}}(\mu_h)\right) - \left(1 + \frac{\alpha(\mu)}{4\pi} c_v^{(1),\mathrm{FO}}(\mu)\right) = \frac{\alpha(\mu_h)}{4\pi}\left[1 - z^{\beta_0}\right] c_v^{(1),\mathrm{FO}}(\mu_h). \tag{5.138}$$

We now observe that all terms correcting the fixed-order result scale like $\alpha(\mu_h)$, which justifies writing it as a correction to $c_v^{(1),\mathrm{FO}}(\mu)$. Accounting for the overall factor of $\frac{\alpha(\mu)}{4\pi}$, we obtain

$$\begin{aligned}
c_v^{(1),\mathrm{RG}} = \frac{4\pi}{\alpha(\mu)} \times \Bigg\{ & \frac{\alpha(\mu_h)}{4\pi}\left[1 - z^{\beta_0}\right] c_v^{(1),\mathrm{FO}}(\mu_h) \\
& + \alpha(\mu_h)\left[1 - z^{\beta_0}\right] \frac{\pi C_F \left(C_A C_F (9C_A - 100C_F) + \beta_0(-26C_A^2 - 19C_A C_F + 32C_F^2)\right)}{26 C_A \beta_0^2} \\
& + \alpha(\mu_h)\left[1 - z^{\beta_0}\right] V_A^2 \frac{8\pi C_F (C_A + C_F)(C_A + 2C_F)}{3\beta_0^2} \\
& + \alpha(\mu_h)\left[2 - z^{\beta_0}\right] \ln\left(\frac{1}{2 - z^{\beta_0}}\right) V_A^2 \frac{8\pi C_F (C_A + C_F)(C_A + 2C_F)}{3\beta_0^2} \\
& + \alpha(\mu_h)\left[1 - z^{\beta_0 - \frac{13}{6}C_A}\right] \frac{24\pi C_F^2 (5C_A + 8C_F)(11C_A - 3\beta_0)}{13 C_A (13C_A - 6\beta_0)^2} \\
& + \alpha(\mu_h)\left[1 - z^{\beta_0 - 2C_A}\right] \frac{\pi C_F^2 (-13C_A + 5\beta_0)}{6(2C_A - \beta_0)^2} \\
& + \alpha(\mu_h) \ln\left(z^{\beta_0}\right) \\
& \quad \times \frac{\pi C_F^2 \left(C_A^2 (9C_A - 100C_F) + 2C_A \beta_0 (-8C_A + 37C_F) + 6\beta_0^2 (C_A - 2C_F)\right)}{\beta_0^2 (13C_A - 6\beta_0)(2C_A - \beta_0)} \Bigg\}.
\end{aligned} \tag{5.139}$$

This result completes the RG improvements necessary for determining the R-ratio at NLL, which we discuss in the next section.

5.5 The R-Ratio at NLL

5.5.1 Incorporation the Resummation Correction into the R-Ratio

We conclude this chapter by relating the results obtained in the previous sections with the RG improvement of the R-ratio discussed in section 4.4.

As we have discussed extensively above, the quantities encoding the RG improvement are given by a_2^{RGI}, b_1^{RGI}, v_0^{RGI}, and p_0^{RGI} (cf. section 5.3.3), as well as $c_v^{(1),\mathrm{RGI}}$ (cf. section 5.4.4). The first four contribute to δV_2, which first arises in the R-ratio in $\delta_2 G(E)$ at NNLO, see equation (4.22). However, $c_v^{(1),\mathrm{RGI}}$ already modifies the R-ratio at NLO as given in equation (4.21). Therefore, this is the quantity necessary for determining the first RG correction. In fact, a_2^{RGI}, b_1^{RGI}, v_0^{RGI}, and p_0^{RGI} were only relevant to determine the full potential running encoded in $c_v^{(1),\mathrm{RGI}}$ and will not be used themselves in the R-ratio.

Therefore, the leading RG correction is encoded in the R-ratio solely by substituting

$$2c_{v,1}\,\mathrm{Im}\{G_0(E)\} \;\longrightarrow\; 2\frac{\alpha(\mu)}{4\pi}c_v^{(1),\mathrm{RGI}}\,\mathrm{Im}\{G_0(E)\} = 2\frac{\alpha(\mu)}{4\pi}\left(c_v^{(1),\mathrm{FO}} + c_v^{(1),\mathrm{RG}}\right)\mathrm{Im}\{G_0(E)\} \tag{5.140}$$

in equation (4.21).

This corresponds to the NLL contribution, while the LL contribution is zero. This is explicitly seen by observing that $c_v^{(1),\mathrm{RG}}$ resums terms like $\alpha^n \log^n$, which are multiplied by the overall factor of α accompanying $c_v^{(1)}$ in the R-ratio. Therefore, in the R-ratio, the resummed terms are actually of the form $\alpha^{n+1}\log^n$.

5.5.2 Crosscheck: Reexpanding the Resummed Result

Reexpanding the resummed result $c_v^{(1),\mathrm{RG}}$ in α provides a cross-check of our calculation.[9] This should exactly reproduce the large single (double) logarithms in the second (third) order R-ratio. To confirm this, we count

$$\mu_h \sim m,\ \mu \sim m\alpha,\ \mu_{us} \sim m\alpha^2, \tag{5.141}$$

such that the large logarithms read

$$\ln\left(\frac{\mu^2}{\mu_h^2}\right) \sim 2\ln(\alpha), \tag{5.142}$$

$$\ln\left(\frac{\mu^2}{\mu_{us}^2}\right) \sim -2\ln(\alpha), \tag{5.143}$$

$$\ln\left(\frac{\mu}{m}\right) \sim \ln(\alpha), \tag{5.144}$$

[9] For the reexpansion in α, we use the one-loop running (2.13) of the coupling. This is sufficient for our discussion since we are not interested in subleading logarithms related to higher-order coefficients of the β-function $(\beta_1, \beta_2, \dots)$. In the numerical analysis, this choice will lead to a small artefact, as we discuss in section 6.2.3.

where all factors of α are implicitly understood to be evaluated at the scale μ. After reexpanding and using this counting, the resummed expression yields

$$\begin{aligned}
2c_v^{(1),\mathrm{RG}}\,\mathrm{Im}\{G_0(E)\} &= \\
&= \left(\frac{\alpha}{4\pi}\right)^2 \ln(\alpha)\left[4\beta_0 c_v^{(1),\mathrm{FO}}(\mu_h) + C_F\pi^2\left(-16C_A - \frac{32}{3}C_F\right)\right]\mathrm{Im}\{G_0(E)\} \\
&\quad + \left(\frac{\alpha}{4\pi}\right)^3 \ln^2(\alpha)\Bigg[8\beta_0^2 c_v^{(1),\mathrm{FO}}(\mu_h) + C_F\pi^2\beta_0\left(-32C_A - \frac{64}{3}C_F\right) \\
&\qquad + C_F\pi^2 V_A^2\left(-\frac{128}{3}C_A^2 - 128C_AC_F - \frac{256}{3}C_F^2\right) + C_F\pi^2\left(-16C_AC_F - \frac{32}{3}C_F^2\right)\Bigg] \\
&\qquad \times \mathrm{Im}\{G_0(E)\} + \mathcal{O}(\alpha^4) = \qquad (5.145) \\
&= \left(\frac{\alpha}{4\pi}\right)^2 \ln(\alpha)\left[4\beta_0 c_v^{(1),\mathrm{FO}}(\mu_h) + C_F\pi^2\left(-16C_A - \frac{32}{3}C_F\right)\right]\mathrm{Im}\{G_0(E)\} \\
&\quad + \left(\frac{\alpha}{4\pi}\right)^3 \ln^2(\alpha)\Bigg[8\beta_0^2 c_v^{(1),\mathrm{FO}}(\mu_h) + C_F\pi^2\beta_0\left(-32C_A - \frac{64}{3}C_F\right) \\
&\qquad + C_F\pi^2\left(-\frac{128}{3}C_A^2 - 144C_AC_F - 96C_F^2\right)\Bigg]\mathrm{Im}\{G_0(E)\} + \mathcal{O}(\alpha^4), \qquad (5.146)
\end{aligned}$$

where we have set $V_A = 1$ in the last line.

The NNLO logarithms directly correspond to the large logarithms in $2c_{v,2}\,\mathrm{Im}\{G_0(E)\}$ in R_{NNLO} (cf. equation (4.22)), as can be seen by comparing to the fixed-order matching coefficient $c_v^{(2),\mathrm{FO}}$ given in equation (4.6). We note that in the RGE for c_v, the terms responsible for these second-order logarithms are entirely made up of terms already present at fixed order, which are written in the first line of equation (5.127).

For the NNNLO logarithms in equation (4.23), the structure is a bit more involved: Both the term $2c_{v,3}\,\mathrm{Im}\{G_0(E)\}$ as well as $\mathrm{Im}\{\delta_3 G(E)\}$ contain large double logarithms. For the former, we read off from equation (4.7) that the large logarithms are given by

$$\begin{aligned}
2c_{v,3}\,\mathrm{Im}\{G_0(E)\} \supset \left(\frac{\alpha}{4\pi}\right)^3 \ln^2(\alpha)\Bigg\{&8\beta_0^2 c_v^{(1),\mathrm{FO}}(m) + C_F\pi^2\beta_0\left(-32C_A - \frac{64}{3}C_F\right) \\
&+ C_F\pi^2[-32C_A^2 - 120C_AC_F - 80C_F^2]\Bigg\}\mathrm{Im}\{G_0(E)\}. \qquad (5.147)
\end{aligned}$$

Regarding $\mathrm{Im}\{\delta_3 G(E)\}$, both the ultrasoft interaction $\delta_3^{us} G(E)$ and the non-Coulomb potentials contain large double logarithms. For $\delta_3^{us} G(E)$, we can read off the large double logarithms from [62]. In this reference, C_F and C_A have been set to their numerical values. However, we can infer the colour structure from the large double logarithms contained in the wave function

at the origin, which are given in [61]. This yields

$$\begin{aligned}\delta_3^{us} G(E) \supset \frac{\alpha^3}{\pi} C_F \Bigg\{ & \left[-2C_A^2 - \frac{16}{3} C_A C_F - \frac{8}{3} C_F^2\right] \ln^2(\alpha) \\ & + \left[-\frac{5}{6} C_A^2 - \frac{11}{6} C_A C_F - \frac{1}{3} C_F^2\right] \ln^2\left(\frac{\mu}{m}\right) \\ & + \left[\frac{8}{3} C_A^2 + \frac{20}{3} C_A C_F + \frac{8}{3} C_F^2\right] \ln(\alpha) \ln\left(\frac{\mu}{m}\right) \Bigg\} G_0(E). \end{aligned} \tag{5.148}$$

Counting $\ln\left(\frac{\mu}{m}\right) \sim \ln(\alpha)$ and pulling out a factor of $\left(\frac{\alpha}{4\pi}\right)^3$, we obtain

$$\operatorname{Im}\{\delta_3^{us} G(E)\} \supset \left(\frac{\alpha}{4\pi}\right)^3 \ln^2(\alpha) C_F \pi^2 \left[-\frac{32}{3} C_A^2 - 32 C_A C_F - \frac{64}{3} C_F^2\right] \operatorname{Im}\{G_0(E)\}. \tag{5.149}$$

Lastly, we consider the large logarithms in $\delta_3^{nC} G(E)$, where the superscript "nC" stands for "non-Coulomb". Inferring them from the non-Coulomb correction to the wave function given in [79] analogously to the ultrasoft expression we just discussed, we obtain

$$\operatorname{Im}\{\delta_3^{nC} G(E)\} \supset \left(\frac{\alpha}{4\pi}\right)^3 \ln^2(\alpha) C_F \pi^2 \left[8 C_A C_F + \frac{16}{3} C_F^2\right] \operatorname{Im}\{G_0(E)\}. \tag{5.150}$$

Taking the expressions for $2c_{v,3} \operatorname{Im}\{G_0(E)\}$, $\operatorname{Im}\{\delta_3^{us} G(E)\}$, and $\operatorname{Im}\{\delta_3^{nC} G(E)\}$ together, we obtain the following double logarithms in the R-ratio at NNNLO (cf. equation (4.23)):

$$\begin{aligned} & 2c_{v,3} \operatorname{Im}\{G_0(E)\} + \operatorname{Im}\{\delta_3^{us} G(E)\} + \operatorname{Im}\{\delta_3^{nC} G(E)\} \supset \\ & \quad \left(\frac{\alpha}{4\pi}\right)^3 \ln^2(\alpha) \Bigg\{ 8\beta_0^2 c_v^{(1),\mathrm{FO}}(m) + C_F \pi^2 \beta_0 \left(-32 C_A - \frac{64}{3} C_F\right) \\ & \qquad + C_F \pi^2 \left[-\frac{128}{3} C_A^2 - 144 C_A C_F - 96 C_F^2\right] \Bigg\} \operatorname{Im}\{G_0(E)\}. \end{aligned} \tag{5.151}$$

Since the other terms in R_{NNNLO} do not contain any large double logarithms, this confirms the reproduction of logarithms from equation (5.146) and concludes the check.

5.5.3 Subtracting Double Counted Logarithms from the R-Ratio

The logarithms reproduced by reexpanding the resummed R-ratio are at the same time already included in the fixed-order R-ratio. Therefore, to avoid double counting, these logarithms have to be subtracted. To be precise, reexpanding $c_v^{(1),\mathrm{RGI}}$ reproduces logarithms of the form $\ln\left(\frac{\mu}{\mu_h}\right)$, which is the quantity we will subtract. The logarithms that need to be subtracted

read:

$$c_v^{(2),\mathrm{FO}}: \quad \left\{2\beta_0 c_v^{(1),\mathrm{FO}}(\mu_h) + C_F\pi^2\left[-8C_A - \frac{16}{3}C_F\right]\right\}\ln\left(\frac{\mu}{\mu_h}\right), \tag{5.152}$$

$$c_v^{(3),\mathrm{FO}}: \quad \left\{4\beta_0^2 c_v^{(1),\mathrm{FO}}(\mu_h) + C_F\pi^2\beta_0\left[-16C_A - \frac{32}{3}C_F\right] + C_F\pi^2\left[-16C_A^2 - 60C_AC_F - 40C_F^2\right]\right\}\ln^2\left(\frac{\mu}{\mu_h}\right), \tag{5.153}$$

$$\delta_3^{us}G(E): \quad \left(\frac{\alpha}{4\pi}\right)^3 C_F\pi^2\left[-\frac{32}{3}C_A^2 - 32C_AC_F - \frac{64}{3}C_F^2\right]\ln^2\left(\frac{\mu}{\mu_h}\right)G_0(E), \tag{5.154}$$

$$\delta_3^{nC}G(E): \quad \left(\frac{\alpha}{4\pi}\right)^3 C_F\pi^2\left[8C_AC_F + \frac{16}{3}C_F^2\right]\ln^2\left(\frac{\mu}{\mu_h}\right)G_0(E). \tag{5.155}$$

This result poses the end of the analytical calculation performed in this thesis. In the next chapter, we will apply our findings by performing a numerical analysis of the R-ratio at NLL.

Chapter 6

Numerical Analysis of the R-Ratio at NLL

6.1 Numerical Implementation of the NLL Correction

We conclude this thesis by applying the findings of the previous chapters to a numerical analysis of the R-ratio at NLL. We start from the `TTbarXSection` code, which implements the calculation of the top anti-top cross section near threshold up to NNNLO. In this code, we implement the NLL contribution by modifying the R-ratio as described in equation (5.140), using expression (5.139) for the RG improved coefficient $c_v^{(1),\mathrm{RG}}$. Details on the implementation are provided in appendix D. Eventually, the results of this thesis will be incorporated into the `QQbar_threshold` code [42] in an analogous manner, which has however not been done yet.

For the following numerical results, we always use the default call

```
TTbarXSection[sqrts - 2*171.5, {{musoft, 350}, {muhard}},
Constants -> {171.5, 1.33, 0.1181}, Order -> {order, logorder},
MassDef -> "PSshift", BeyondQCD -> {"None"}, ResonantOnly -> True,
Production -> "SWaveOnly", Rratio -> True].
```

This uses the following constants:

$$\begin{aligned}
m_t^{\mathrm{PS}} &= 171.5\,\mathrm{GeV} && \text{Top mass in the PS shift scheme,}[1] \\
\mu_w &= 350\,\mathrm{GeV} && \text{Finite width scale related to non-resonant contributions,} \\
\Gamma &= 1.33\,\mathrm{GeV} && \text{Width of the top quark,} \\
\alpha(m_Z) &= 0.1181 && \text{Strong coupling at the mass of the Z-boson.}
\end{aligned} \tag{6.1}$$

The desired fixed-order precision is specified via the parameter `order`, where the possible values are 0, 1, 2, and 3. The inclusion of resummation results is determined through the parameter `logorder`, which is set to `"NLL"` for the inclusion of NLL improvements and to `"None"` when this resummation should not be considered. We have also allowed for the use of the truncated log-series instead of the full NLL result, as we describe in appendix D. As described in section 5.5.3, there are large logarithms at NNLO and NNNLO that would be double counted when the RG improvement is simply added to the fixed-order results. The code automatically accounts for this by subtracting these large logarithms.

The center-of-mass energy $\sqrt{s}$, as well as the soft and hard scale, are set individually via `sqrts`, `musoft`, and `muhard`, respectively. Note the use of two sets of brackets when defining the scales in the default call. This is only necessary for the NLL case, where (besides μ_s and μ_w) the hard scale μ_h must also be set to a specific value. When no resummation is asked for, it is enough to fix μ_s and μ_w. In that case, the original syntax of the `TTbarXSection` code before the implementation of RG improvements still holds. A more in-depth description is again provided in appendix D.

In this work, we do not consider EW, QED or Higgs effects and focus on the pure QCD result. We also discard non-resonant contributions as well as the axial coupling to the Z-boson, which is achieved through the `ResonantOnly -> True` and `"SWaveOnly"`-commands. Finally, we will analyse the R-ratio instead of the cross section, which is the reason for setting `Rratio -> True`.

6.2 Numerical Results

In the following, we analyse the effect of the inclusion of NLL contributions on the R-ratio. We are particularly interested in the scale dependence of the results. For the fixed-order calculation,

[1] The PS shift scheme is a mass scheme suitable for dealing with IR divergences in the pole mass. The index "PS" stands for "potential-subtracted" and indicates that divergent contributions related to the Coulomb potential are subtracted [88]. Based on this method, the PS shift scheme then allows to calculate the cross section in the pole scheme while still avoiding the IR divergences [77].

a breakdown of perturbation theory at small scales μ_s is observed, starting already at values of $\mu_s \lesssim 40\,\text{GeV}$ [26, 77, 78]. This is particularly notable since a natural scale choice for the top anti-top pair would be $\mu_s \sim 20\,\text{GeV}$. Including the NLL effects, we observe an overall reduction of the scale dependence and an increased stability for small values of μ_s. Additionally, we assess the behaviour of the truncated, reexpanded series of logarithms. This allows us to analyse the convergence behaviour of the log-series and gives us an opportunity to gauge the size of the non-logarithmic contributions at NNLO and NNNLO.

Our analysis will not consider LO results but instead focus on NLO and higher orders. The reason for this is twofold: On the one hand, the LO result does not provide an accurate description of top anti-top pair production since higher-order corrections have a large impact. On the other hand, the resummation effects considered in this thesis only start at NLL (there are no LL contributions), such that the natural starting point for our analysis is at NLO.

6.2.1 Qualitative Look at the Scale Dependence for NLO+NLL

We start by comparing the R-ratio at NLO and at NLO+NLL for different values of μ_s. Figure 6.1 shows the R-ratio as a function of the center-of-mass energy $\sqrt{s}$ both at NLO and at NLO+NLL, where the soft scale μ_s is varied between 20 GeV and 80 GeV in steps of 10 GeV in progressively lighter shades of blue and red, respectively. The range of the soft scale is chosen such that the lower bound $\mu_s = 20\,\text{GeV}$ corresponds to the natural choice for the top anti-top pair. However, as we will see, perturbation theory is not valid for this value of μ_s. At the upper bound $\mu_s = 80\,\text{GeV}$, perturbation theory is reliable, and at the same time, this choice still fulfils the hierarchy $\mu_{us} \ll \mu_s \ll \mu_h$. The top mass is set to $m = 171.5\,\text{GeV}$ according to the PS shift scheme, as we mentioned for the default call above. The hard scale is fixed at $\mu_h = 180\,\text{GeV}$. This choice is consistent with the natural choice of $\mu_h \sim m$ and still captures some effects of the logarithms $\ln\left(\frac{\mu_h}{m}\right)$.

For small values of μ_s, the fixed-order NLO R-ratio strongly depends on the scale. This is caused by the aforementioned breakdown of perturbation theory. In contrast, for the NLO+NLL R-ratio including the RG improvements determined in this thesis, the overall scale dependence is reduced significantly. While for $\mu_s = 20\,\text{GeV}$, we still observe a large deviation, all larger values of μ_s result in similar curves. The same behaviour has been found in reference [35], where μ_s is varied between 30 GeV and 80 GeV. We observe from figure 6.1 that for the NLO result, the largest values of R (for the range of μ_s considered above) are mostly obtained for soft scales around the maximum $\mu_s = 80\,\text{GeV}$, while for the case including NLL corrections, the maximum of R is mostly obtained for $\mu_s \sim 50\,\text{GeV}$. We also note an overall increase of the

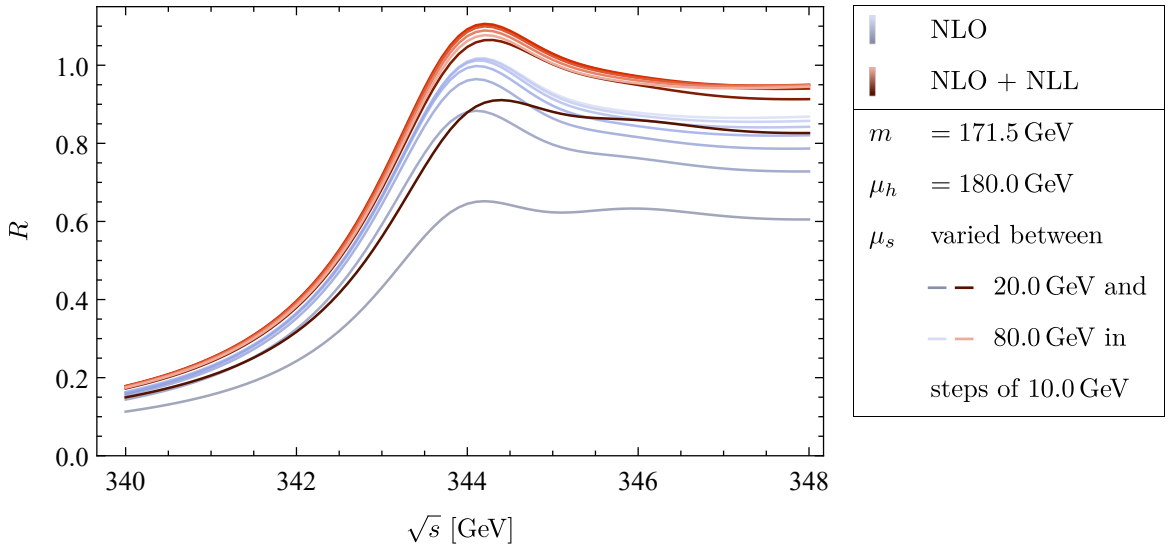

Figure 6.1: R-ratio at NLO (blue) and NLO+NLL (red) for center-of-mass energies $\sqrt{s}$ around the top anti-top production threshold. The soft scale μ_s is varied between 20 GeV and 80 GeV in steps of 10 GeV in progressively lighter shades of colour. The top mass is set to $m = 171.5\,\text{GeV}$, while for the hard scale $\mu_h = 180\,\text{GeV}$ is used.

R-ratio when including the NLL effects. This increase is in accordance with the NNLO R-ratio, which is larger than the one at NLO. We will discuss this in more detail in section 6.2.2.

Keeping the parameters the same, we now normalize the R-ratio at NLO and at NLO+NLL to its respective value at the midpoint $\mu_s = 50\,\text{GeV}$. The result is shown in figure 6.2, which compares the NLO result (upper panel) and the NLO+NLL expression (lower panel) for the R-ratio. The entire shaded regions (including both light and dark shaded areas) correspond to a scale variation between 20 GeV and 80 GeV. In contrast, the darker regions represent a variation of μ_s between 50 GeV and 80 GeV. The axes of the two panels are scaled the same to facilitate an easier comparison. The reduction of the scale dependence for small μ_s achieved by incorporating NLL corrections is now particularly visible.

Apart from the dependence on the soft scale, the R-ratio at NLO+NLL also depends on the hard scale μ_h. However, this dependence is minimal in comparison, as we demonstrate in figure 6.3, where we fix the soft scale to $\mu_s = 50\,\text{GeV}$ and vary μ_h between 150 GeV and 210 GeV in steps of 10 GeV. We observe only a weak dependence of the R-ratio on the hard scale.

In the same way, we are interested in the dependence on the ultrasoft scale μ_{us}. Since the scales have been correlated when solving the RGE for the coefficient c_v, we cannot consider

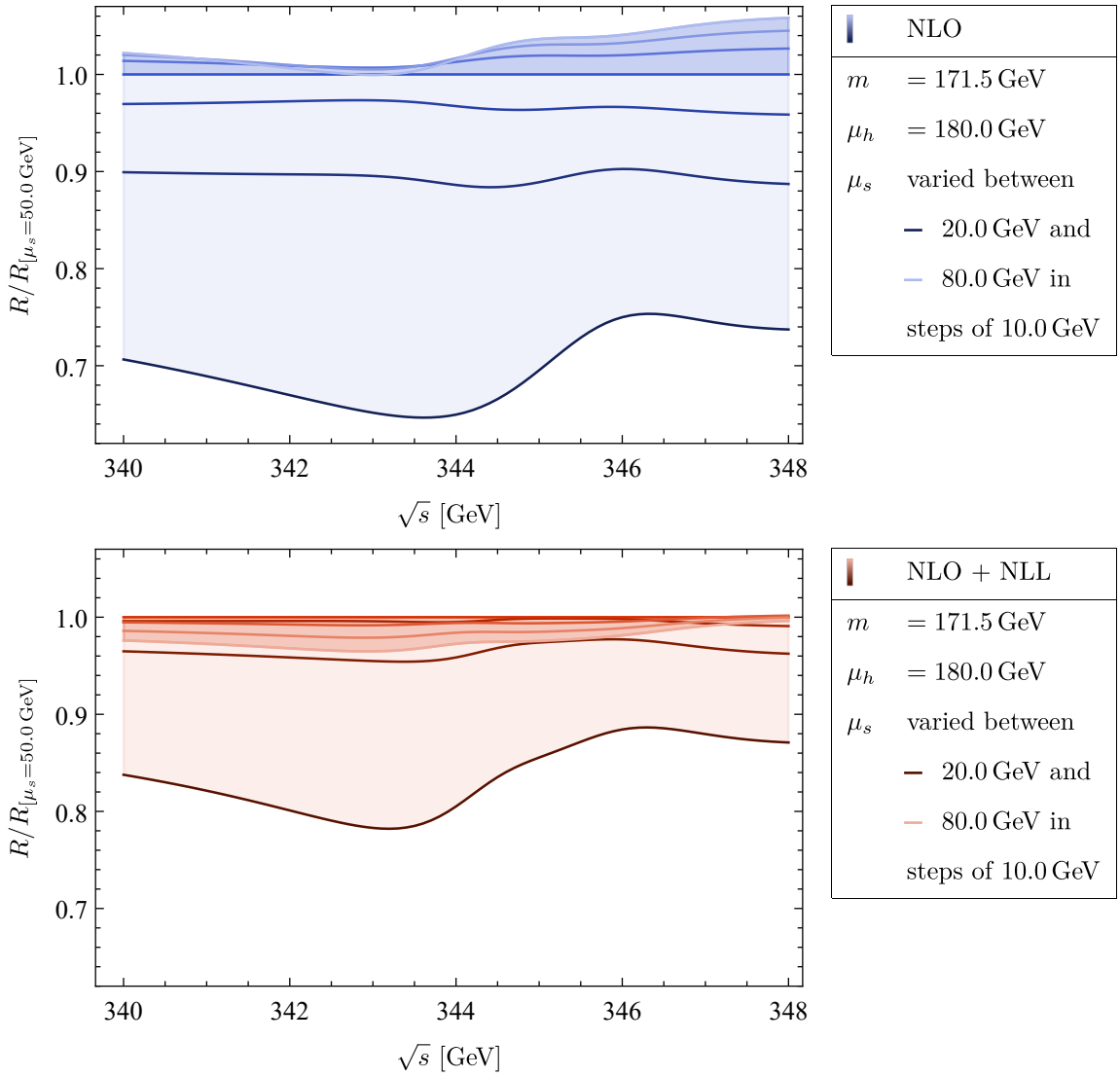

Figure 6.2: R-ratio at NLO (lower panel: NLO+NLL) normalized to its value for $\mu_s = 50\,\text{GeV}$. The lines denote the normalized R-ratio for different values of μ_s, which is varied between 20 GeV and 80 GeV in steps of 10 GeV and depicted in progressively lighter shades of blue (red). The entire shaded regions (including both light and dark shaded areas) correspond to a variation of μ_s in the full parameter region of 20 GeV to 80 GeV, while the dark shaded regions show a variation of μ_s between 50 GeV and 80 GeV. The top mass and hard scale are fixed at $m = 171.5\,\text{GeV}$ and $\mu_h = 180\,\text{GeV}$, respectively.

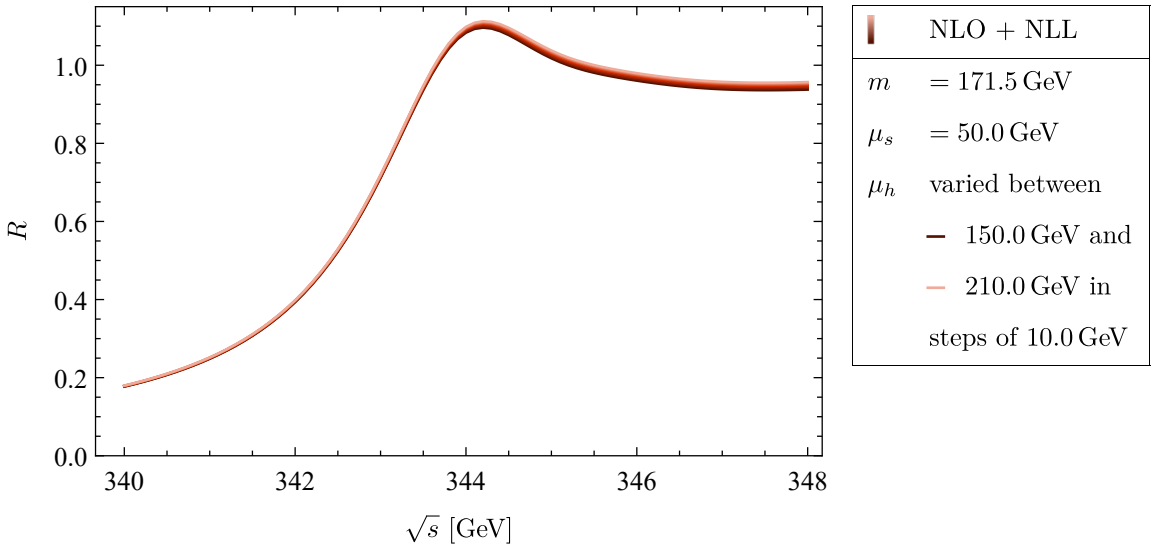

Figure 6.3: R-ratio at NLO+NLL with variation of the hard scale μ_h. The soft scale is fixed to $\mu_s = 50\,\text{GeV}$. μ_h is varied between 150 GeV and 210 GeV in steps of 10 GeV in progressively lighter shades of red.

the variation of the ultrasoft scale $\mu_{us} = \frac{\mu_s^2}{\mu_h}$ independently. However, using this correlation, we note that the variation of μ_h between 150 GeV and 210 GeV in figure 6.3 corresponds to a variation of μ_{us} between 11.9 GeV and 16.7 GeV for $\mu_s = 50\,\text{GeV}$. That is, a small change in μ_{us} is sufficient to cause the same effect on the R-ratio as a much larger variation of μ_h. This makes sense intuitively: The R-ratio is much more sensitive to a variation of μ_{us} than of μ_h because the strong coupling varies a lot quicker for small scales.

In the following, we will not consider the influence of μ_h or μ_{us} further and instead concentrate on the much more significant variation of the soft scale.

6.2.2 Comparison of Resummed Logarithmic Terms and Full Fixed-Order Results

Besides analysing the effect of integrating the fully resummed result, we can extract another kind of useful information from the resummation procedure: Reexpanding the full resummed log-series, we obtain the large logarithms $\alpha^{n+1}\log^n$ at any order. This allows us to analyse the size of these logarithmic terms at NNLO and NNNLO in comparison to the respective full fixed-order expression (including terms not regarded by resummation).

Figure 6.4 shows the R-ratio at NLO (solid blue line), which we considered before, together with the NNLO result (solid green line). The figure illustrates this situation for different

values of μ_s between 20 GeV and 80 GeV, while the hard scale is fixed to $\mu_h = 180\,\text{GeV}$ for all panels. In order to check how much of the NNLO expression for the R-ratio is captured by the log-series, we depict the effect of adding the NNLO logarithm to the NLO expression as a dashed green line. This correction is obtained by reexpanding the resummed expression for $c_v^{(1)}$ in α and extracting only the first logarithm. While this logarithm partly shifts the R-ratio at NLO towards the NNLO result, there is still a large remainder not accounted for by the logarithm. This is not unexpected since at NLO, only the Coulomb potential contributes to the R-ratio, while extending to NNLO introduces new potentials suppressed in m. These new contributions can contain large effects not encoded in the logarithms, such that the NNLO result is not dominated by the NLL correction. We observe that the energy dependence of the curve with the added logarithm is different than the full NNLO curve, which is particularly visible in a shift of the peak.

In a similar sentiment, we show the R-ratio at NNLO and NNNLO in figure 6.5 as solid green and yellow lines, respectively. Additionally, we depict the effect of adding the NNNLO logarithm to the NNLO result as a yellow dashed line, as well as adding the fourth-order (N4LO) logarithm to the NNNLO result as a purple dashed line. Similar to the situation before, we observe that adding the NNNLO logarithm to the NNLO expression reproduces parts of the full NNNLO result but does not dominate it. For the N4LO logarithm, we cannot compare to the full fixed-order result, as it is not known. However, we observe that while the correction from this logarithm is quite large for small parameters of μ_s, it has almost no effect for $\mu_s = 80\,\text{GeV}$.

Comparing the panels with $\mu_s = 20\,\text{GeV}$ with the other panels for both figure 6.4 and 6.5, we explicitly observe the poorly behaved fixed-order results at small scales. For $\mu_s = 20\,\text{GeV}$, the NLO and NNNLO curves are too low and exhibit an unexpected dip above the peak, while the NNLO curve is too high. This is particularly visible when comparing the curves in these panels to the ones for higher values of μ_s. When the logarithmic effects are included, these problems are tempered but still prominent. We will discuss the scale dependence in more detail in section 6.2.4 below.

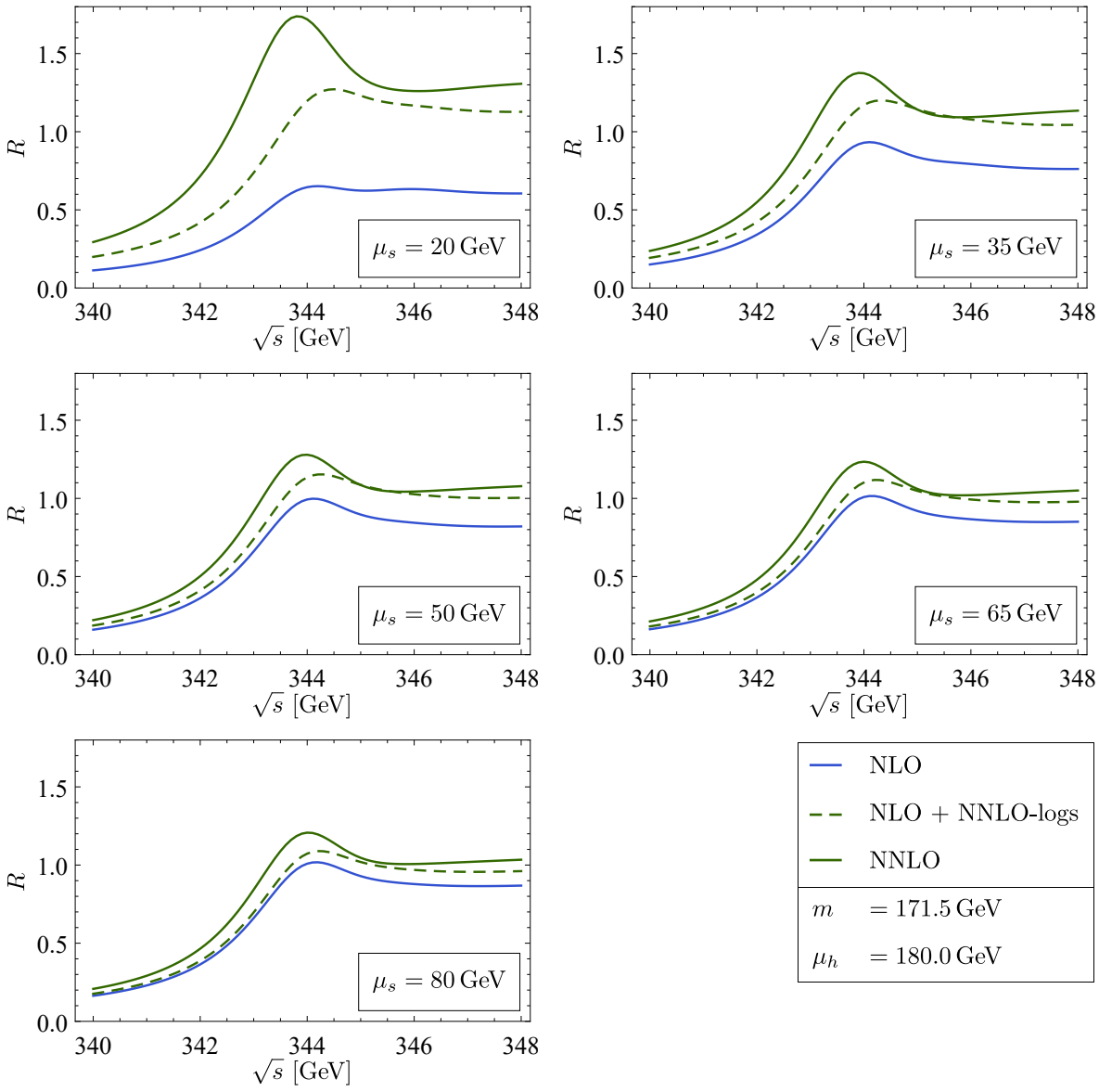

Figure 6.4: Comparison of the R-ratio at NLO and NNLO (solid lines in blue and green, respectively). Additionally, the dashed green line depicts the R-ratio where the NNLO logarithm from the reexpanded log-tower has been added to the NLO result. Between the separate panels, μ_s is varied between 20 GeV and 80 GeV in steps of 15 GeV. The hard scale is fixed to $\mu_h = 180\,\text{GeV}$ for all curves.

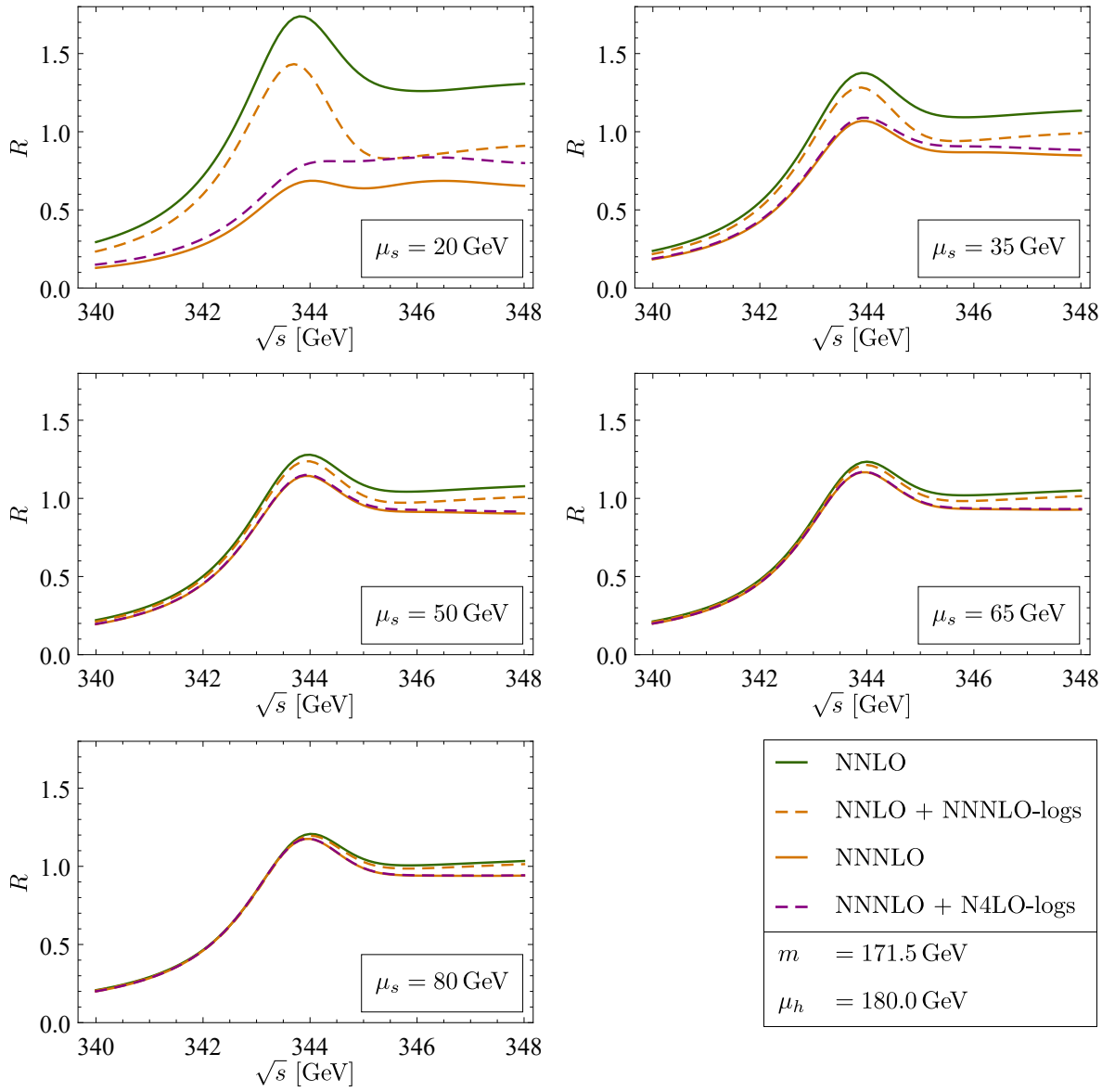

Figure 6.5: Comparison of the R-ratio at NNLO and NNNLO (solid lines in green and orange, respectively). The dashed yellow line depicts the R-ratio where the NNNLO logarithm from the reexpanded log-tower has been added to the NNLO result, while the dashed purple line shows the NNNLO contribution with added N4LO logarithms. Between the separate panels, μ_s changes between 20 GeV and 80 GeV in steps of 15 GeV, while the hard scale is fixed to $\mu_h = 180\,\text{GeV}$.

6.2.3 Convergence of the Reexpanded Series of Logarithms

The truncated log-series from the previous discussion can be further used to assess the convergence behaviour of the resummed series. To illustrate this, we first look at the aspect depicted in figure 6.6, which shows the R-ratio at NLO (blue) together with successively added terms from the reexpanded log-series (red dashed lines, the length of the dashes increases order by order). One observes the convergence of the truncated log-series to the full NLO+NLL result, which is shown as a solid red line.[2] This convergence is much faster for larger values of μ_s: For $\mu_s = 20\,\text{GeV}$, five terms of the log-series are noticeably different from the full result, while for $\mu_s = 35\,\text{GeV}$ this already only holds for three terms. Starting from $\mu_s = 65\,\text{GeV}$, even the second term already results in a curve close to the one using the full resummed result. We conclude that at scales above $\mu_s \sim 65\,\text{GeV}$, only the first new logarithm in the resummed series is really relevant. For smaller scales, the series still converges, but the convergence is much slower, and logarithms up to higher orders are of relevance.

In the same way, we consider the truncated log-series added to the R-ratio at NNNLO, which is depicted in figure 6.7. We note that adding the NNLO and NNNLO logarithm to this result has no effect since they are already contained in the fixed-order expression and subtracted to avoid double counting. Therefore, the first correction is obtained by adding the N4LO logarithm. Figure 6.5 suggests that already this first correction from the logarithms is very small (especially for larger values of μ_s), which is why we depict this scenario normalized to the respective third-order R-ratio R_{NNNLO}. This normalization is done separately for each panel, such that for every μ_s, we have $R/R_{\text{NNNLO}} = 1$ for the purely fixed-order expression. This is shown as a solid yellow line. The successively added logarithms are shown as dashed purple lines, where again, the length of the dashes increases order by order. The full NNNLO+NLL result is shown as a solid purple line. Note that for this figure, the axis showing the normalized R-ratio is not uniform over the individual panels, instead corresponding to successively smaller intervals.

When depicting the results normalized in this way, we observe a clear disparity between the apparent limit of the individual curves of the truncated log-series and the full NNNLO+NLL result. This discrepancy is of similar size for all values of μ_s, as we show in table 6.1. The table shows the numerical values for the R-ratio at a center-of-mass energy of $\sqrt{s} = 348\,\text{GeV}$, where according to figure 6.7, the discrepancy is particularly large. We compare values for the full NNNLO+NLL R-ratio and the scenario where the NLL logarithms up to order N7LO from the truncated log-series have been added to the NNNLO case. We consider the latter as an approximation for the limit of the reexpanded log-series. While this is only an estimate, it

[2] There is a subtlety to this apparent convergence, which we will discuss in detail for the NNNLO case.

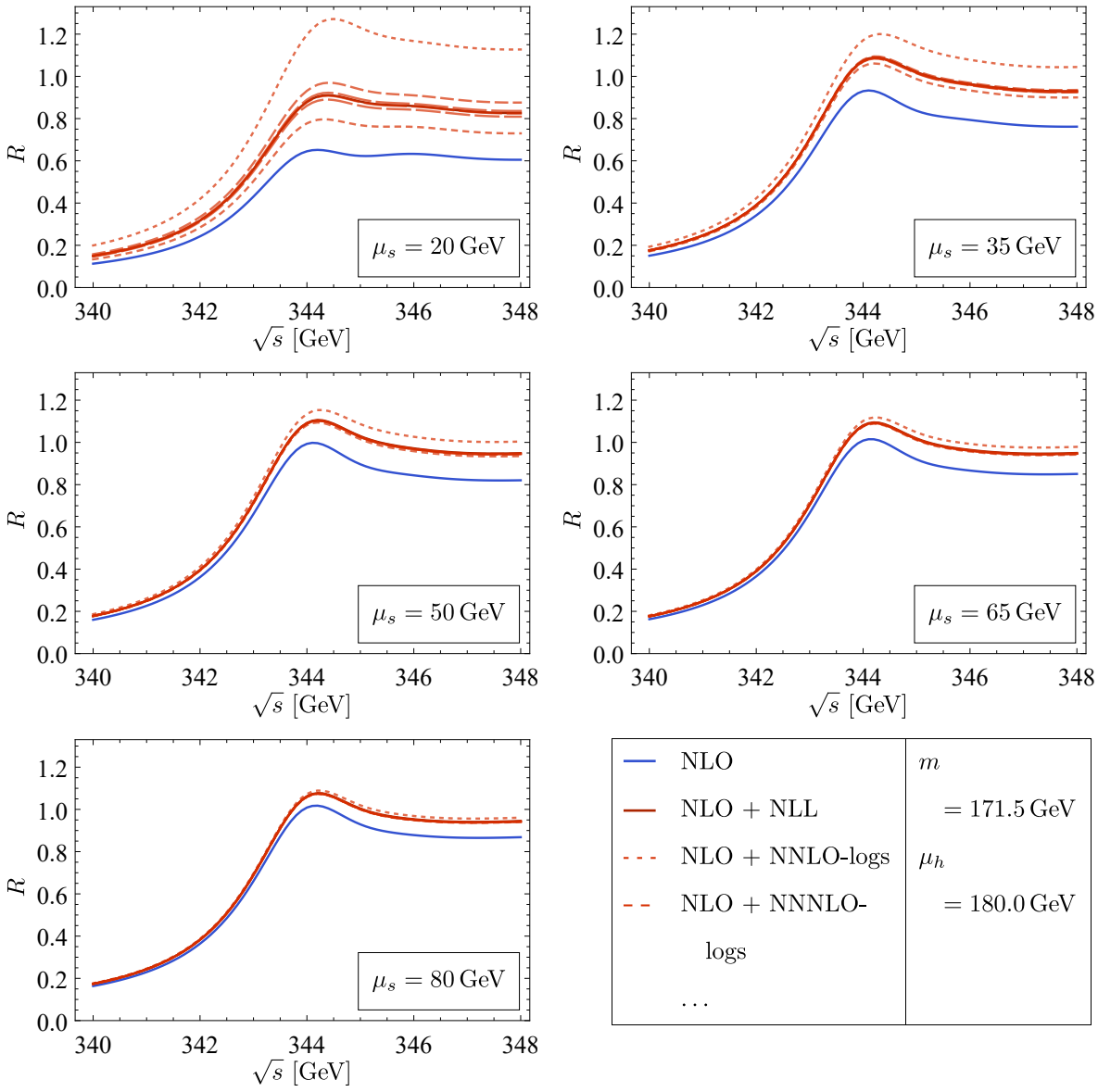

Figure 6.6: Convergence of the reexpanded log-series for different values of μ_s, where the NLO result is shown in blue. Added to this are the corrections obtained from the reexpanded log-series order by order, depicted in red and increasing from short to longer dashes. Additionally, the full NLO+NLL expression is shown as a solid red line. For the results using resummation, the hard scale has been fixed to $\mu_h = 180\,\text{GeV}$.

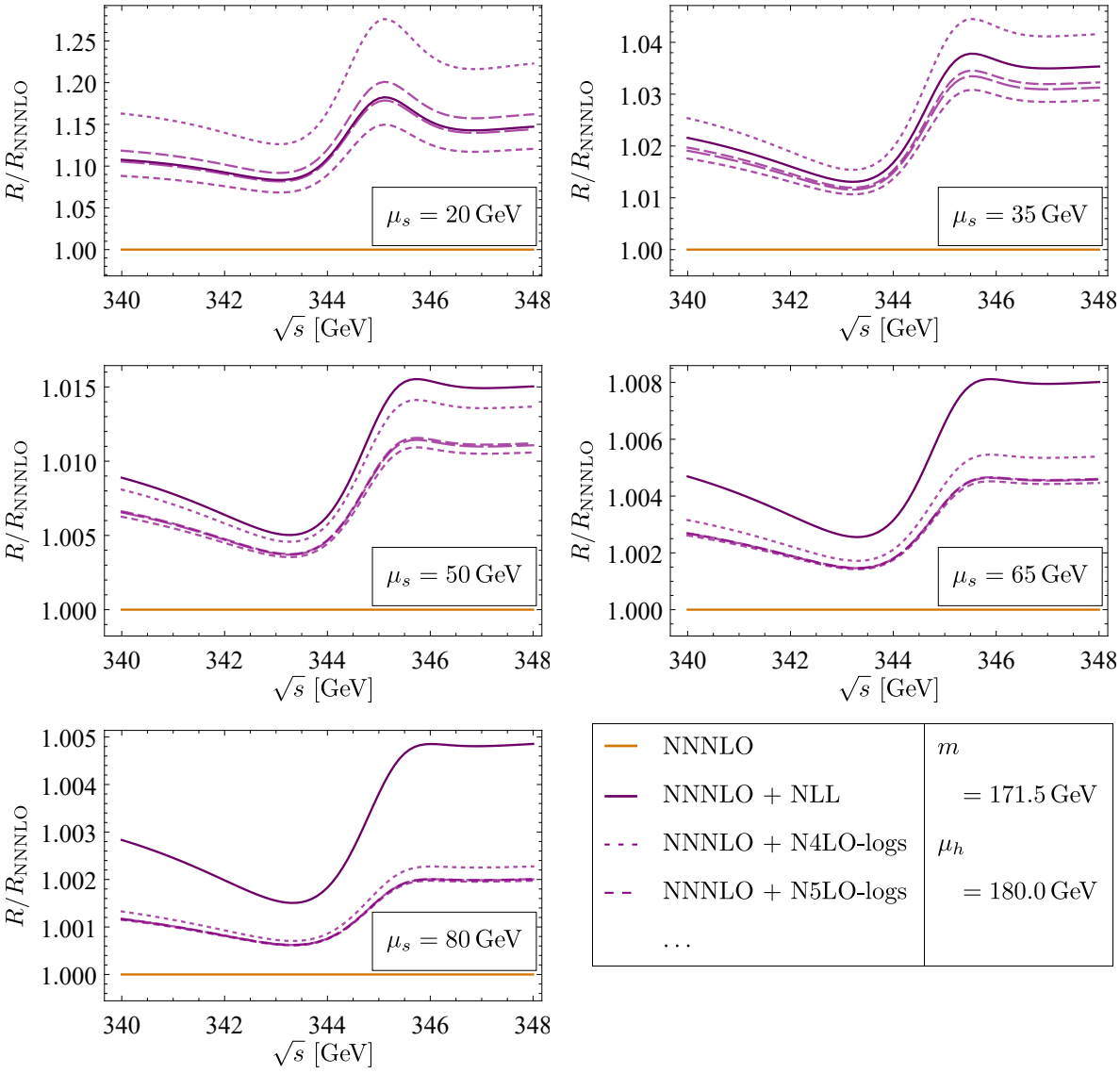

Figure 6.7: Convergence of the reexpanded log-series for different values of μ_s for the R-ratio at NNNLO. Each panel has been normalized to its respective fixed-order expression at NNNLO, such that the fixed-order result (yellow) corresponds to a constant line at $R/R_{\text{NNNLO}} = 1$. The dashed purple lines show the corrections obtained from the truncated log-series order by order, increasing from short to longer dashes. Additionally, the full NNNLO+NLL expression is shown as a solid purple line. For all panels, we use the standard hard scale $\mu_h = 180\,\text{GeV}$.

seems reasonable according to the fast convergence of the log-series in figure 6.7. Note that even though in figure 6.7 the discrepancy between the solid purple line (full NNNLO+NLL result) and the apparent limit of the dashed lines (successively truncated log-series) seems to increase for increasing scales μ_s, this is not actually the case: This impression is due to the faster convergence of the log-series and a decrease in the range of the vertical axis. Instead, as the numbers in table 6.1 suggest, the disparity is similar for all individual panels. For comparison, the table also contains the disparity for the NLO case, which, after rounding to four decimal places, is exactly the same as for the NNNLO case (even though it is not visible in figure 6.6).

Table 6.1: Comparison of the R-ratio at NNNLO+NLL and at NNNLO+N7LO logarithms, where we use the latter as an approximation of the limit of the reexpanded log-series. $|\Delta R_{\text{NNNLO}}| = |R_{\text{NNNLO+NLL}} - R_{\text{NNNLO+N7LO logs}}|$ denotes the discrepancy between the two. For comparison, we also show the same quantity for $|\Delta R_{\text{NLO}}| = |R_{\text{NLO+NLL}} - R_{\text{NLO+N7LO logs}}|$. All numbers are determined for $\sqrt{s} = 348\,\text{GeV}$ and rounded to four decimal places.

	$R_{\text{NNNLO+NLL}}$	$R_{\text{NNNLO+N7LO logs}}$	$\lvert\Delta R_{\text{NNNLO}}\rvert$	$\lvert\Delta R_{\text{NLO}}\rvert$
$\mu_s = 20\,\text{GeV}$	0.7499	0.7479	0.0020	0.0020
$\mu_s = 35\,\text{GeV}$	0.8785	0.8751	0.0035	0.0035
$\mu_s = 50\,\text{GeV}$	0.9170	0.9134	0.0036	0.0036
$\mu_s = 65\,\text{GeV}$	0.9349	0.9317	0.0032	0.0032
$\mu_s = 80\,\text{GeV}$	0.9452	0.9425	0.0027	0.0027

We attribute this systematical discrepancy to a subtlety in the implementation of the reexpanded log-series. For the reexpansion in section 5.5.2, we have used the one-loop running of α as given in equation (2.13), which does not hold to higher orders. However, in the code, the running coupling is always evaluated with five-loop running. This produces a small disparity between the truncated reexpanded log-series of $c_v^{(1),\text{RGI}}$ and its actual limit, which influences the R-ratio. Therefore, we view the discrepancy between the limit of the truncated log-series and the full NLL result as an artefact of the choice we made when reexpanding the resummed result.

6.2.4 Reduction of the Scale Dependence at Various Orders

We conclude our numerical analysis with a more detailed discussion of the scale dependence of the R-ratio. We have already demonstrated in section 6.2.1 that for NLO, the dependence on μ_s is reduced once NLL modifications are added. This becomes even more apparent when considering the R-ratio at a specific center-of-mass energy while varying the scale μ_s. This is depicted in figure 6.8, 6.9, and 6.10 for the NLO, NNLO, and NNNLO case, respectively. All figures display the μ_s-dependence of the R-ratio after normalizing it to its value for $\mu_s = 50\,\text{GeV}$.

Here, we always normalize to the R-ratio considered in the respective case. That is, the R-ratio at NLO is normalized with respect to the NLO result at $\mu_s = 50\,\text{GeV}$, while the NLO+NLL result is normalized to the NLO+NLL value at $\mu_s = 50\,\text{GeV}$, and so on. Therefore, all lines intersect at a ratio of one for $\mu_s = 50\,\text{GeV}$. A curve constant at one would correspond to a quantity independent of the scale. We consider values of $\sqrt{s} = 340\,\text{GeV}$ (below the peak), $\sqrt{s} = 344\,\text{GeV}$ (close to the peak), and $\sqrt{s} = 348\,\text{GeV}$ (above the peak).

In figure 6.8, we depict the situation at NLO. The blue line shows the fixed-order NLO result for the R-ratio normalized to its value at $\mu_s = 50\,\text{GeV}$, while the solid red line shows the full NLO+NLL result. The dashed lines denote the individual results for the successively truncated log-series as in figure 6.6. We note that the NNLO logarithm (line with shortest dashes) overshoots significantly, such that the NNNLO logarithm is particularly relevant. We observe a clear decrease in the scale dependence once NLL corrections are added to the fixed-order expression. This is particularly visible for the point where the curves start to rapidly drop off for small scales μ_s, which indicates a breakdown of perturbation theory. For the fixed-order result, this breakdown is already visible for $\mu_s \lesssim 40\,\text{GeV}$, confirming the statements in the literature [26, 77, 78]. When adding the NLL modification, a similarly large drop-off is only observed for scales below $\mu_s = 30\,\text{GeV}$, posing a significant improvement. While for scales below this value, the breakdown of perturbation theory still happens, it is now shifted to lower scales compared to the pure fixed-order calculation. We also observe that even for higher values of μ_s, the curves overall deviate less from a horizontal line, corresponding to a decreased scale dependence also in this range. This behaviour is similar for all three values of $\sqrt{s}$.

Analogously, we show this analysis for the NNLO case in figure 6.9, where the green line denotes the fixed-order NNLO result, and the yellow solid line corresponds to NNLO+NLL. The dashed yellow lines demonstrate the convergence of the terms in the truncated log-series with increasingly longer dash size. Again, we observe a significant reduction of the scale μ_s for which perturbation theory breaks down to below $\mu_s = 30\,\text{GeV}$. Especially for $\sqrt{s} = 348\,\text{GeV}$ (above the peak), the overall scale dependence is very small, resulting in a nearly horizontal line.

This improvement in the scale dependence of the R-ratio when including NLL effects has already been observed in [35]. In this reference, the discussion also included a partial inclusion of NNLL effects, which we do not consider here. However, we now also present the RG improvement for the NNNLO calculation at NLL, which has not been shown before. Analogously to the previous figures, figure 6.10 shows the situation at NNNLO, where the yellow line corresponds to the fixed-order expression and the purple lines show the behaviour for NNNLO+NLL (with dashed lines again denoting the successively truncated log-series). While at this order the

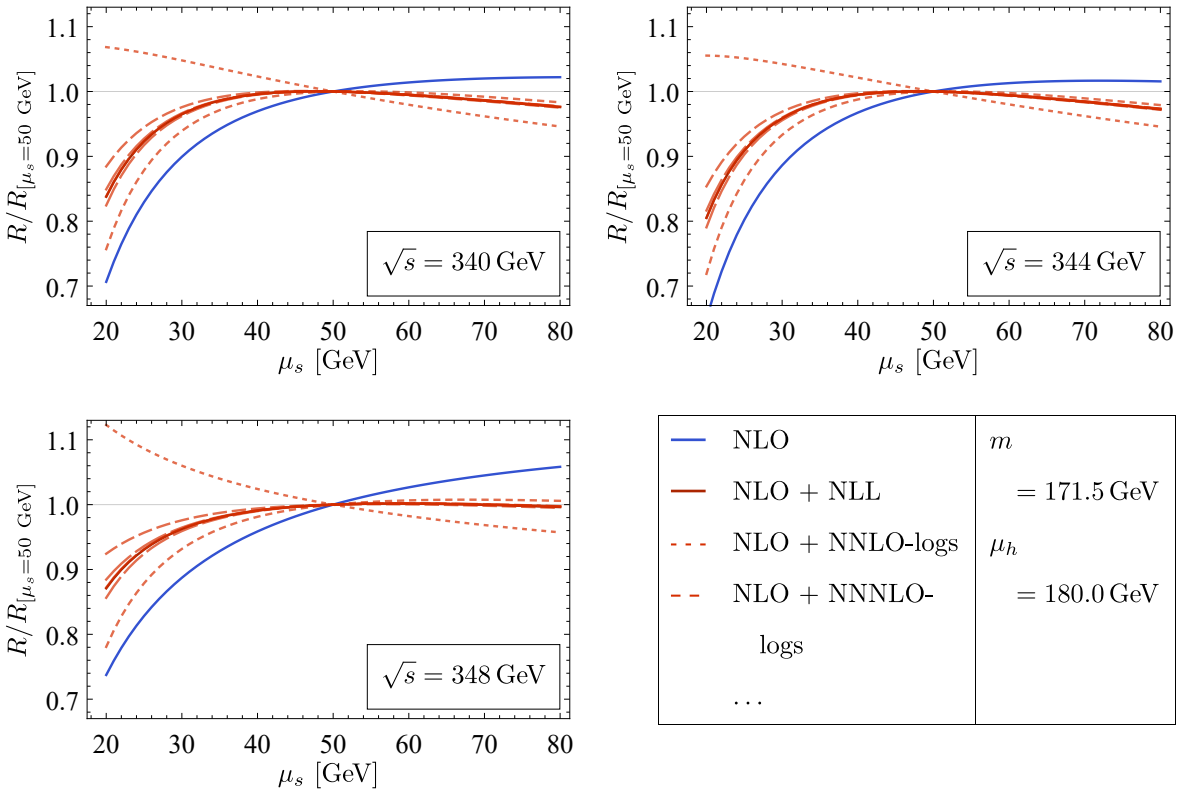

Figure 6.8: μ_s-dependence of the R-ratio at NLO compared to RG improved results at the same order. Each line shows the R-ratio normalized to its respective value at $\mu_s = 50\,\mathrm{GeV}$. In the individual panels, we consider center-of-mass energies below the peak ($\sqrt{s} = 340\,\mathrm{GeV}$), approximately at the peak ($\sqrt{s} = 344\,\mathrm{GeV}$), and above the peak ($\sqrt{s} = 348\,\mathrm{GeV}$). The blue line depicts the NLO result, while the solid red line corresponds to NLO+NLL. Dashed lines show the effect of using the log-series truncated at increasingly higher orders with increasing dash sizes. For all panels, the hard scale is set to $\mu_h = 180\,\mathrm{GeV}$.

effect of adding the RG improvements is not as drastic as for NLO and NNLO (as was already expected from figure 6.5), we still observe an improvement for the resummed result. Again, the curve is overall more horizontal, corresponding to a decreased scale dependence, which moves the point where perturbation theory breaks down to smaller scales of around $\mu_s \sim 30\,\mathrm{GeV}$.

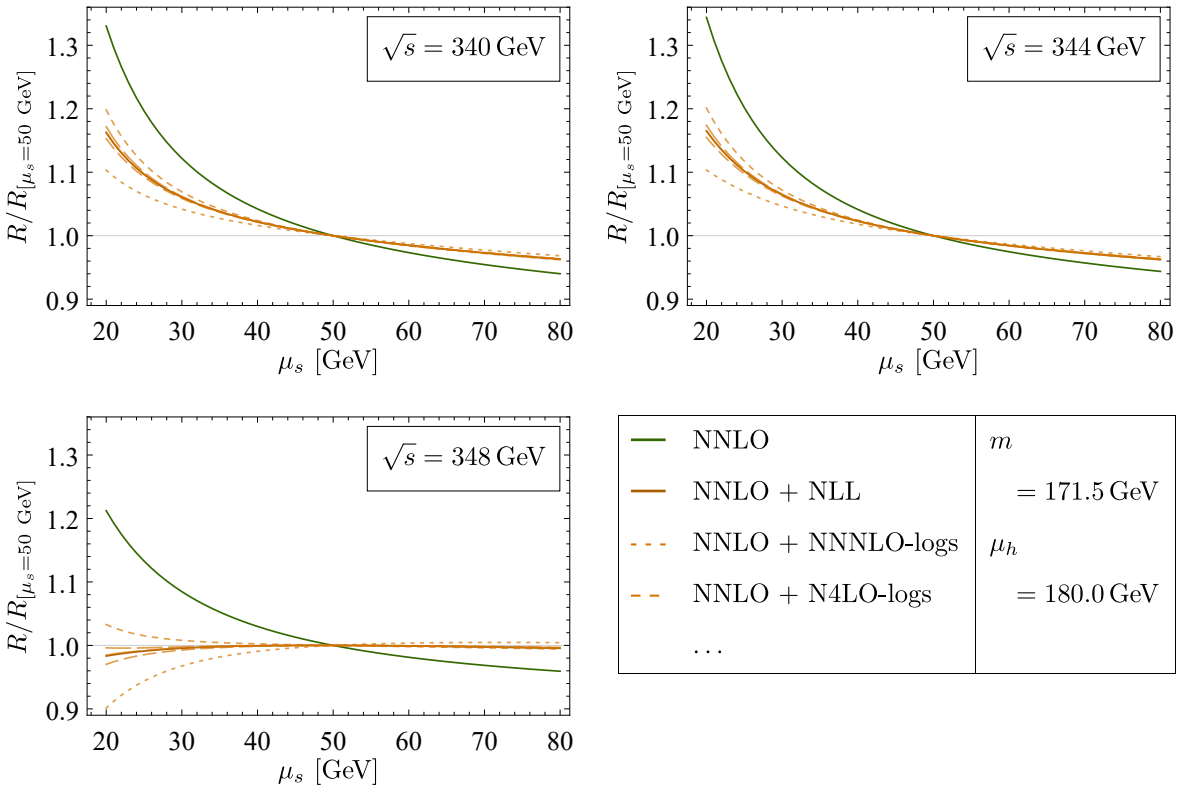

Figure 6.9: μ_s-dependence of the R-ratio at NNLO compared to results where NLL effects have been included at the same order. As in figure 6.8, for each line, the R-ratio is normalized to its respective value at $\mu_s = 50\,\text{GeV}$. The individual panels show different center-of-mass energies of $\sqrt{s} = 340\,\text{GeV}$, $\sqrt{s} = 344\,\text{GeV}$, and $\sqrt{s} = 348\,\text{GeV}$. The green line shows the NNLO result, while the solid yellow line corresponds to NNLO+NLL. As before, dashed lines demonstrate the convergence of the truncated log-series, where increasing dash size corresponds to higher-order logarithms.

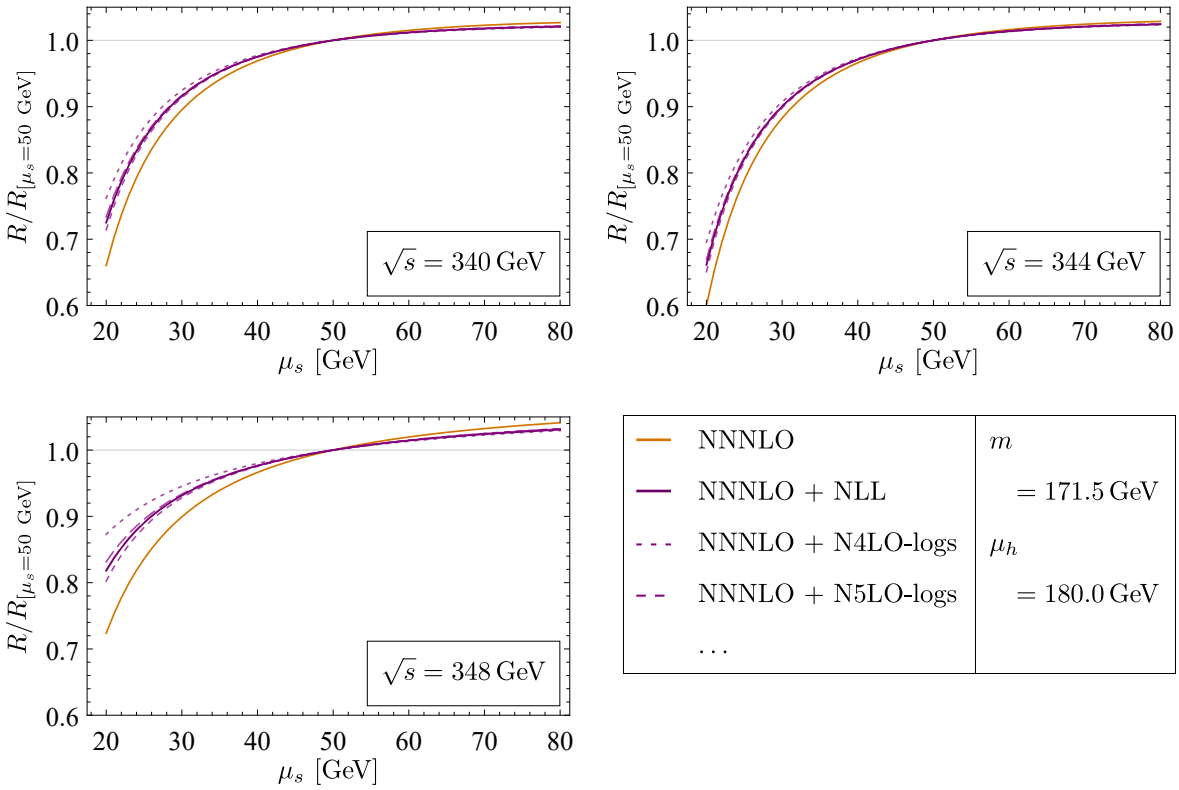

Figure 6.10: μ_s-dependence of the R-ratio at NNNLO and NNNLO+NLL. Analogously to figures 6.8 and 6.9, the R-ratio is normalized to its respective value at $\mu_s = 50\,\mathrm{GeV}$. The NNNLO result is shown as a solid yellow line, while the solid purple line corresponds to NNNLO+NLL. Dashed lines (longer dashes corresponding to higher-order logarithms) show the convergence of the reexpanded log-series.

Chapter 7

Conclusion

In this thesis, we presented an in-depth analysis of the RG improvement for the R-ratio of top anti-top pair production near threshold at NLL. Building onto the discussion in the review [34] and related papers, we transformed the calculations to momentum space and placed particular focus on the use of conventions compatible with reference [27]. This reference, together with [77], discusses the R-ratio up to NNNLO at fixed order and is used as a basis for the `QQbar_threshold` code [42].

The large mass of the top quark allows for an EFT treatment of the top anti-top pair production near threshold, where the velocity v of the heavy quark is small. In this framework, we considered first NRQCD and then PNRQCD, performing the RG improvement in multiple steps.

First, we considered the hard running of the matching coefficients d_i and d_{ij} in the NRQCD Lagrangian, which is discussed, for example, in references [33, 53]. This procedure resums large logarithms of the form $\ln\left(\frac{\mu^2}{\mu_h^2}\right)$, where μ_h denotes the hard scale, which is of the order of the top mass m, while the renormalization scale μ has been associated with the soft scale $\mu_s \sim mv$. We encoded the correction obtained from the hard running in an additive modification of the PNRQCD potential $\mathcal{V}_{1/m^2}$. In particular, this contributed to the coefficient v_0, which is given in equation (5.33).

As a second step, we looked at the ultrasoft running of the potentials. This is closely related to divergences in diagrams involving the ultrasoft interaction $g\mathbf{x}\cdot\mathbf{E}$ from the PNRQCD Lagrangian. For this calculation, we followed reference [34], providing additional details in the process. We then transformed the result to momentum space using a fully d-dimensional Fourier transform. While for the NLL correction only terms of order $\mathcal{O}(\varepsilon^0)$ are relevant, this provides a starting point for future extensions to higher orders in the resummation of logarithms

in the momentum space framework of reference [27]. This especially holds since we additionally gave the analogous two-loop expressions in the appendix, which are also required once one extends to higher orders in resummation. For the NLL case, we again wrote the corrections as a modification of coefficients in the PNRQCD potentials, specifically a_2, b_1, v_0, and p_0. The results resum logarithms $\ln\left(\frac{\mu^2}{\mu_{us}^2}\right)$, where μ_{us} is the ultrasoft scale, and are given in equations (5.93)-(5.96).

The last part of the resummation procedure is given by the potential running. It is encoded in the matching coefficient c_v of the non-relativistic vector current $j^{(v)}$. To determine the associated RGE, we extracted the divergences in c_v from the divergences in the imaginary part of the Green's function, $\mathrm{Im}\{G_0(E)\}$, which they are closely related to. When solving the RGE, we correlated the scales as $\mu_{us} = k\frac{\mu^2}{\mu_h}$. Our result agrees with the expression given in [32, 34]. To facilitate an easier numerical implementation, we again encoded the correction obtained from the RG improvement as an additive modification of the fixed-order result, as it is given in equation (5.139).

Finally, to conclude the analytic calculation, we incorporated these results into the R-ratio, obtaining an RG improved expression for this quantity at NLL. The relevant modification is given in equation (5.140). We observe that while the corrections to the potential coefficients a_2, b_1, v_0, and p_0 were necessary to determine the full running of the coefficient c_v, only the latter actually contributes to the R-ratio at this order. We checked explicitly that our result reproduces the correct large logarithms in the fixed-order expressions at NNLO and NNNLO. We also took care to avoid double-counting by subtracting these logarithms accordingly.

After this analytical calculation, we analysed the numerical effect of the RG improvement by incorporating the modification of $c_v^{(1)}$ into the `Mathematica` code `TTbarXSection`. Using this implementation, we compared different aspects of the fixed-order and RG improved R-ratio. After a qualitative comparison of the NLO and NLO+NLL results, we analysed the behaviour of the truncated, reexpanded log-series, where we observed a generally good convergence which is particularly fast for larger scales μ_s. We also considered the NNLO and NNNLO logarithms individually, comparing how much of the respective fixed-order contribution is encoded in the logarithmic part. We observed that while a significant part of the respective next order is contained in the next-to-leading logarithms, the other contributions are also sizable. The main focus of the numerical analysis was placed on the scale dependence of the R-ratio. While for the fixed-order case, a large scale dependence is observed for $\mu_s \lesssim 40\,\mathrm{GeV}$, indicating a breakdown of perturbation theory [26, 77, 78], this is significantly improved once NLL corrections are included. We observed that the scale dependence is overall reduced, with the point where perturbation theory becomes unreliable moved to $\mu_s \lesssim 30\,\mathrm{GeV}$.

Thus, we demonstrated that including the NLL correction improves the numerical behaviour of the R-ratio. This has been discussed in a similar manner in [35] for the NLL and partial NNLL with fixed-order results at NNLO. In this thesis, we extended this result by additionally combining NLL with NNNLO, observing an analogous reduction of the scale dependence also in this case.

The topic of top anti-top pair production near threshold provides a natural possible extension for future work, where it would be desirable to determine the full RG improvement at NNLL. Reference [35], as well as [38–41] (which consider this topic in the formalism of vNRQCD), already achieve partial resummation at this order. Throughout this thesis, we have repeatedly alluded to possible future extensions in the framework chosen in this work. In particular, we have transformed the two-loop ultrasoft counterterm from reference [34] to momentum space in a fully d-dimensional manner and given the result in appendix C. When considering NNLL resummation in this scheme, one needs to place special care on $\mathcal{O}(\varepsilon)$-terms in matching coefficients and counterterms. While they did not contribute in this thesis, they might multiply $\frac{1}{\varepsilon}$-poles in higher-order calculations, resulting in relevant finite terms. In general, a careful analysis of the calculation in position versus momentum space and the resulting scheme dependence is necessary. Also, we note again that the running of the coefficient V_A (cf. equation (5.42)) calls for further discussion.

While the numerical implementation in this thesis has been performed for the `TTbarXSection` code, the renormalization group improvements will also be incorporated into the publicly available `QQbar_threshold` code [42] in the future.

Appendix A

Acronyms

SM	Standard Model
LHC	Large Hadron Collider
ILC	International Linear Collider
EFT	effective field theory
QCD	Quantum Chromodynamics
QED	Quantum Electrodynamics
EW	electroweak
NRQCD	non-relativistic QCD
PNRQCD	potential non-relativistic QCD
vNRQCD	velocitiy non-relativistic QCD
HQET	heavy quark effective theory
FO	fixed order
LO	leading order
NLO	next-to-leading order
NNLO	next-to-next-to-leading order
NNNLO	next-to-next-to-next-to-leading order
N4LO	fourth-order
LL	leading logarithm
NLL	next-to-leading logarithm
NNLL	next-to-next-to-leading logarithm
RG	renormalization group
RGE	renormalization group equation
RGI	renormalization group improved

EOM	equation of motion
IR	infrared
UV	ultraviolet
PS	position space

Appendix B

Comparison of Conventions

B.1 Conventions in the NRQCD Lagrangian

For ease of reference, we want to explicitly compare the conventions used in the papers providing the main intermediate results we need for our work. The covariant derivative and the field strength tensor are defined as given in table B.1. The left column shows the notation we are using in this thesis, following reference [27]. The right column gives the corresponding conventions in references [33, 34, 89], which coincide. We use tildes to denote the difference in signs these quantities show compared to the conventions of our choice. We also note that reference [53] uses the convention shown in the right column ($\tilde{g}$ instead of g) for the coupling.

Therefore, the quantities appearing in the NRQCD Lagrangian in [27] and [34] are related as presented in table B.2.

Table B.1: Definitions of the covariant derivative and the field strength tensor used in relevant references. In this thesis, we will follow the notation of the left column.

Conventions from [27] (Beneke et al.)	Conventions from [33, 34, 89] (Pineda et al.)
$D^\mu = \partial^\mu - ig_s A^\mu$	$\tilde{D}^\mu = \partial^\mu + i\tilde{g} A^\mu$
$D^\mu = (D^0, \mathbf{D})$	$\tilde{D}^\mu = (\tilde{D}^0, -\tilde{\mathbf{D}})$
$G^{\mu\nu} = \frac{i}{g_s}[D^\mu, D^\nu] =$	$\tilde{G}^{\mu\nu} = -\frac{i}{\tilde{g}}[\tilde{D}^\mu, \tilde{D}^\nu] =$
$= (\partial^\mu A^\nu) - (\partial^\nu A^\mu) - ig_s[A^\mu, A^\nu]$	$= (\partial^\mu A^\nu) - (\partial^\nu A^\mu) + i\tilde{g}[A^\mu, A^\nu]$

Table B.2: Conversion between the relevant quantities appearing in the Lagrangians in references [27] and [34].

Conventions from [27]	Conventions from [34]
$-g_s$	$\tilde{g}$
D^0	$\tilde{D}^0$
$-D^i$	$\tilde{D}^i$
$G^{\mu\nu}$	$\tilde{G}^{\mu\nu}$
E^i	$\tilde{E}^i$
$\boldsymbol{\sigma}\cdot\mathbf{B}$	$\boldsymbol{\sigma}\cdot\tilde{\mathbf{B}}$

B.1.1 Choice of Operator Basis in the Gluonic Lagrangian

Apart from these differences in defining the fundamental quantities, there is also another source of difference in notation: The non-relativistic Lagrangian is usually written in terms of an operator basis containing redundant operators. There are different choices for eliminating operators from this redundant basis. We start by discussing some possible choices within the general gluonic Lagrangian up to $\mathcal{O}\left(\frac{1}{m^2}\right)$, which is given by

$$\mathcal{L}_g = -\frac{1}{4}G^{A\mu\nu}G^A_{\mu\nu} + \frac{\hat{c}_g^1}{m^2}gf^{ABC}G^A_{\mu\nu}G^{B\mu}{}_\alpha G^{C\nu\alpha} + \frac{\hat{c}_g^2}{m^2}D^\mu G^A_{\mu\alpha}D_\nu G^{A\nu\alpha} + \frac{\hat{c}_g^3}{m^2}G^A_{\mu\nu}D^2G^{A\mu\nu}. \tag{B.1}$$

One way to eliminate operators from this is to use the identity (cf. [34])

$$0 = \int \mathrm{d}^4x \left(2D^\mu G^A_{\mu\alpha}D_\nu G^{A\nu\alpha} - 2gf^{ABC}G^A_{\mu\nu}G^{B\mu}{}_\alpha G^{C\nu\alpha} + G^A_{\mu\nu}D^2G^{A\mu\nu}\right). \tag{B.2}$$

We list the different choices of operator bases made in some references relevant to this thesis in table B.3.

Operator Basis Chosen in [27] (By Beneke, Kiyo, Schuller)

We now relate the coefficients used in the Lagrangians in the different references with the ones in the general Lagrangian (B.1).

Table B.3: Overview of the choice of operators from the redundant basis in the gluonic Lagrangian in some relevant references. The coefficient in brackets denotes the coefficient associated with that particular operator in the respective reference. The first line is the one used in this thesis.

	$f^{ABC}G^AG^BG^C$	DG^ADG^A	$G^AD^2G^A$
Ref. [27], Beneke et al.	included $[d_6]$	eliminated using (B.2)	included $[d_5]$
Ref. [53], Bauer, Manohar	included $\left[\frac{c_1^g}{4}\right]$	included $\left[\frac{c_2^g}{4}\right]$, but rewritten in terms of four-fermion operators and not considered	eliminated using (B.2)
Ref. [33, 34], Pineda	included $\left[\frac{c_1^g}{4}\right]$	eliminated using (B.2)	eliminated using field redefinition $A\mu \to A_\mu + 2c[D^\alpha, G_{\alpha\mu}]$

For the case used in this thesis, following the notation from [27], we eliminate the operator DG^ADG^A using equation (B.2) and get

$$\mathcal{L}_{g,\text{ref.[27]}} = -\frac{1}{4}G^{A\mu\nu}G^A_{\mu\nu} + \underbrace{\left(\hat{c}_g^1 + \hat{c}_g^2\right)}_{\equiv d_6}\frac{1}{m^2}gf^{ABC}G^A_{\mu\nu}G^{B\mu}{}_\alpha G^{C\nu\alpha} + \underbrace{\left(\hat{c}_g^3 - \frac{1}{2}\hat{c}_g^2\right)}_{\equiv d_5}\frac{1}{m^2}G^A_{\mu\nu}D^2G^{A\mu\nu}. \tag{B.3}$$

We obtain

$$d_5 = \hat{c}_g^3 - \frac{1}{2}\hat{c}_g^2, \tag{B.4}$$

$$d_6 = \hat{c}_g^1 + \hat{c}_g^2, \tag{B.5}$$

expressing the gluonic coefficients in the Lagrangian in [27] in terms of the more general coefficients $\hat{c}_g^i$ defined in equation (B.1). We will perform the same procedure for the choices made in the other references (cf. table B.3), providing a way to easily relate the different conventions.

Operator Basis Chosen in [53] (By Bauer, Manohar)

To account for the calculation in [53], we eliminate the operator $G^A D^2 G^A$ instead, leading to

$$\mathcal{L}_{g,\text{ref.[53]}} = -\frac{1}{4} G^{A\mu\nu} G^A_{\mu\nu} + \underbrace{\left(-\hat{c}^1_g - 2\hat{c}^3_g\right)}_{\equiv \frac{c^g_1}{4}} \frac{1}{m^2} \tilde{g} f^{ABC} G^A_{\mu\nu} G^{B\mu}{}_{\alpha} G^{C\nu\alpha} + \underbrace{\left(\hat{c}^2_g - 2\hat{c}^3_g\right)}_{\equiv \frac{c^g_2}{4}} D^\mu G^A_{\mu\alpha} D_\nu G^{A\nu\alpha}. \tag{B.6}$$

We obtain

$$c^g_1 = -4\hat{c}^1_g - 8\hat{c}^3_g, \tag{B.7}$$

$$c^g_2 = 4\hat{c}^2_g - 8\hat{c}^3_g \tag{B.8}$$

for the coefficients in the Lagrangian in [53]. We have rewritten the Lagrangian in terms of $\tilde{g}$, corresponding to the convention of that reference. We note that in [53], the operator corresponding to c^g_2 is not considered further since it can be rewritten in terms of four-fermion operators, which are not relevant to the calculation performed there. Since, in our case, the four-fermion operators are relevant, we instead choose to also eliminate the c^g_2-term from the gluonic Lagrangian. This was done in the same way in [34], as we discuss below in section B.1.2. This discussion will modify the coefficient of the Darwin operator.

Operator Basis Chosen in [33, 34] (By Pineda)

Finally, we derive the Lagrangian used in references [33] and [34]. First, we eliminate the operator $DG^A DG^A$ as we did above for the Lagrangian from reference [27], obtaining

$$\mathcal{L}_{g,\text{ref.[34]}} = -\frac{1}{4} G^{A\mu\nu} G^A_{\mu\nu} + \left(-\hat{c}^1_g - \hat{c}^2_g\right) \frac{1}{m^2} \tilde{g} f^{ABC} G^A_{\mu\nu} G^{B\mu}{}_{\alpha} G^{C\nu\alpha} + \left(\hat{c}^3_g - \frac{1}{2}\hat{c}^2_g\right) \frac{1}{m^2} G^A_{\mu\nu} D^2 G^{A\mu\nu}. \tag{B.9}$$

We have again rewritten the second term to include $\tilde{g}$ instead of g. Additionally, these references eliminate the last term $G^A D^2 G^A$ by performing the field redefinition

$$A_\mu \to A_\mu + 2c[D^\alpha, G_{\alpha,\mu}] + \mathcal{O}(c^2), \tag{B.10}$$

where $c \sim \frac{1}{m^2}$. Up to order $\mathcal{O}\left(\frac{1}{m^2}\right)$, this leads to the following modification of the gluonic Lagrangian:

$$-\frac{1}{4} G^{A\mu\nu} G^A_{\mu\nu} \to -\frac{1}{4} G^{A\mu\nu} G^A_{\mu\nu} - \frac{c}{2} G^A_{\mu\nu} D^2 G^{A\mu\nu} - c\tilde{g} f^{ABC} G^A_{\mu\nu} G^{B\mu}{}_{\alpha} G^{C\nu\alpha} + \mathcal{O}(c^2), \tag{B.11}$$

as is discussed in reference [89]. Plugging this into the Lagrangian yields

$$\mathcal{L}_{g,\text{ref.[34]}} = -\frac{1}{4}G^{A\mu\nu}G^{A}_{\mu\nu} + \left(-\frac{\hat{c}_g^1}{m^2} - \frac{\hat{c}_g^2}{m^2} - c\right)\tilde{g}f^{ABC}G^{A}_{\mu\nu}G^{B\mu}{}_{\alpha}G^{C\nu\alpha} + \left(\frac{\hat{c}_g^3}{m^2} - \frac{1}{2}\frac{\hat{c}_g^2}{m^2} - \frac{1}{2}c\right)G^{A}_{\mu\nu}D^2G^{A\mu\nu}. \tag{B.12}$$

In order to eliminate the last term, we choose $c = 2\frac{\hat{c}_g^3}{m^2} - \frac{\hat{c}_g^2}{m^2}$, leading to

$$\mathcal{L}_{g,\text{ref.[34]}} = -\frac{1}{4}G^{A\mu\nu}G^{A}_{\mu\nu} + \underbrace{\left(-\frac{\hat{c}_g^1}{m^2} - 2\frac{\hat{c}_g^3}{m^2}\right)}_{\equiv\frac{c_1^g}{4}}\tilde{g}f^{ABC}G^{A}_{\mu\nu}G^{B\mu}{}_{\alpha}G^{C\nu\alpha}. \tag{B.13}$$

We now identify the coefficient of the leftover operator with the one from [34], obtaining

$$c_1^g = -4\hat{c}_g^1 - 8\hat{c}_g^3. \tag{B.14}$$

This coincides with the coefficient given the same name in [53], which was derived above.

It is important to stress that the change in the gluonic coefficients is not the only consequence of the field redefinition (B.10): As discussed in [89], this also modifies

$$i\tilde{D}_0 \to i\tilde{D}_0 - c\tilde{g}(\tilde{\mathbf{D}}\cdot\tilde{\mathbf{E}} - \tilde{\mathbf{E}}\cdot\tilde{\mathbf{D}}) = iD_0 - cg([D^i, E^i]), \tag{B.15}$$

where $[\tilde{\mathbf{D}}\cdot, \tilde{\mathbf{E}}] = \tilde{\mathbf{D}}\cdot\tilde{\mathbf{E}} - \tilde{\mathbf{E}}\cdot\tilde{\mathbf{D}}$. This leads to a redefinition of the coefficient of the Darwin operator:

$$\frac{\hat{c}_D}{8m^2}\tilde{g}[\tilde{\mathbf{D}}\cdot, \tilde{\mathbf{E}}] \to \left(\frac{\hat{c}_D}{8m^2} - c\right)\tilde{g}[\tilde{\mathbf{D}}\cdot, \tilde{\mathbf{E}}] = \underbrace{\left(\frac{\hat{c}_D}{8m^2} - 2\frac{\hat{c}_g^3}{m^2} + \frac{\hat{c}_g^2}{m^2}\right)}_{\equiv\frac{c_D}{8m^2}}\tilde{g}[\tilde{\mathbf{D}}\cdot, \tilde{\mathbf{E}}]. \tag{B.16}$$

This shows that the coefficient c_D used in [34] is related to the coefficients in the more general Lagrangian given in (B.1) by

$$c_D = \hat{c}_D - 16\left(\hat{c}_g^3 - \frac{1}{2}\hat{c}_g^2\right). \tag{B.17}$$

We can identify the last term with d_5 from equation (B.4), obtaining

$$c_{D,\text{ref.[34]}} = (d_2 - 16d_5)_{\text{ref.[27]}}. \tag{B.18}$$

This explicitly shows how to use the results for the running of the Darwin coefficient from reference [34] in our calculation following the notation in [27]. However, we additionally need to consider a possible elimination in the heavy-light sector of the Lagrangian, which we will discuss now.

B.1.2 Choice of Operator Basis in the Heavy-Light Lagrangian

There is also an ambiguity in choosing the operators in the heavy-light part of the Lagrangian, which we did not write in (3.9). There is one operator from this class that could contribute to the calculation at the order we are considering, which is $\psi^\dagger T^A \psi \bar{q}\gamma^0 T^A q$ (and the analogous operator with $\psi \to \chi$). However, this operator can be absorbed into the Darwin operator and one of the four-fermion operators, making it possible to remove this operator from the Lagrangian. This is what we choose to do in this work. We demonstrate the elimination of this operator by starting from a general Lagrangian still including it in its basis:

$$\begin{aligned}\mathcal{L}_{\text{including } O_1^{hl}} \supset\ & \hat{c}_D \frac{1}{8m^2}\psi^\dagger g[D^i, E^i]\psi + \hat{c}_D \frac{1}{8m^2}\chi^\dagger g[D^i, E^i]\chi + \hat{d}_{vs}\frac{1}{m^2}\psi^\dagger T^a \psi \chi^\dagger T^a \chi \\ & + \hat{c}_1^{hl}\frac{g^2}{8m^2}\sum_i \psi^\dagger T^A \psi \bar{q}\gamma^0 T^A q + \hat{c}_1^{hl}\frac{g^2}{8m^2}\sum_i \chi^\dagger T^A \chi \bar{q}\gamma^0 T^A q = \\ \equiv\ & \hat{c}_D O_D^\psi + \hat{c}_D O_D^\chi + \hat{d}_{vs} O_{vs} + \hat{c}_1^{hl} O_1^{hl,\psi} + \hat{c}_1^{hl} O_1^{hl,\chi}.\end{aligned} \tag{B.19}$$

Similar to the section before, we use hats on the coefficients to indicate an operator basis different from the one we are choosing to use.

The elimination of O_1^{hl} is discussed in detail in reference [53] in the context of HQET. We follow the calculation performed there, translated to NRQCD. We start with the EOM for the gluon field, derived from the terms in the Lagrangian not suppressed in m:

$$\mathcal{L}_{\mathcal{O}(m^0)} = \psi^\dagger i D^0 \psi + \chi^\dagger i D^0 \chi - \frac{1}{4} G^A_{\mu\nu} G^{A\mu\nu} + \sum_i \bar{q}_i i \not{D} q_i. \tag{B.20}$$

The EOM takes the form

$$D_\mu G^{A\mu\nu} = -g \sum_i \bar{q}_i \gamma^\nu T^A q_i - g\delta_0^\nu (\psi^\dagger T^A \psi + \chi^\dagger T^A \chi). \tag{B.21}$$

Combining this equation with $\frac{g}{8m^2}\psi^\dagger T^A \psi \delta^0_\nu$ or $\frac{g}{8m^2}\chi^\dagger T^A \chi \delta^0_\nu$ yields[1]

$$-O_D^\psi = -O_1^{hl,\psi} - \frac{g^2}{8} O_{vs} - \frac{g^2}{8m^2}\psi^\dagger T^A \psi \psi^\dagger T^A \psi \tag{B.23}$$

and

$$-O_D^\chi = -O_1^{hl,\chi} - \frac{g^2}{8} O_{vs} - \frac{g^2}{8m^2}\chi^\dagger T^A \chi \chi^\dagger T^A \chi, \tag{B.24}$$

respectively. The last terms in these two equations involve four heavy quarks (four heavy anti-quarks) and contribute only beyond the order of our calculation.

Plugging these relations into the Lagrangian still containing $O_1^{hl,\psi/\chi}$, we obtain

$$\mathcal{L}_{\text{eliminated } O_1^{hl}} \supset (\hat{c}_D + \hat{c}_1^{hl}) O_D^\psi + (\hat{c}_D + \hat{c}_1^{hl}) O_D^\chi + \left(\hat{d}_{vs} - \frac{g^2}{4}\hat{c}_1^{hl}\right) O_{vs}. \tag{B.25}$$

In our choice of basis, we define

$$d_2 = \hat{c}_D + \hat{c}_1^{hl}, \tag{B.26}$$

$$d_{vs} = \hat{d}_{vs} - \frac{g^2}{4}\hat{c}_1^{hl} = \hat{d}_{vs} - \pi\alpha\hat{c}_1^{hl}. \tag{B.27}$$

Reference [53] discusses the running of the d_i in both the case where O_1^{hl} has not been removed and the one where it has. While in [34] the operator has not been eliminated, we choose to consider the case where it has been removed since we prefer to work with a non-redundant operator basis.

We have written the comparison in this general manner in order to facilitate an easier comparison with different choices of conventions in various references. Therefore, the discussion in this section should be viewed separately from the one in appendix B.1.1 discussing the choice of operator basis in the gluonic part of the Lagrangian. Specifically, the coefficient to the Darwin operator, d_2 in our conventions, is modified by both a field redefinition in the gluonic sector and the elimination in the heavy-light sector of the Lagrangian.

[1] Use that

$$\psi^\dagger [D^i, E^i]\psi = \psi^\dagger (D^i G^{i0} - G^{i0} D^i)\psi = \psi^\dagger (D^i G^{i0})\psi = -\psi^\dagger (D_i G^{i0})\psi, \tag{B.22}$$

where the derivative is only acting on the field strength tensor in the end. This relates the usual expression for the Darwin operator O_D to the one obtained after combining the EOM with these factors.

B.2 Relation between Different Conventions for the Potentials

In this work, we consider references with mainly two different definitions of the potentials in PNRQCD. The one we choose to use is the one also used in [27], where the spin-projected potentials take the form (cf. equation (3.59))

$$V(\mathbf{p},\mathbf{p}') = -\mathcal{V}_C(\alpha)\frac{4\pi C_F\alpha(\mu)}{\mathbf{q}^2} + \mathcal{V}_{1/m}(\alpha)\frac{\pi^2(4\pi)C_F\alpha(\mu)}{m|\mathbf{q}|} - \mathcal{V}_p(\alpha)\frac{2\pi C_F\alpha(\mu)(\mathbf{p}^2+\mathbf{p}'^2)}{m^2\mathbf{q}^2} - \mathcal{V}_{1/m^2}(\alpha)\frac{4\pi C_F\alpha(\mu)}{m^2}. \tag{B.28}$$

The other relevant choice of notation is the one used, for example, in [34], where the potential is given by

$$\begin{aligned} V_s = &-\frac{C_F\alpha_{V_s}}{r} - \frac{C_FC_AD_s^{(1)}}{2mr^2} \\ &- \frac{C_FD_{1,s}^{(2)}}{2m^2}\left\{\mathbf{p}^2,\frac{1}{r}\right\} + \frac{C_FD_{2,s}^{(2)}}{2m^2r^3}\mathbf{L}^2 + \frac{\pi C_FD_{d,s}^{(2)}}{m^2}\delta^{(3)}(r) \\ &+ \frac{3C_FD_{LS,s}^{(2)}}{2m^2r^3}\mathbf{L}\cdot\mathbf{S} + \frac{4\pi C_FD_{S^2,s}^{(2)}}{3m^2}\mathbf{S}^2\delta^{(3)}(r) + \frac{C_FD_{\mathbf{S}_{12},s}^{(2)}}{4m^2r^3}\mathbf{S}_{12}(\hat{\mathbf{r}}). \end{aligned} \tag{B.29}$$

The $\mathbf{L}^2$-term can be rewritten and absorbed into the delta- and $\frac{1}{m}$-potentials. This is easiest seen by considering the momentum space expression

$$\frac{C_FD_2^{(2)}}{2m^2r^3}\mathbf{L}^2 \to \frac{\pi C_FD_2^{(2)}}{m^2}\left[\left(\frac{\mathbf{p}^2-\mathbf{p}'^2}{\mathbf{q}^2}\right)^2 - 1\right], \tag{B.30}$$

where the last term immediately shows the same structure as a delta-potential. An insertion of the first term can be rewritten [35] and absorbed into the $\frac{1}{m}$-potential.

For the sake of the comparison of these expressions, it is enough to consider the potentials in four dimensions, $\varepsilon \to 0$. Additionally, it is sufficient to use the spin-projected expressions $\mathbf{S}^2 \to s(s+1)$, $\mathbf{L}\cdot\mathbf{S} \to 0$ and $\mathbf{S}_{12}(\hat{\mathbf{r}}) \to 0$.

We use the three-dimensional Fourier transforms

$$\frac{1}{r} \xrightarrow[\text{FT}]{} \frac{4\pi}{\mathbf{q}^2}, \tag{B.31}$$

$$\frac{1}{r^2} \xrightarrow[\text{FT}]{} \frac{2\pi^2}{|\mathbf{q}|}, \tag{B.32}$$

$$\left\{\frac{1}{r}, \mathbf{p}^2\right\} \xrightarrow[\text{FT}]{} 4\pi\frac{\mathbf{p}^2+\mathbf{p}'^2}{\mathbf{q}^2}, \tag{B.33}$$

$$\delta^{(3)}(r) \xrightarrow[\text{FT}]{} 1. \tag{B.34}$$

For the Coulomb potential, we can thus associate

$$-\frac{4\pi\alpha C_F}{\mathbf{q}^2}\mathcal{V}_C \longleftrightarrow -\frac{4\pi C_F \alpha_{V_s}}{\mathbf{q}^2}. \tag{B.35}$$

For the $\frac{1}{m}$-potential, we get

$$\frac{(4\pi)\pi^2\alpha C_F}{m|\mathbf{q}|}\mathcal{V}_{1/m} \longleftrightarrow -\frac{\pi^2 C_F C_A D^{(1)}}{m|\mathbf{q}|} + \frac{\pi^2 C_F^2 \alpha D_2^{(2)}}{2m|\mathbf{q}|}. \tag{B.36}$$

The $\frac{1}{m^2}$-potentials are related by

$$-\frac{4\pi\alpha C_F}{m^2}\mathcal{V}_{1/m^2} \longleftrightarrow \frac{\pi C_F D_d^{(2)}}{m^2} + \frac{4\pi C_F D_{S^2}^{(2)}}{3m^2}s(s+1) - \frac{\pi C_F D_2^{(2)}}{m^2} \tag{B.37}$$

and

$$-\frac{4\pi\alpha C_F}{m^2}\mathcal{V}_p\frac{\mathbf{p}^2+\mathbf{p}'^2}{2\mathbf{q}^2} \longleftrightarrow -\frac{4\pi C_F D_1^{(2)}}{m^2}\frac{\mathbf{p}^2+\mathbf{p}'^2}{2\mathbf{q}^2}. \tag{B.38}$$

In terms of the coefficients $\mathcal{V}_i$ and D_i, these relations can be expressed in the compact form depicted in table B.4.

Table B.4: Relation between the coefficients used in the potential in references [27] and [34].

Coefficients $\mathcal{V}_i$ from [27]	Coefficients D_i from [34]
$\alpha\mathcal{V}_C$	α_{V_s}
$4\pi\alpha\mathcal{V}_{1/m}$	$-C_A D^{(1)} + \frac{C_F}{2}\alpha D_2^{(2)}$
$-4\alpha\mathcal{V}_{1/m^2}$	$D_d^{(2)} + \frac{4}{3}s(s+1)D_{S^2}^{(2)} - D_2^{(2)}$
$\alpha\mathcal{V}_p$	$D_1^{(2)}$

Appendix C

Derivation of the Two-Loop Ultrasoft Counterterm

In this appendix, we provide the derivation of the two-loop ultrasoft counterterm as an extension of the one-loop calculation presented in section 5.3. When performing the ultrasoft calculation in the course of this thesis, we have worked with the more general two-loop expressions from the beginning, closely following reference [34]. However, since only the one-loop result is relevant to the NLL contribution discussed in this thesis, we extracted these lower-order terms when presenting the results in the main text. In the following, we now give the full calculation. We also provide some additional details of the calculation in this appendix.

C.1 Two-Loop Correlator Σ_B

In equation (5.43), we have given the chromomagnetic correlator Σ_B at one-loop. We now turn to the two-loop result including terms up to $\mathcal{O}(\alpha^2)$, where the correlator reads [34, 80, 82, 90]

$$\begin{aligned}\Sigma_B^{\text{2-loop}} &= g_B^4 C_F C_A V_A^2 \Gamma(-3+4\varepsilon)\left[\mathcal{D}^{(1)}(\varepsilon)-(1-2\varepsilon)\mathcal{D}_1^{(1)}(\varepsilon)\right]\mathbf{r}(h_o^B-E)^{3-4\varepsilon}\mathbf{r} = \\ &\equiv c_{\text{2-loop}}\tilde{\mu}^{4\varepsilon}\mathbf{r}(h_o^B-E)^{3-4\varepsilon}\mathbf{r}, \end{aligned} \tag{C.1}$$

using the same notation as for the one-loop case. The constants in the two-loop expression read

$$\mathcal{D}^{(1)}(\varepsilon) = \frac{1}{(2\pi)^2}\frac{1}{4\pi^{2-2\varepsilon}}\Gamma^2(1-\varepsilon)g(\varepsilon), \tag{C.2}$$

$$\mathcal{D}_1^{(1)}(\varepsilon) = \frac{1}{(2\pi)^2}\frac{1}{4\pi^{2-2\varepsilon}}\Gamma^2(1-\varepsilon)g_1(\varepsilon) \tag{C.3}$$

with

$$g(\varepsilon) = -\frac{-2\varepsilon^3+6\varepsilon^2-8\varepsilon+3}{\varepsilon(2\varepsilon^2-5\varepsilon+3)} + \frac{2\varepsilon\Gamma(2\varepsilon-2)\Gamma(2\varepsilon-1)}{(-2\varepsilon+3)\Gamma(4\varepsilon-3)}, \tag{C.4}$$

$$g_1(\varepsilon) = \frac{-6\varepsilon^3+17\varepsilon^2-18\varepsilon+6}{\varepsilon^2(2\varepsilon^2-5\varepsilon+3)} - \frac{4(-\varepsilon+1)n_f T_F}{\varepsilon(-2\varepsilon+3)N} - \frac{2(\varepsilon^2-\varepsilon+1)\Gamma(2\varepsilon-2)\Gamma(2\varepsilon-1)}{\varepsilon(-2\varepsilon+3)\Gamma(4\varepsilon-3)}. \tag{C.5}$$

The divergent terms in the coefficients are given by

$$\begin{aligned} c_{\text{1-loop}} &= -\frac{C_F V_A^2 \beta_0}{12\pi^2}\frac{\alpha^2}{\varepsilon^2} + \left[\frac{C_F V_A^2}{3\pi}\alpha + \frac{C_F V_A^2 \beta_0(-5+3\gamma_E-3\ln(\pi))}{36\pi^2}\alpha^2\right]\frac{1}{\varepsilon} + \mathcal{O}(\varepsilon^0) = \\ &\equiv c^{(2)}_{\text{1-loop}}\frac{1}{\varepsilon^2} + c^{(1)}_{\text{1-loop}}\frac{1}{\varepsilon} + \mathcal{O}(\varepsilon^0), \end{aligned} \tag{C.6}$$

$$\begin{aligned} c_{\text{2-loop}} &= -\frac{C_A C_F V_A^2(-11N+4T_F n_f)}{72\pi^2 N}\frac{\alpha^2}{\varepsilon^2} + \left[\frac{C_A C_F V_A^2\left(34+2\pi^2-11\gamma_E+11\ln(\pi)\right)}{36\pi^2}\right. \\ &\quad \left. + \frac{C_A C_F V_A^2 T_F n_f\left(-10+4\gamma_E-4\ln(\pi)\right)}{36\pi^2 N}\right]\frac{\alpha^2}{\varepsilon} + \mathcal{O}(\varepsilon^0) = \\ &\equiv c^{(2)}_{\text{2-loop}}\frac{1}{\varepsilon^2} + c^{(1)}_{\text{2-loop}}\frac{1}{\varepsilon} + \mathcal{O}(\varepsilon^0), \end{aligned} \tag{C.7}$$

where we now include terms up to $\mathcal{O}(\alpha^2)$ also in $c_{\text{1-loop}}$.

In $\Sigma_B^{n\text{-loop}}$ $(n=1,2)$, these coefficients multiply an operator structure of the form

$$\tilde{\mu}^{2n\varepsilon}\mathbf{r}(h_o^B-E)^{3-2n\varepsilon}\mathbf{r} = \mathbf{r}(h_o^B-E)^3\mathbf{r} - 2n\mathbf{r}(h_o^B-E)^3\ln\left(\frac{h_o^B-E}{\tilde{\mu}}\right)\mathbf{r}\varepsilon + \mathcal{O}(\varepsilon^2), \tag{C.8}$$

respectively. For $\Sigma_B^{\text{1-loop}}$, we noted that the $\mathcal{O}(\varepsilon)$-term is not relevant to the divergence. The same holds for the result up to two-loop, even though, in this case, the argument is a bit more involved, as we discuss now. Summing the one- and two-loop expressions yields

$$\begin{aligned} \Sigma_B^{\text{1-loop}} + \Sigma_B^{\text{2-loop}} &= \left[\left(c^{(2)}_{\text{1-loop}} + c^{(2)}_{\text{2-loop}}\right)\frac{1}{\varepsilon^2} + \left(c^{(1)}_{\text{1-loop}} + c^{(1)}_{\text{2-loop}}\right)\frac{1}{\varepsilon}\right]\mathbf{r}(h_o^B-E)^3\mathbf{r} \\ &\quad - 2\underbrace{\left(c^{(2)}_{\text{1-loop}} + 2c^{(2)}_{\text{2-loop}}\right)}_{=0}\frac{1}{\varepsilon}\mathbf{r}(h_o^B-E)^3\ln\left(\frac{h_o^B-E}{\tilde{\mu}}\right)\mathbf{r} + \mathcal{O}(\varepsilon^0). \end{aligned} \tag{C.9}$$

Using the explicit expressions for $c^{(2)}_{\text{1-loop}}$ and $c^{(2)}_{\text{2-loop}}$ with $\beta_0 = \frac{11}{3}C_A - \frac{4}{3}T_F n_f$ and $C_A = N$, one observes that the second line is zero and not actually contributing to the divergence. Therefore, it is enough to consider the leading order term $\mathbf{r}(h_o^B-E)^3\mathbf{r}$ in the expansion of the operator

structure also for $\Sigma_B^{\text{2-loop}}$. In total, the divergence is given by

$$\Sigma_B^{\text{1-loop}} + \Sigma_B^{\text{2-loop}} = C_F V_A^2 \Bigg\{ \left[\frac{\alpha}{3\pi} - \frac{\alpha^2}{36\pi^2} \left(C_A \left(-\frac{47}{3} - 2\pi^2 \right) + \frac{10}{3} T_F n_f \right) \right] \frac{1}{\varepsilon} - \frac{\alpha^2}{24\pi^2} \beta_0 \frac{1}{\varepsilon^2} \Bigg\} \times \mathbf{r}(h_o - E)^3 \mathbf{r} + \mathcal{O}(\varepsilon^0). \tag{C.10}$$

Therefore, the two-loop ultrasoft counterterm in position space reads

$$\delta V_{us}^{\text{PS}} = C_F V_A^2 \Bigg\{ \left[\frac{\alpha}{3\pi} - \frac{\alpha^2}{36\pi^2} \left(C_A \left(-\frac{47}{3} - 2\pi^2 \right) + \frac{10}{3} T_F n_f \right) \right] \frac{1}{\varepsilon} - \frac{\alpha^2}{24\pi^2} \beta_0 \frac{1}{\varepsilon^2} \Bigg\} \mathbf{r}(h_o - E)^3 \mathbf{r}. \tag{C.11}$$

C.2 Operator Identity in Position Space for Rewriting the Ultrasoft Counterterm

In this section, we detail the derivation of equation (5.48), which is used in [34, 82] when deriving the counterterm encoding the ultrasoft running. The identity provides a way to rewrite the operator $\mathbf{r}(h_o - E)\mathbf{r}$ in terms of the potentials. In this context, it is enough to consider only the leading potentials in the singlet and octet Hamiltonian, that is

$$h_s = \frac{\mathbf{p}^2}{m} + V_s^{(0)} \quad \text{and} \quad h_o = \frac{\mathbf{p}^2}{m} + V_o^{(0)}, \tag{C.12}$$

where the momentum operator is given by $p_k = -i\frac{\partial}{\partial r_k}$. We defined the difference between the octet and singlet static potential as $\Delta V = V_o^{(0)} - V_s^{(0)}$.

As was discussed in section 5.3.1, external factors of positive powers of $(h_s - E)$ can be neglected since they multiply factors $\frac{1}{(h_s - E)}$ from the Green's functions.

We will use the canonical commutation relation

$$[r_i, p_j] = i\delta_{ij}, \tag{C.13}$$

which allows to substitute

$$p_k r_k = r_k p_k - i(d-1), \tag{C.14}$$

where we sum over repeated indices. The first term on the right-hand side can be reexpressed in terms of the absolute value r of $\mathbf{r}$ as

$$r_k p_k = -ir_k \frac{\partial}{\partial r_k} = -ir_k \frac{\partial r}{\partial r_k}\frac{\partial}{\partial r} = -ir\frac{\partial}{\partial r}, \tag{C.15}$$

where $r^2 = \sum_{i=1}^{d-1} r_i^2$. Applying the basic commutation relation (C.13), we obtain the useful relations

$$[f(r), p_k] = i\left(\frac{\partial}{\partial r_k} f(r)\right) \quad \text{and} \quad [\mathbf{p}^2, f(r)] = -\left(\frac{\partial^2}{\partial r_k^2} f(r)\right) - 2i\left(\frac{\partial}{\partial r_k} f(r)\right) p_k. \tag{C.16}$$

In order to use the fact that we can neglect external factors of $(h_s - E)$, we rewrite the operator in question as

$$\begin{aligned}\mathbf{r}(h_o - E)\mathbf{r} &= r_k(h_o - h_s + h_s - E)^3 r_k = r_k(\Delta V + h_s - E)^3 r_k = \\ &= r_k\Big((\Delta V)^3 + (\Delta V)^2(h_s - E) + (\Delta V)(h_s - E)(\Delta V) + (h_s - E)(\Delta V)^2 \\ &\quad + (\Delta V)(h_s - E)^2 + (h_s - E)(\Delta V)(h_s - E) + (h_s - E)^2(\Delta V) + (h_s - E)^3\Big) r_k.\end{aligned} \tag{C.17}$$

We now move the (still internal) factors of $(h_s - E)$ to the furthermost right or left of all other factors in a suitable manner. As discussed in the main text, this is an ambiguous process from which we choose one particular procedure.

We first note two general relations:[1] Moving one factor of $(h_s - E)$ to the right of r_k, we get

$$\begin{aligned}[\dots](h_s - E)r_k &= [\dots][(h_s - E), r_k] + [\dots]r_k(h_s - E) = \\ &= [\dots][\frac{\mathbf{p}^2}{m}, r_k] + \mathcal{O}((h_s - E)) = \\ &= [\dots]\left(-\frac{2i}{m}\right) p_k + \mathcal{O}((h_s - E)),\end{aligned} \tag{C.18}$$

[1] Note that while these relations are true in general, the $\mathcal{O}((h_s - E))$-terms can only be neglected if they are external factors (as, for example, in $[\dots]r_k(h_s - E)$ with no further factors to the right). If they appear in the middle of an expression, they must be considered explicitly.

where the dots $[\dots]$ denote any terms to the left of this expression. On the other hand, moving one factor of $(h_s - E)$ to the left of r_k, we get

$$\begin{aligned} r_k(h_s - E)[\dots] &= [r_k, (h_s - E)][\dots] + (h_s - E) r_k[\dots] = \\ &= [r_k, \frac{\mathbf{p}^2}{m}][\dots] + \mathcal{O}((h_s - E)) = \\ &= \left(\frac{2i}{m}\right) p_k[\dots] + \mathcal{O}((h_s - E)). \end{aligned} \tag{C.19}$$

Using these considerations, we now rewrite the terms in (C.17). In the following, we use equal signs to denote expressions that are equal up to terms containing external factors of $\mathcal{O}((h_s - E))$, which we do not indicate explicitly anymore.

$r_k(\Delta V)^3 r_k$

This term directly produces $\mathbf{r}^2(\Delta V)^3$.

$r_k(\Delta V)^2(h_s - E)r_k$, $r_k(\Delta V)(h_s - E)(\Delta V)r_k$ and $r_k(h_s - E)(\Delta V)^2 r_k$

The terms involving two factors of (ΔV) can be rewritten in the form of $\frac{1}{m}$-terms: We use

$$r_k(\Delta V)^2(h_s - E)r_k = -\frac{2i}{m} r_k(\Delta V)^2 p_k, \tag{C.20}$$

$$r_k(h_s - E)(\Delta V)^2 r_k = \frac{2i}{m} p_k(\Delta V)^2 r_k \tag{C.21}$$

and symmetrize the term where the factors of (ΔV) appear to both sides of $(h_s - E)$:

$$\begin{aligned} r_k(\Delta V)(h_s-E)(\Delta V)r_k &= \frac{1}{2}\Big\{(\Delta V)r_k(h_s-E)(\Delta V)r_k + r_k(\Delta V)(h_s-E)r_k(\Delta V)\Big\} = \\ &= \frac{1}{2}\Big\{(\Delta V)[r_k,(h_s-E)](\Delta V)r_k + (\Delta V)(h_s-E)r_k(\Delta V)r_k \\ &\qquad + r_k(\Delta V)[(h_s-E),r_k](\Delta V) + r_k(\Delta V)r_k(h_s-E)(\Delta V)\Big\} = \\ &= \frac{1}{2}\Big\{\frac{1}{m}(\Delta V)[r_k,\mathbf{p}^2](\Delta V)r_k + [(\Delta V),(h_s-E)]r_k(\Delta V)r_k \\ &\qquad + \frac{1}{m}r_k(\Delta V)[\mathbf{p}^2,r_k](\Delta V) + r_k(\Delta V)r_k[(h_s-E),(\Delta V)]\Big\} = \\ &= \frac{1}{2m}\Big\{2i(\Delta V)p_k(\Delta V)r_k + [(\Delta V),\mathbf{p}^2]r_k(\Delta V)r_k \\ &\qquad - 2ir_k(\Delta V)p_k(\Delta V) + r_k(\Delta V)r_k[\mathbf{p}^2,(\Delta V)]\Big\}. \end{aligned} \tag{C.22}$$

Taking the three terms together, we obtain

$$\begin{aligned} &r_k(\Delta V)^2(h_s-E)r_k + r_k(\Delta V)(h_s-E)(\Delta V)r_k + r_k(h_s-E)(\Delta V)^2r_k = \\ &\quad = \frac{1}{m}\Big\{-2i(\Delta V)^2r_kp_k + 2ip_kr_k(\Delta V)^2 + i(\Delta V)p_kr_k(\Delta V) - i(\Delta V)r_kp_k(\Delta V) \\ &\qquad + \frac{1}{2}[(\Delta V),\mathbf{p}^2]r_k(\Delta V)r_k + \frac{1}{2}r_k(\Delta V)r_k[\mathbf{p}^2,(\Delta V)]\Big\}. \end{aligned} \tag{C.23}$$

Using $p_kr_k = r_kp_k - i(d-1)$, the terms in the first line of this result simplifies to

$$\begin{aligned} &-2i(\Delta V)^2r_kp_k + 2ip_kr_k(\Delta V)^2 + i(\Delta V)p_kr_k(\Delta V) - i(\Delta V)r_kp_k(\Delta V) = \\ &\quad = 3(d-1)(\Delta V)^2 + 2ir_k[p_k,(\Delta V)^2] = \\ &\quad = 3(d-1)(\Delta V)^2 + 4(\Delta V)\left(r\frac{\mathrm{d}}{\mathrm{d}r}\Delta V\right) \end{aligned} \tag{C.24}$$

and the second line reduces to

$$\begin{aligned}\frac{1}{2}[(\Delta V),\mathbf{p}^2]r_k(\Delta V)r_k+\frac{1}{2}r_k(\Delta V)r_k[\mathbf{p}^2,(\Delta V)]&=\\ &=i(\partial_{r_k}(\Delta V))p_k r^2(\Delta V)-i(\partial_{r_k}(\Delta V))r^2(\Delta V)p_k=\\ &=i(\partial_{r_k}(\Delta V))[p_k,r^2(\Delta V)]=\\ &=r^2(\partial_{r_k}(\Delta V))^2+2r_k(\partial_{r_k}(\Delta V))(\Delta V)\\ &=\left(r\frac{\mathrm{d}}{\mathrm{d}r}\Delta V\right)^2+2\left(r\frac{\mathrm{d}}{\mathrm{d}r}\Delta V\right)(\Delta V).\end{aligned}\tag{C.25}$$

In total, these three terms yield the contribution

$$\begin{aligned}r_k(\Delta V)^2(h_s-E)r_k+r_k(\Delta V)(h_s-E)(\Delta V)r_k+r_k(h_s-E)(\Delta V)^2r_k&=\\ =\frac{1}{m}\left\{3(d-1)(\Delta V)^2+6(\Delta V)\left(r\frac{\mathrm{d}}{\mathrm{d}r}\Delta V\right)+\left(r\frac{\mathrm{d}}{\mathrm{d}r}\Delta V\right)^2\right\}.\end{aligned}\tag{C.26}$$

$r_k(\Delta V)(h_s-E)^2r_k$ and $r_k(h_s-E)^2(\Delta V)r_k$

These two terms involving the square of (h_s-E) also contribute at order $\mathcal{O}\left(\frac{1}{m}\right)$. In the first expression, we move both factors of (h_s-E) to the right of the other factors, while in the second term, we move both factors of (h_s-E) to the left. This leads to

$$\begin{aligned}r_k(\Delta V)(h_s-E)^2r_k&=-\frac{2i}{m}r_k(\Delta V)(h_s-E)p_k=\\ &=-\frac{2i}{m}r_k(\Delta V)[(h_s-E),p_k]=\\ &=-\frac{2i}{m}r_k(\Delta V)[V_s^{(0)},p_k]\end{aligned}\tag{C.27}$$

and

$$r_k(h_s-E)^2(\Delta V)r_k=\frac{2i}{m}[p_k,V_s^{(0)}](\Delta V)r_k.\tag{C.28}$$

Together, we obtain

$$\begin{aligned} r_k(\Delta V)(h_s-E)^2 r_k + r_k(h_s-E)^2(\Delta V)r_k = \\ = \frac{2}{m}\left(r_k(\Delta V)\left(\partial_{r_k}V_s^{(0)}\right) + \left(\partial_{r_k}V_s^{(0)}\right)(\Delta V)r_k\right) = \\ = \frac{4}{m}(\Delta V)\left(r\frac{\mathrm{d}}{\mathrm{d}r}V_s^{(0)}\right). \end{aligned} \tag{C.29}$$

$r_k(h_s-E)(\Delta V)(h_s-E)r_k$

While this term also includes two factors of (h_s-E), we write it in a way such that it contributes at order $\mathcal{O}\left(\frac{1}{m^2}\right)$. We move the left factor of (h_s-E) to the left and the right one to the right and obtain

$$r_k(h_s-E)(\Delta V)(h_s-E)r_k = \frac{4}{m^2}p_k(\Delta V)p_k. \tag{C.30}$$

$r_k(h_s-E)^3 r_k$

The last missing term also contributes at order $\mathcal{O}\left(\frac{1}{m^2}\right)$. We first move one factor to the right and one to the left:

$$r_k(h_s-E)^3 r_k = \frac{4}{m^2}p_k(h_s-E)p_k. \tag{C.31}$$

We then symmetrize the remaining operation, moving $\frac{1}{2}(h_s-E)$ to the left and $\frac{1}{2}(h_s-E)$ to the right of p_k.

$$\begin{aligned} r_k(h_s-E)^3 r_k = \frac{2}{m^2}\left([p_k,(h_s-E)]p_k + p_k[(h_s-E),p_k]\right) = \\ = \frac{2}{m^2}\left([p_k,V_s^{(0)}]p_k + p_k[V_s^{(0)},p_k]\right) = \\ = \frac{2}{m^2}\left(2p_kV_s^{(0)}p_k - V_s^{(0)}\mathbf{p}^2 - \mathbf{p}^2V_s^{(0)}\right). \end{aligned} \tag{C.32}$$

Taking this together with (C.30), we obtain

$$\begin{aligned} r_k(h_s-E)(\Delta V)(h_s-E)r_k + r_k(h_s-E)^3 r_k = \\ &= \frac{2}{m^2}\left(2p_k(\Delta V)p_k + 2p_k V_s^{(0)} p_k - V_s^{(0)}\mathbf{p}^2 - \mathbf{p}^2 V_s^{(0)}\right) = \\ &= \frac{2}{m^2}\left(2p_k V_o^{(0)} p_k + (\Delta V - V_o^{(0)})\mathbf{p}^2 + \mathbf{p}^2(\Delta V - V_o^{(0)})\right) = \\ &= \frac{2}{m^2}\left(\{\mathbf{p}^2, \Delta V\} - [\mathbf{p},[\mathbf{p}, V_o^{(0)}]]\right) \end{aligned} \tag{C.33}$$

for the terms contributing at order $\mathcal{O}\left(\frac{1}{m^2}\right)$.

Taking all terms in equation (C.17) together, we obtain

$$\begin{aligned} \mathbf{r}(h_o-E)\mathbf{r} &= \mathbf{r}^2(\Delta V)^3 + \frac{1}{m}\left(3(d-1)(\Delta V)^2 + 6(\Delta V)\left(r\frac{\mathrm{d}}{\mathrm{d}r}\Delta V\right) + \left(r\frac{\mathrm{d}}{\mathrm{d}r}\Delta V\right)^2\right) \\ &\quad + \frac{4}{m}(\Delta V)\left(r\frac{\mathrm{d}}{\mathrm{d}r}V_s^{(0)}\right) + \frac{2}{m^2}\left(\{\mathbf{p}^2,\Delta V\} - [\mathbf{p},[\mathbf{p},V_o^{(0)}]]\right) = \qquad \text{(C.34)} \\ &= \mathbf{r}^2(\Delta V)^3 + \frac{1}{m}\Bigg[4\Delta V\left(r\frac{\mathrm{d}}{\mathrm{d}r}V_s^{(0)}\right) + (\Delta V)^2(3d-8) \\ &\qquad\qquad + 4\Delta V\left(\left(r\frac{\mathrm{d}}{\mathrm{d}r}\Delta V\right) + \Delta V\right) + \left(\left(r\frac{\mathrm{d}}{\mathrm{d}r}\Delta V\right) + \Delta V\right)^2\Bigg] \\ &\quad + \frac{1}{m^2}\left[-2[\mathbf{p},[\mathbf{p},V_o^{(0)}]] + 2\{\mathbf{p}^2,\Delta V\}\right], \qquad \text{(C.35)} \end{aligned}$$

where, as a final step, we have rewritten the $\frac{1}{m}$-terms in a way that includes the combination $\left(\left(r\frac{\mathrm{d}}{\mathrm{d}r}\Delta V\right) + \Delta V\right)$, which is suppressed in ε. This will become obvious in the explicit Fourier transform of these terms in section 5.3.2. This concludes the derivation of equation (5.48).

C.3 Expanding the Ultrasoft Counterterm in α

We recall the explicit expressions for the static potentials in position space from equation (5.56):

$$V_{s/o/\Delta}^{(0),\mathrm{PS}} = \alpha c_1^{s/o/\Delta}\mathcal{F}_2(r) + \alpha^2\left[c_{21}^{s/o/\Delta}\mathcal{F}_{2+2\varepsilon}(r) + c_{22}^{s/o/\Delta}\mathcal{F}_2(r)\right] + \mathcal{O}(\alpha^3). \tag{C.36}$$

Plugging this into the identity for the counterterm derived above, we expand the separate terms to next-to-leading order in α and obtain:

$$\mathbf{r}^2(\Delta V)^3 = \left[\alpha^3\left(c_1^\Delta\right)^3 + \alpha^4 3\left(c_1^\Delta\right)^2\left(c_{22}^\Delta\right)\right] r^2\mathcal{F}_2(r)^3 + \alpha^4 3\left(c_1^\Delta\right)^2\left(c_{21}^\Delta\right) r^2\mathcal{F}_2(r)^2\mathcal{F}_{2+2\varepsilon}(r) + \mathcal{O}(\alpha^5), \tag{C.37}$$

$$\Delta V\left(r\frac{\mathrm{d}}{\mathrm{d}r}V_s^{(0)}\right) = \left[\alpha^2\left(c_1^\Delta\right)\left(c_1^s\right) + \alpha^3\left(\left(c_1^\Delta\right)\left(c_{22}^s\right) + \left(c_{22}^\Delta\right)\left(c_1^s\right)\right)\right]\mathcal{F}_2(r)\left(r\frac{\mathrm{d}}{\mathrm{d}r}\mathcal{F}_2(r)\right) + \alpha^3\left(c_1^\Delta\right)\left(c_{21}^s\right)\mathcal{F}_2(r)\left(r\frac{\mathrm{d}}{\mathrm{d}r}\mathcal{F}_{2+2\varepsilon}(r)\right) + \alpha^3\left(c_{21}^\Delta\right)\left(c_1^s\right)\mathcal{F}_{2+2\varepsilon}(r)\left(r\frac{\mathrm{d}}{\mathrm{d}r}\mathcal{F}_2(r)\right) + \mathcal{O}(\alpha^4), \tag{C.38}$$

$$(\Delta V)^2 = \left[\alpha^2\left(c_1^\Delta\right)^2 + \alpha^3 2\left(c_1^\Delta\right)\left(c_{22}^\Delta\right)\right]\mathcal{F}_2(r)^2 + \alpha^3 2\left(c_1^\Delta\right)\left(c_{21}^\Delta\right)\mathcal{F}_2(r)\mathcal{F}_{2+2\varepsilon}(r) + \mathcal{O}\left(\alpha^4\right), \tag{C.39}$$

$$(\Delta V)\left(r\frac{\mathrm{d}}{\mathrm{d}r}\Delta V + \Delta V\right) = \left[\alpha^2\left(c_1^\Delta\right)^2 + \alpha^3 2\left(c_1^\Delta\right)\left(c_{22}^\Delta\right)\right]\mathcal{F}_2(r)\left(r\frac{\mathrm{d}}{\mathrm{d}r}\mathcal{F}_2(r)\right) + \alpha^3\left(c_1^\Delta\right)\left(c_{21}^\Delta\right)\left\{\mathcal{F}_2(r)\left(r\frac{\mathrm{d}}{\mathrm{d}r}\mathcal{F}_{2+2\varepsilon}(r)\right) + \mathcal{F}_{2+2\varepsilon}(r)\left(r\frac{\mathrm{d}}{\mathrm{d}r}\mathcal{F}_2(r)\right)\right\} + \left[\alpha^2\left(c_1^\Delta\right)^2 + \alpha^3 2\left(c_1^\Delta\right)\left(c_{22}^\Delta\right)\right]\mathcal{F}_2(r)^2 + \alpha^3 2\left(c_1^\Delta\right)\left(c_{21}^\Delta\right)\mathcal{F}_2(r)\mathcal{F}_{2+2\varepsilon}(r) + \mathcal{O}\left(\alpha^4\right), \tag{C.40}$$

$$\left(r\frac{\mathrm{d}}{\mathrm{d}r}\Delta V + \Delta V\right)^2 = \left[\alpha^2\left(c_1^\Delta\right)^2 + \alpha^3 2\left(c_1^\Delta\right)\left(c_{22}^\Delta\right)\right]\left(r\frac{\mathrm{d}}{\mathrm{d}r}\mathcal{F}_2(r)\right)^2 + \alpha^3 2\left(c_1^\Delta\right)\left(c_{21}^\Delta\right)\left(r\frac{\mathrm{d}}{\mathrm{d}r}\mathcal{F}_2(r)\right)\left(r\frac{\mathrm{d}}{\mathrm{d}r}\mathcal{F}_{2+2\varepsilon}(r)\right) + \left[\alpha^2 2\left(c_1^\Delta\right)^2 + \alpha^3 4\left(c_1^\Delta\right)\left(c_{22}^\Delta\right)\right]\mathcal{F}_2(r)\left(r\frac{\mathrm{d}}{\mathrm{d}r}\mathcal{F}_2(r)\right) + \alpha^3 2\left(c_1^\Delta\right)\left(c_{21}^\Delta\right)\left\{\mathcal{F}_2(r)\left(r\frac{\mathrm{d}}{\mathrm{d}r}\mathcal{F}_{2+2\varepsilon}(r)\right) + \mathcal{F}_{2+2\varepsilon}(r)\left(r\frac{\mathrm{d}}{\mathrm{d}r}\mathcal{F}_2(r)\right)\right\} + \left[\alpha^2\left(c_1^\Delta\right)^2 + \alpha^3 2\left(c_1^\Delta\right)\left(c_{22}^\Delta\right)\right]\mathcal{F}_2(r)^2 + \alpha^3 2\left(c_1^\Delta\right)\left(c_{21}^\Delta\right)\mathcal{F}_2(r)\mathcal{F}_{2+2\varepsilon}(r) + \mathcal{O}\left(\alpha^4\right), \tag{C.41}$$

$$[\mathbf{p},[\mathbf{p},V_o^{(0)}]] = \left(\alpha\left(c_1^o\right) + \alpha^2\left(c_{22}^o\right)\right)[\mathbf{p},[\mathbf{p},\mathcal{F}_2(r)]] + \alpha^2\left(c_{21}^o\right)[\mathbf{p},[\mathbf{p},\mathcal{F}_{2+2\varepsilon}(r)]] + \mathcal{O}(\alpha^3), \tag{C.42}$$

$$\{\mathbf{p}^2,\Delta V\} = \left(\alpha\left(c_1^\Delta\right) + \alpha^2\left(c_{22}^\Delta\right)\right)\{\mathbf{p}^2,\mathcal{F}_2(r)\} + \alpha^2\left(c_{21}^\Delta\right)\{\mathbf{p}^2,\mathcal{F}_{2+2\varepsilon}(r)\} + \mathcal{O}(\alpha^3). \tag{C.43}$$

C.4 Fourier Transform of the Individual Structures in the Counterterm

In table C.1, we list the Fourier transforms of the individual structures in position space appearing in the expressions above. Table 5.1 in the main text provides the relations needed for this calculation. The functions $\mathcal{F}_n(r)$ and $f(n)$ were defined in equation (5.55) and read

$$\mathcal{F}_n(r) = f(n)\tilde{\mu}^{2\varepsilon} r^{-d+1+n} = f(n)\tilde{\mu}^{2\varepsilon} r^{-3+n+2\varepsilon}, \quad \text{where} \quad f(n) = 2^{-n}\pi^{-\frac{d-1}{2}} \frac{\Gamma\left(\frac{d-1}{2} - \frac{n}{2}\right)}{\Gamma\left(\frac{n}{2}\right)}. \tag{C.44}$$

Table C.1: Fourier transforms of r-dependent structures appearing in the counterterm.

Position Space	Momentum Space
$r^2\mathcal{F}_2(r)^3 = \tilde{\mu}^{6\varepsilon} f(2)^3 r^{-1+6\varepsilon}$	$\tilde{\mu}^{4\varepsilon} \frac{f(2)^3}{f(2+4\varepsilon)} \frac{1}{\lvert\mathbf{q}\rvert^{2+4\varepsilon}}$
$r^2\mathcal{F}_2(r)^2\mathcal{F}_{2+2\varepsilon}(r) = \tilde{\mu}^{6\varepsilon} f(2)^2 f(2+2\varepsilon) r^{-1+8\varepsilon}$	$\tilde{\mu}^{4\varepsilon} \frac{f(2)^2 f(2+2\varepsilon)}{f(2+6\varepsilon)} \frac{1}{\lvert\mathbf{q}\rvert^{2+6\varepsilon}}$
$\mathcal{F}_2(r)\left(r\frac{\mathrm{d}}{\mathrm{d}r}\mathcal{F}_2(r)\right) = \tilde{\mu}^{4\varepsilon} f(2)^2(-1+2\varepsilon) r^{-2+4\varepsilon}$	$\tilde{\mu}^{2\varepsilon}(-1+2\varepsilon) \frac{f(2)^2}{f(1+2\varepsilon)} \frac{1}{\lvert\mathbf{q}\rvert^{1+2\varepsilon}}$
$\mathcal{F}_2(r)\left(r\frac{\mathrm{d}}{\mathrm{d}r}\mathcal{F}_{2+2\varepsilon}(r)\right) = \tilde{\mu}^{4\varepsilon} f(2) f(2+2\varepsilon)((-1+4\varepsilon) r^{-2+6\varepsilon}$	$\tilde{\mu}^{2\varepsilon}(-1+4\varepsilon) \frac{f(2) f(2+2\varepsilon)}{f(1+4\varepsilon)} \frac{1}{\lvert\mathbf{q}\rvert^{1+4\varepsilon}}$
$\mathcal{F}_{2+2\varepsilon}(r)\left(r\frac{\mathrm{d}}{\mathrm{d}r}\mathcal{F}_2(r)\right) = \tilde{\mu}^{4\varepsilon} f(2+2\varepsilon) f(2)(-1+2\varepsilon) r^{-2+6\varepsilon}$	$\tilde{\mu}^{2\varepsilon}(-1+2\varepsilon) \frac{f(2) f(2+2\varepsilon)}{f(1+4\varepsilon)} \frac{1}{\lvert\mathbf{q}\rvert^{1+4\varepsilon}}$
$\mathcal{F}_2(r)^2 = \tilde{\mu}^{4\varepsilon} f(2)^2 r^{-2+4\varepsilon}$	$\tilde{\mu}^{2\varepsilon} \frac{f(2)^2}{f(1+2\varepsilon)} \frac{1}{\lvert\mathbf{q}\rvert^{1+2\varepsilon}}$
$\mathcal{F}_2(r)\mathcal{F}_{2+2\varepsilon}(r) = \tilde{\mu}^{4\varepsilon} f(2) f(2+2\varepsilon) r^{-2+6\varepsilon}$	$\tilde{\mu}^{2\varepsilon} \frac{f(2) f(2+2\varepsilon)}{f(1+4\varepsilon)} \frac{1}{\lvert\mathbf{q}\rvert^{1+4\varepsilon}}$
$\left(r\frac{\mathrm{d}}{\mathrm{d}r}\mathcal{F}_2(r)\right)^2 = \tilde{\mu}^{4\varepsilon} f(2)^2(-1+2\varepsilon)^2 r^{-2+4\varepsilon}$	$\tilde{\mu}^{2\varepsilon}(-1+2\varepsilon)^2 \frac{f(2)^2}{f(1+2\varepsilon)} \frac{1}{\lvert\mathbf{q}\rvert^{1+2\varepsilon}}$
$\left(r\frac{\mathrm{d}}{\mathrm{d}r}\mathcal{F}_2(r)\right)\left(r\frac{\mathrm{d}}{\mathrm{d}r}\mathcal{F}_{2+2\varepsilon}(r)\right) =$ $= \tilde{\mu}^{4\varepsilon} f(2) f(2+2\varepsilon)(-1+2\varepsilon)(-1+4\varepsilon) r^{-2+6\varepsilon}$	$\tilde{\mu}^{2\varepsilon}(-1+2\varepsilon)(-1+4\varepsilon) \frac{f(2) f(2+2\varepsilon)}{f(1+4\varepsilon)} \frac{1}{\lvert\mathbf{q}\rvert^{1+4\varepsilon}}$
$[\mathbf{p}, [\mathbf{p}, \mathcal{F}_2(r)]]$	1
$[\mathbf{p}, [\mathbf{p}, \mathcal{F}_{2+2\varepsilon}(r)]]$	$\frac{1}{\lvert\mathbf{q}\rvert^{2\varepsilon}}$
$\{\mathbf{p}^2, \mathcal{F}_2(r)\}$	$\frac{(\mathbf{p}^2+\mathbf{p}'^2)}{\lvert\mathbf{q}\rvert^2}$
$\{\mathbf{p}^2, \mathcal{F}_{2+2\varepsilon}(r)\}$	$\frac{(\mathbf{p}^2+\mathbf{p}'^2)}{\lvert\mathbf{q}\rvert^{2+2\varepsilon}}$

Using these relations together with the results from the previous section, we determine the full Fourier transformed terms in the counterterm up to two-loop:

For the term $\mathbf{r}^2(\Delta V)^3$, we obtain

$$\begin{aligned}\mathbf{r}^2(\Delta V)^3 \longrightarrow\ & \alpha^3 C_\Delta^3 (4\pi)^3 \frac{f(2)^3}{f(2+4\varepsilon)} \tilde{\mu}^{4\varepsilon} \frac{1}{|\mathbf{q}|^{2+4\varepsilon}} + \alpha^4 \Bigg\{ -3C_\Delta^3 (4\pi)^2 \frac{\beta_0}{\varepsilon} \frac{f(2)^3}{f(2+4\varepsilon)} \tilde{\mu}^{4\varepsilon} \frac{1}{|\mathbf{q}|^{2+4\varepsilon}} \\ & + 3C_\Delta^3 (4\pi)^2 \left(a_1(\varepsilon) + \frac{\beta_0}{\varepsilon}\right) \frac{f(2)^2 f(2+2\varepsilon)}{f(2+6\varepsilon)} \tilde{\mu}^{4\varepsilon} \mu^{2\varepsilon} \frac{1}{|\mathbf{q}|^{2+6\varepsilon}} \Bigg\} + \mathcal{O}(\alpha^5). \end{aligned} \tag{C.45}$$

The terms suppressed in $\frac{1}{m}$ yield

$$\begin{aligned}\Delta V\left(r\frac{\mathrm{d}}{\mathrm{d}r}V_s^{(0)}\right) \longrightarrow{}& \alpha^2 C_\Delta C_S (4\pi)^2(-1+2\varepsilon)\frac{f(2)^2}{f(1+2\varepsilon)}\tilde{\mu}^{2\varepsilon}\frac{1}{|\mathbf{q}|^{1+2\varepsilon}}\\ &+\alpha^3\Bigg\{-C_\Delta C_S 2(4\pi)\frac{\beta_0}{\varepsilon}(-1+2\varepsilon)\frac{f(2)^2}{f(1+2\varepsilon)}\tilde{\mu}^{2\varepsilon}\frac{1}{|\mathbf{q}|^{1+2\varepsilon}}\\ &\quad+C_\Delta C_S(4\pi)\left(a_1(\varepsilon)+\frac{\beta_0}{\varepsilon}\right)(-2+6\varepsilon)\frac{f(2)f(2+2\varepsilon)}{f(1+4\varepsilon)}\tilde{\mu}^{2\varepsilon}\mu^{2\varepsilon}\frac{1}{|\mathbf{q}|^{1+4\varepsilon}}\Bigg\}+\mathcal{O}(\alpha^4),\end{aligned} \tag{C.46}$$

$$\begin{aligned}(\Delta V)^2 \longrightarrow{}& \alpha^2 C_\Delta^2 (4\pi)^2\frac{f(2)^2}{f(1+2\varepsilon)}\tilde{\mu}^{2\varepsilon}\frac{1}{|\mathbf{q}|^{1+2\varepsilon}}\\ &+\alpha^3\Bigg\{-C_\Delta^2 2(4\pi)\frac{\beta_0}{\varepsilon}\frac{f(2)^2}{f(1+2\varepsilon)}\tilde{\mu}^{2\varepsilon}\frac{1}{|\mathbf{q}|^{1+2\varepsilon}}\\ &\quad+C_\Delta^2 2(4\pi)\left(a_1(\varepsilon)+\frac{\beta_0}{\varepsilon}\right)\frac{f(2)f(2+2\varepsilon)}{f(1+4\varepsilon)}\tilde{\mu}^{2\varepsilon}\mu^{2\varepsilon}\frac{1}{|\mathbf{q}|^{1+4\varepsilon}}\Bigg\}+\mathcal{O}(\alpha^4),\end{aligned} \tag{C.47}$$

$$\begin{aligned}(\Delta V)\left(r\frac{\mathrm{d}}{\mathrm{d}r}\Delta V+\Delta V\right) \longrightarrow{}& \alpha^2 C_\Delta^2 (4\pi)^2(2\varepsilon)\frac{f(2)^2}{f(1+2\varepsilon)}\tilde{\mu}^{2\varepsilon}\frac{1}{|\mathbf{q}|^{1+2\varepsilon}}\\ &+\alpha^3\Bigg\{-C_\Delta^2 2(4\pi)\frac{\beta_0}{\varepsilon}(2\varepsilon)\frac{f(2)^2}{f(1+2\varepsilon)}\tilde{\mu}^{2\varepsilon}\frac{1}{|\mathbf{q}|^{1+2\varepsilon}}\\ &\quad+C_\Delta^2(4\pi)\left(a_1(\varepsilon)+\frac{\beta_0}{\varepsilon}\right)(6\varepsilon)\frac{f(2)f(2+2\varepsilon)}{f(1+4\varepsilon)}\tilde{\mu}^{2\varepsilon}\mu^{2\varepsilon}\frac{1}{|\mathbf{q}|^{1+4\varepsilon}}\Bigg\}+\mathcal{O}(\alpha^4),\end{aligned} \tag{C.48}$$

$$\begin{aligned}\left(r\frac{\mathrm{d}}{\mathrm{d}r}\Delta V+\Delta V\right)^2 \longrightarrow{}& \alpha^2 C_\Delta^2 (4\pi)^2(4\varepsilon^2)\frac{f(2)^2}{f(1+2\varepsilon)}\tilde{\mu}^{2\varepsilon}\frac{1}{|\mathbf{q}|^{1+2\varepsilon}}\\ &+\alpha^3\Bigg\{-C_\Delta^2 2(4\pi)\frac{\beta_0}{\varepsilon}(4\varepsilon^2)\frac{f(2)^2}{f(1+2\varepsilon)}\tilde{\mu}^{2\varepsilon}\frac{1}{|\mathbf{q}|^{1+2\varepsilon}}\\ &\quad+C_\Delta^2 2(4\pi)\left(a_1(\varepsilon)+\frac{\beta_0}{\varepsilon}\right)(8\varepsilon^2)\frac{f(2)f(2+2\varepsilon)}{f(1+4\varepsilon)}\tilde{\mu}^{2\varepsilon}\mu^{2\varepsilon}\frac{1}{|\mathbf{q}|^{1+4\varepsilon}}\Bigg\}+\mathcal{O}(\alpha^4).\end{aligned} \tag{C.49}$$

Adding all of these $\frac{1}{m}$-terms as in the counterterm, we obtain

$$\begin{aligned}
&\frac{1}{m}\Bigg[4\Delta V\left(r\frac{\mathrm{d}}{\mathrm{d}r}V_s^{(0)}\right)+(\Delta V)^2(3d-8)+4\Delta V\left(\left(r\frac{\mathrm{d}}{\mathrm{d}r}\Delta V\right)+\Delta V\right)+\left(\left(r\frac{\mathrm{d}}{\mathrm{d}r}\Delta V\right)+\Delta V\right)^2\Bigg]\\
&\longrightarrow \frac{1}{m}\Bigg[\alpha^2(4\pi)^2\left(C_AC_F(2-4\varepsilon)+C_A^2\left(1+\frac{1}{2}\varepsilon+\varepsilon^2\right)\right)\frac{f(2)^2}{f(1+2\varepsilon)}\tilde{\mu}^{2\varepsilon}\frac{1}{|\mathbf{q}|^{1+2\varepsilon}}\\
&\quad+\alpha^3\Bigg\{-2(4\pi)\frac{\beta_0}{\varepsilon}\left(C_AC_F(2-4\varepsilon)+C_A^2\left(1+\frac{1}{2}\varepsilon+\varepsilon^2\right)\right)\frac{f(2)^2}{f(1+2\varepsilon)}\tilde{\mu}^{2\varepsilon}\frac{1}{|\mathbf{q}|^{1+2\varepsilon}}\\
&\qquad+(4\pi)\left(a_1(\varepsilon)+\frac{\beta_0}{\varepsilon}\right)\left(C_AC_F(4-12\varepsilon)+C_A^2\left(2+3\varepsilon+4\varepsilon^2\right)\right)\frac{f(2)f(2+2\varepsilon)}{f(1+4\varepsilon)}\tilde{\mu}^{2\varepsilon}\mu^{2\varepsilon}\frac{1}{|\mathbf{q}|^{1+4\varepsilon}}\Bigg\}\\
&\quad+\mathcal{O}(\alpha^4)\Bigg].
\end{aligned}\tag{C.50}$$

The terms suppressed by $\frac{1}{m^2}$ are given by

$$[\mathbf{p},[\mathbf{p},V_o^{(0)}]]\longrightarrow\alpha C_o(4\pi)+\alpha^2\Bigg\{-C_o\frac{\beta_0}{\varepsilon}+C_o\left(a_1(\varepsilon)+\frac{\beta_0}{\varepsilon}\right)\mu^{2\varepsilon}\frac{1}{|\mathbf{q}|^{2\varepsilon}}\Bigg\}+\mathcal{O}(\alpha^3)\tag{C.51}$$

$$\begin{aligned}
\{\mathbf{p}^2,\Delta V\}\longrightarrow{}&\alpha C_\Delta(4\pi)\frac{(\mathbf{p}^2+\mathbf{p}'^2)}{|\mathbf{q}|^2}\\
&+\alpha^2\Bigg\{-C_\Delta\frac{\beta_0}{\varepsilon}\frac{(\mathbf{p}^2+\mathbf{p}'^2)}{|\mathbf{q}|^2}+C_\Delta\left(a_1(\varepsilon)+\frac{\beta_0}{\varepsilon}\right)\mu^{2\varepsilon}\frac{(\mathbf{p}^2+\mathbf{p}'^2)}{|\mathbf{q}|^{2+2\varepsilon}}\Bigg\}+\mathcal{O}(\alpha^3).
\end{aligned}\tag{C.52}$$

In the counterterm, these terms correspond to

$$\begin{aligned}
&\frac{1}{m^2}\left[-2[\mathbf{p},[\mathbf{p},V_o^{(0)}]]+2\{\mathbf{p}^2,\Delta V\}\right]\\
&\longrightarrow\frac{1}{m^2}\Bigg[\alpha(4\pi)\left(-C_A+2C_F+C_A\frac{(\mathbf{p}^2+\mathbf{p}'^2)}{|\mathbf{q}|^2}\right)\\
&\quad+\alpha^2\Bigg\{-\frac{\beta_0}{\varepsilon}\left(-C_A+2C_F+C_A\frac{(\mathbf{p}^2+\mathbf{p}'^2)}{|\mathbf{q}|^2}\right)\\
&\qquad+\left(a_1(\varepsilon)+\frac{\beta_0}{\varepsilon}\right)\left(-C_A+2C_F+C_A\frac{(\mathbf{p}^2+\mathbf{p}'^2)}{|\mathbf{q}|^2}\right)\mu^{2\varepsilon}\frac{1}{|\mathbf{q}|^{2\varepsilon}}\Bigg\}+\mathcal{O}(\alpha^3)\Bigg].
\end{aligned}\tag{C.53}$$

Putting all contributions together, we obtain the following expression for the two-loop counterterm in momentum space up to NLO in α:

$$\begin{aligned}
\delta V_{us} = {} & C_F V_A^2 \left[\frac{1}{\varepsilon} \left[\frac{\alpha(\mu_{(us)})}{3\pi} - \frac{\alpha^2(\mu_{(us)})}{36\pi^2} \left(C_A \left(-\frac{47}{3} - 2\pi^2 \right) + \frac{10}{3} T_F n_f \right) \right] - \frac{1}{\varepsilon^2} \frac{\alpha^2(\mu_{(us)})}{24\pi^2} \beta_0 \right] \\
& \times \Bigg\{ \alpha^3(\mu_{(s)}) \frac{C_A^3}{8} (4\pi)^3 \frac{f(2)^3}{f(2+4\varepsilon)} \tilde{\mu}_{(s)}^{4\varepsilon} \frac{1}{|\mathbf{q}|^{2+4\varepsilon}} + \alpha^4(\mu_{(s)}) \Bigg\{ -3 \frac{C_A^3}{8} (4\pi)^2 \frac{\beta_0}{\varepsilon} \frac{f(2)^3}{f(2+4\varepsilon)} \tilde{\mu}_{(s)}^{4\varepsilon} \frac{1}{|\mathbf{q}|^{2+4\varepsilon}} \\
& \quad + 3 \frac{C_A^3}{8} (4\pi)^2 \left(a_1(\varepsilon) + \frac{\beta_0}{\varepsilon} \right) \frac{f(2)^2 f(2+2\varepsilon)}{f(2+6\varepsilon)} \tilde{\mu}_{(s)}^{4\varepsilon} \mu_{(s)}^{2\varepsilon} \frac{1}{|\mathbf{q}|^{2+6\varepsilon}} \Bigg\} \\
& \quad + \frac{1}{m} \Bigg[\alpha^2(\mu_{(s)}) (4\pi)^2 \left(C_A C_F (2-4\varepsilon) + C_A^2 \left(1 + \frac{1}{2}\varepsilon + \varepsilon^2 \right) \right) \frac{f(2)^2}{f(1+2\varepsilon)} \tilde{\mu}_{(s)}^{2\varepsilon} \frac{1}{|\mathbf{q}|^{1+2\varepsilon}} \\
& \qquad + \alpha^3(\mu_{(s)}) \Bigg\{ -2(4\pi) \frac{\beta_0}{\varepsilon} \left(C_A C_F (2-4\varepsilon) + C_A^2 \left(1 + \frac{1}{2}\varepsilon + \varepsilon^2 \right) \right) \frac{f(2)^2}{f(1+2\varepsilon)} \tilde{\mu}_{(s)}^{2\varepsilon} \frac{1}{|\mathbf{q}|^{1+2\varepsilon}} \\
& \qquad + (4\pi) \left(a_1(\varepsilon) + \frac{\beta_0}{\varepsilon} \right) \left(C_A C_F (4-12\varepsilon) + C_A^2 \left(2 + 3\varepsilon + 4\varepsilon^2 \right) \right) \frac{f(2) f(2+2\varepsilon)}{f(1+4\varepsilon)} \tilde{\mu}_{(s)}^{2\varepsilon} \mu_{(s)}^{2\varepsilon} \frac{1}{|\mathbf{q}|^{1+4\varepsilon}} \Bigg\} \Bigg] \\
& \quad + \frac{1}{m^2} \Bigg[\alpha(\mu_{(s)}) (4\pi) \left(-C_A + 2C_F + C_A \frac{(\mathbf{p}^2 + \mathbf{p}'^2)}{|\mathbf{q}|^2} \right) \\
& \qquad + \alpha^2(\mu_{(s)}) \Bigg\{ -\frac{\beta_0}{\varepsilon} \left(-C_A + 2C_F + C_A \frac{(\mathbf{p}^2 + \mathbf{p}'^2)}{|\mathbf{q}|^2} \right) \\
& \qquad + \left(a_1(\varepsilon) + \frac{\beta_0}{\varepsilon} \right) \left(-C_A + 2C_F + C_A \frac{(\mathbf{p}^2 + \mathbf{p}'^2)}{|\mathbf{q}|^2} \right) \mu_{(s)}^{2\varepsilon} \frac{1}{|\mathbf{q}|^{2\varepsilon}} \Bigg\} \Bigg] \Bigg\}. \qquad \text{(C.54)}
\end{aligned}$$

In section 5.3.2, these expressions are quoted from here at leading order in α.

C.5 Constraint for the Two-Loop Counterterm

Finally, we show that the two-loop counterterm (C.11) actually fulfils the constraint

$$0 = -2\alpha(\mu_{(us)}) \frac{\partial}{\partial \alpha(\mu_{(us)})} Z_V^{(2)} + \alpha(\mu_{(us)}) \beta\left(\alpha(\mu_{(us)})\right) Z_V^{(1)} + \mu_{(us)} \frac{\mathrm{d}\mathcal{O}_V}{\mathrm{d}\mu_{(us)}} \frac{\partial}{\partial \mathcal{O}_V} Z_V^{(1)} \qquad \text{(C.55)}$$

(cf. equation (5.84)) at the relevant order. This is easiest seen in position space, where we read off the coefficients

$$Z_V^{(1),\mathrm{PS}} = C_F V_A^2 \left[\frac{\alpha(\mu_{(us)})}{3\pi} - \frac{\alpha^2(\mu_{(us)})}{36\pi^2} \left(C_A \left(-\frac{47}{3} - 2\pi^2 \right) + \frac{10}{3} T_F n_f \right) \right] \mathcal{O}_V, \tag{C.56}$$

$$Z_V^{(2),\mathrm{PS}} = -C_F V_A^2 \frac{\alpha^2(\mu_{(us)})}{24\pi^2} \beta_0 \mathcal{O}_V. \tag{C.57}$$

Counting $\mathbf{p} \sim m\alpha$ and $r \sim \frac{1}{m\alpha}$ in the explicit expression for $\mathcal{O}_V$ deduced in section 5.3.1 (see equation (5.48)), we deduce that the operator $\mathcal{O}_V$ scales like $\alpha^4(\mu_{(s)})$. Considering the terms in the constraint separately, we observe

$$-2\alpha(\mu_{(us)}) \frac{\partial}{\partial \alpha(\mu_{(us)})} Z_V^{(2)} = \frac{\alpha^2(\mu_{(us)})}{6\pi^2} \beta_0 C_F V_A^2 \mathcal{O}_V + \mathcal{O}(\alpha^7), \tag{C.58}$$

$$\alpha(\mu_{(us)}) \beta\left(\alpha(\mu_{(us)})\right) Z_V^{(1)} = \alpha(\mu_{(us)}) \left(-\frac{\alpha(\mu_{(us)})}{2\pi} \beta_0 \right) C_F V_A^2 \frac{1}{3\pi} \mathcal{O}_V + \mathcal{O}(\alpha^7), \tag{C.59}$$

$$\mu_{(us)} \frac{\mathrm{d}\mathcal{O}_V}{\mathrm{d}\mu_{(us)}} \frac{\partial}{\partial \mathcal{O}_V} Z_V^{(1)} = \mathcal{O}(\alpha^8). \tag{C.60}$$

The first two lines cancel, and the third term contributes only beyond the order we are considering, which confirms that the constraint is fulfilled at leading order. The last line calls for some more details: As can be inferred from the explicit counterterm (C.54), the ultrasoft scale $\mu_{(us)}$ first appears explicitly in the potentials (and thus in $\mathcal{O}_V$) at the level of $\mathcal{V}_C^{(3)}$, $\mathcal{V}_{1/m}^{(2)}$, $\mathcal{V}_{1/m^2}^{(1)}$, and $\mathcal{V}_p^{(1)}$. In position space, this corresponds to a contribution from the potentials at order α^5. These potentials are contained in h_o in $\mathcal{O}_V$, which includes h_o to the third power. To get the leading term explicitly dependent on $\mu_{(us)}$, we pair the potentials containing it with two powers of the leading order Coulomb potential, each scaling like α^2. Finally, accounting for the two factors of $\mathbf{r} \sim \frac{1}{m\alpha}$ in $\mathcal{O}_V$ and the overall factor of α in $Z_V^{(1),\mathrm{PS}}$, we deduce that the last line starts contributing only at order $\mathcal{O}(\alpha^8)$.

Appendix D

Details on the Numerical Implementation

This section details the implementation of the analytical RG improvement of the R-ratio into the `TTbarXSection` code. The resulting code has been used to obtain the numerical results presented in chapter 6.

The main quantity encoding the RG correction at NLL is the correction $c_v^{(1),\mathrm{RG}}$ to the coefficient of the non-relativistic current. It is introduced as `QCDc1RG` in the `TTbarConstants` file. For further analysis of the convergence of the reexpanded log-series, we have also defined the variable `QCDc1RGTrunc[n]`, which denotes the reexpanded log-series truncated after the term $\alpha^n(\mu)$. That is, `QCDc1RGTrunc[1]` only includes the $\alpha \times \ln\left(\frac{\mu^2}{\mu_h^2}\right)$-term, which corresponds to the NNLO logarithm. In the code `TTbarXSection`, this is implemented up to $n = 6$.

The NLL correction is implemented in the following way:

- `SetQCDConstants` now also sets `c1RG->QCDc1RG` and `c1RGTrunc->QCDc1RGTrunc` to the expressions given in `TTbarConstants`.
- The `Scales` in the input parameters of `TTbarXSection` now also need to allow for inputting the hard scale μ_h. The syntax is the following:
  - If only one scale is input, either as `Scales = mus` or as `Scales = {mus}`, the input value is set for `muweak=musoft` as before the implementation of the NLL expression. In this case, `muhard` is not set.

  - If two scales are input in single brackets (`Scales = {mus, muw}`), it is assumed that no resummation is asked for and (as before the implementation of the NLL expression) `{musoft, muweak}` are set as the input values, while again `muhard` is not set.

  - For setting also the hard scale μ_h, we introduce additional brackets: `Scales = {{mus, muw}, {muh}}` is the syntax for setting all scales individually, while `Scales = {{mus}, {muh}}` uses the same value for `mus` and `muweak`.

- The input parameter `Order->{order,pot}` of the function `TTbarXSection` has been changed to `Order>{order,logorder,pot}`. The options for `logorder` are `"None"` (default), `"NLL"`, or `"NLLTrunc1"`, ..., `"NLLTrunc6"`. We have also defined corresponding factors `LogOrder`, `LogOrderTrunc1`,...,`LogOrderTrunc6` which are set to one if the respective contribution is called for when evaluating the `TTbarXSection`-function, while the rest is set to zero. Using the option `"None"` sets all factors to zero.

- We have defined the term `HWCNLORG`, which is added to `HWCNLO` in the `PertOrder[1]`-term of `PiV`. It encodes the corrections `c1RG` or `c1RGTruncn`, which are then multiplied by the `LogOrder`-factors defined above.

The terms subtracting otherwise double counted NLL logarithms (cf. equations (5.152)-(5.155)) are given by substituting `HWCNNLO` in the `PertOrder[2]`-term of `PiV` by (`HWCNNLO + HWCNNLOSub`), where the latter contains the (negative of the) large log, and the same for `HWCNNNLO`, which is replaced by (`HWCNNNLO + HWCNNNLOSub`) in the `PerOrder[3]`-term. Additionally, the large logarithms contained in $\delta_3 G(E)$ are subtracted from `GreenFunctionNNNLO` and `USCorr`. Note that the subtraction for the third-order terms is only switched on when the options `"NLL"` or `"NLLTrunc2"`, ..., `"NLLTrunc6"` are used, but not for `"NLLTrunc1"`, which only reproduces the second-order logarithm.

Bibliography

[1] ATLAS and CMS Collaborations. *Combination of measurements of the top quark mass from data collected by the ATLAS and CMS experiments at $\sqrt{s}$ = 7 and 8 TeV*. ATLAS-CONF-2023-066, CMS-PAS-TOP-22-001.

[2] A. H. Hoang. *What is the Top Quark Mass?* In: *Ann. Rev. Nucl. Part. Sci.* 70 (2020), pp. 225–255. arXiv: 2004.12915 [hep-ph].

[3] G. Degrassi, S. Di Vita, J. Elias-Miro, J. R. Espinosa et al. *Higgs mass and vacuum stability in the Standard Model at NNLO*. In: *JHEP* 08 (2012), p. 098. arXiv: 1205.6497 [hep-ph].

[4] S. Alekhin, A. Djouadi and S. Moch. *The top quark and Higgs boson masses and the stability of the electroweak vacuum*. In: *Phys. Lett. B* 716 (2012), pp. 214–219. arXiv: 1207.0980 [hep-ph].

[5] A. V. Bednyakov, B. A. Kniehl, A. F. Pikelner and O. L. Veretin. *Stability of the Electroweak Vacuum: Gauge Independence and Advanced Precision*. In: *Phys. Rev. Lett.* 115.20 (2015), p. 201802. arXiv: 1507.08833 [hep-ph].

[6] T. Horiguchi, A. Ishikawa, T. Suehara, K. Fujii et al. *Study of top quark pair production near threshold at the ILC*. 2013. arXiv: 1310.0563 [hep-ex].

[7] M. Martinez and R. Miquel. *Multiparameter fits to the t anti-t threshold observables at a future e+ e- linear collider*. In: *Eur. Phys. J. C* 27 (2003), pp. 49–55. arXiv: hep-ph/0207315.

[8] K. Seidel, F. Simon, M. Tesar and S. Poss. *Top quark mass measurements at and above threshold at CLIC*. In: *Eur. Phys. J. C* 73.8 (2013), p. 2530. arXiv: 1303.3758 [hep-ex].

[9] Navas, S. et al (Particle Data Group). *The Review of Particle Physics*. To be published in Phys. Rev. D 110, 030001 (2024).

[10] I. I. Y. Bigi, Y. L. Dokshitzer, V. A. Khoze, J. H. Kühn et al. *Production and Decay Properties of Ultraheavy Quarks*. In: *Phys. Lett. B* 181 (1986), pp. 157–163.

[11] B. A. Thacker and G. P. Lepage. *Heavy quark bound states in lattice QCD*. In: *Phys. Rev. D* 43 (1991), pp. 196–208.

[12] G. P. Lepage, L. Magnea, C. Nakhleh, U. Magnea et al. *Improved nonrelativistic QCD for heavy quark physics*. In: *Phys. Rev. D* 46 (1992), pp. 4052–4067. arXiv: hep-lat/9205007.

[13] G. T. Bodwin, E. Braaten and G. P. Lepage. *Rigorous QCD analysis of inclusive annihilation and production of heavy quarkonium*. In: *Phys. Rev. D* 51 (1995). [Erratum: Phys.Rev.D 55, 5853 (1997)], pp. 1125–1171. arXiv: hep-ph/9407339.

[14] A. Pineda and J. Soto. *Effective field theory for ultrasoft momenta in NRQCD and NRQED*. In: *Nucl. Phys. B Proc. Suppl.* 64 (1998), pp. 428–432. arXiv: hep-ph/9707481.

[15] A. Pineda and J. Soto. *The Lamb shift in dimensional regularization*. In: *Phys. Lett. B* 420 (1998), pp. 391–396. arXiv: hep-ph/9711292.

[16] M. Beneke. *New results on heavy quarks near threshold*. In: *3rd Workshop on Continuous Advances in QCD (QCD 98)*. 1998, pp. 293–309. arXiv: hep-ph/9806429.

[17] M. Beneke, A. Signer and V. A. Smirnov. *Top quark production near threshold and the top quark mass*. In: *Phys. Lett. B* 454 (1999), pp. 137–146. arXiv: hep-ph/9903260.

[18] N. Brambilla, A. Pineda, J. Soto and A. Vairo. *Potential NRQCD: An Effective theory for heavy quarkonium*. In: *Nucl. Phys. B* 566 (2000), p. 275. arXiv: hep-ph/9907240.

[19] M. E. Luke, A. V. Manohar and I. Z. Rothstein. *Renormalization group scaling in nonrelativistic QCD*. In: *Phys. Rev. D* 61 (2000), p. 074025. arXiv: hep-ph/9910209.

[20] A. V. Manohar and I. W. Stewart. *Renormalization group analysis of the QCD quark potential to order v^2*. In: *Phys. Rev. D* 62 (2000), p. 014033. arXiv: hep-ph/9912226.

[21] A. H. Hoang and I. W. Stewart. *Ultrasoft renormalization in nonrelativistic QCD*. In: *Phys. Rev. D* 67 (2003), p. 114020. arXiv: hep-ph/0209340.

[22] V. S. Fadin and V. A. Khoze. *Threshold Behavior of Heavy Top Production in e^+e^- Collisions*. In: *JETP Lett.* 46 (1987), pp. 525–529.

[23] V. S. Fadin and V. A. Khoze. *Production of a pair of heavy quarks in e^+e^- annihilation in the threshold region*. In: *Sov. J. Nucl. Phys.* 48 (1988), pp. 309–313.

[24] M. J. Strassler and M. E. Peskin. *The Heavy top quark threshold: QCD and the Higgs*. In: *Phys. Rev. D* 43 (1991), pp. 1500–1514.

[25] A. H. Hoang, M. Beneke, K. Melnikov, T. Nagano et al. *Top - anti-top pair production close to threshold: Synopsis of recent NNLO results*. In: *Eur. Phys. J. direct* 2.1 (2000), p. 3. arXiv: hep-ph/0001286.

[26] M. Beneke, Y. Kiyo, P. Marquard, A. Penin et al. *Next-to-Next-to-Next-to-Leading Order QCD Prediction for the Top Antitop S-Wave Pair Production Cross Section Near Threshold in e^+e^- Annihilation*. In: *Phys. Rev. Lett.* 115.19 (2015), p. 192001. arXiv: 1506.06864 [hep-ph].

[27] M. Beneke, Y. Kiyo and K. Schuller. *Third-order correction to top-quark pair production near threshold I. Effective theory set-up and matching coefficients.* 2013. arXiv: 1312.4791 [hep-ph].

[28] M. Beneke, A. Maier, J. Piclum and T. Rauh. *Non-QCD contributions to top-pair production near threshold.* In: *PoS* EPS-HEP2015 (2015), p. 315. arXiv: 1511.00801 [hep-ph].

[29] M. Beneke, A. Maier, T. Rauh and P. Ruiz-Femenia. *Electroweak and non-resonant corrections to top-pair production near threshold at NNLO.* In: *PoS* RADCOR2017 (2017), p. 052. arXiv: 1711.00676 [hep-ph].

[30] M. Beneke, A. Maier, T. Rauh and P. Ruiz-Femenia. *Non-resonant and electroweak NNLO correction to the e^+e^- top anti-top threshold.* In: *JHEP* 02 (2018), p. 125. arXiv: 1711.10429 [hep-ph].

[31] A. Pineda and J. Soto. *The Renormalization group improvement of the QCD static potentials.* In: *Phys. Lett. B* 495 (2000), pp. 323–328. arXiv: hep-ph/0007197.

[32] A. Pineda. *Next-to-leading log renormalization group running in heavy-quarkonium creation and annihilation.* In: *Phys. Rev. D* 66 (2002), p. 054022. arXiv: hep-ph/0110216.

[33] A. Pineda. *Renormalization group improvement of the NRQCD Lagrangian and heavy quarkonium spectrum.* In: *Phys. Rev. D* 65 (2002), p. 074007. arXiv: hep-ph/0109117.

[34] A. Pineda. *Review of Heavy Quarkonium at weak coupling.* In: *Prog. Part. Nucl. Phys.* 67 (2012), pp. 735–785. arXiv: 1111.0165 [hep-ph].

[35] A. Pineda and A. Signer. *Heavy Quark Pair Production near Threshold with Potential Non-Relativistic QCD.* In: *Nucl. Phys. B* 762 (2007), pp. 67–94. arXiv: hep-ph/0607239.

[36] C. Peset, A. Pineda and J. Segovia. *P-wave heavy quarkonium spectrum with next-to-next-to-next-to-leading logarithmic accuracy.* In: *Phys. Rev. D* 98.9 (2018), p. 094003. arXiv: 1809.09124 [hep-ph].

[37] C. Anzai, D. Moreno and A. Pineda. *S-wave heavy quarkonium spectrum with next-to-next-to-next-to-leading logarithmic accuracy.* In: *Phys. Rev. D* 98.11 (2018), p. 114034. arXiv: 1810.11031 [hep-ph].

[38] A. H. Hoang, A. V. Manohar, I. W. Stewart and T. Teubner. *A Renormalization group improved calculation of top quark production near threshold.* In: *Phys. Rev. Lett.* 86 (2001), pp. 1951–1954. arXiv: hep-ph/0011254.

[39] A. H. Hoang, A. V. Manohar, I. W. Stewart and T. Teubner. *The Threshold t anti-t cross-section at NNLL order.* In: *Phys. Rev. D* 65 (2002), p. 014014. arXiv: hep-ph/0107144.

[40] M. Stahlhofen and A. Hoang. *NNLL top-antitop production at threshold.* In: *PoS* RADCOR2011 (2011), p. 025. arXiv: 1111.4486 [hep-ph].

[41] A. H. Hoang and M. Stahlhofen. *The Top-Antitop Threshold at the ILC: NNLL QCD Uncertainties*. In: *JHEP* 05 (2014), p. 121. arXiv: 1309.6323 [hep-ph].

[42] M. Beneke, Y. Kiyo, A. Maier and J. Piclum. *Near-threshold production of heavy quarks with* QQbar_threshold. In: *Comput. Phys. Commun.* 209 (2016), pp. 96–115. arXiv: 1605.03010 [hep-ph].

[43] A. V. Manohar. *Introduction to Effective Field Theories*. 2018. arXiv: 1804.05863 [hep-ph].

[44] T. Cohen. *As Scales Become Separated: Lectures on Effective Field Theory*. 2019. arXiv: 1903.03622 [hep-ph].

[45] A. Pich. *Effective field theory: Course*. In: *Les Houches Summer School in Theoretical Physics, Session 68: Probing the Standard Model of Particle Interactions*. 1998, pp. 949–1049. arXiv: hep-ph/9806303.

[46] M. Neubert. *Renormalization Theory and Effective Field Theories*. 2019. arXiv: 1901.06573 [hep-ph].

[47] W. A. Bardeen, A. J. Buras, D. W. Duke and T. Muta. *Deep Inelastic Scattering Beyond the Leading Order in Asymptotically Free Gauge Theories*. In: *Phys. Rev. D* 18 (1978), p. 3998.

[48] V. A. Smirnov. *Asymptotic expansions in momenta and masses and calculation of Feynman diagrams*. In: *Mod. Phys. Lett. A* 10 (1995), pp. 1485–1500. arXiv: hep-th/9412063.

[49] M. Beneke and V. A. Smirnov. *Asymptotic expansion of Feynman integrals near threshold*. In: *Nucl. Phys. B* 522 (1998), pp. 321–344. arXiv: hep-ph/9711391.

[50] W. E. Caswell and G. P. Lepage. *Effective Lagrangians for Bound State Problems in QED, QCD, and Other Field Theories*. In: *Phys. Lett. B* 167 (1986), pp. 437–442.

[51] N. Brambilla, A. Pineda, J. Soto and A. Vairo. *The QCD potential at O(1/m)*. In: *Phys. Rev. D* 63 (2001), p. 014023. arXiv: hep-ph/0002250.

[52] N. Brambilla, A. Pineda, J. Soto and A. Vairo. *Effective Field Theories for Heavy Quarkonium*. In: *Rev. Mod. Phys.* 77 (2005), p. 1423. arXiv: hep-ph/0410047.

[53] C. W. Bauer and A. V. Manohar. *Renormalization group scaling of the* $1/m^2$ *HQET Lagrangian*. In: *Phys. Rev. D* 57 (1998), pp. 337–343. arXiv: hep-ph/9708306.

[54] E. Eichten and B. R. Hill. *An Effective Field Theory for the Calculation of Matrix Elements Involving Heavy Quarks*. In: *Phys. Lett. B* 234 (1990), pp. 511–516.

[55] M. Gerlach, G. Mishima and M. Steinhauser. *Matching coefficients in nonrelativistic QCD to two-loop accuracy*. In: *Phys. Rev. D* 100.5 (2019), p. 054016. arXiv: 1907.08227 [hep-ph].

[56] O. V. Tarasov, A. A. Vladimirov and A. Y. Zharkov. *The Gell-Mann-Low Function of QCD in the Three Loop Approximation*. In: *Phys. Lett. B* 93 (1980), pp. 429–432.

[57] A. V. Manohar. *The HQET / NRQCD Lagrangian to order α/m^3*. In: *Phys. Rev. D* 56 (1997), pp. 230–237. arXiv: hep-ph/9701294.

[58] A. Pineda and J. Soto. *Matching at one loop for the four quark operators in NRQCD*. In: *Phys. Rev. D* 58 (1998), p. 114011. arXiv: hep-ph/9802365.

[59] M. Beneke, P. Falgari and C. Schwinn. *Threshold resummation for pair production of coloured heavy (s)particles at hadron colliders*. In: *Nucl. Phys. B* 842 (2011), pp. 414–474. arXiv: 1007.5414 [hep-ph].

[60] T. J. G. Rauh. *Precise top and bottom quark masses from pair production near threshold in e^+e^- collisions*. PhD thesis. Munich, Tech. U., 2016.

[61] M. Beneke, Y. Kiyo and A. A. Penin. *Ultrasoft contribution to quarkonium production and annihilation*. In: *Phys. Lett. B* 653 (2007), pp. 53–59. arXiv: 0706.2733 [hep-ph].

[62] M. Beneke and Y. Kiyo. *Ultrasoft contribution to heavy-quark pair production near threshold*. In: *Phys. Lett. B* 668 (2008), pp. 143–147. arXiv: 0804.4004 [hep-ph].

[63] P. Labelle. *Effective field theories for QED bound states: Extending nonrelativistic QED to study retardation effects*. In: *Phys. Rev. D* 58 (1998), p. 093013. arXiv: hep-ph/9608491.

[64] B. Grinstein and I. Z. Rothstein. *Effective field theory and matching in nonrelativistic gauge theories*. In: *Phys. Rev. D* 57 (1998), pp. 78–82. arXiv: hep-ph/9703298.

[65] M. Beneke. *Perturbative heavy quark - anti-quark systems*. 1999. arXiv: hep-ph/9911490.

[66] K. G. Wilson. *Nonlagrangian models of current algebra*. In: *Phys. Rev.* 179 (1969), pp. 1499–1512.

[67] W. Zimmermann. *Normal products and the short distance expansion in the perturbation theory of renormalizable interactions*. In: *Annals Phys.* 77 (1973), pp. 570–601.

[68] Y. Schröder. *The Static potential in QCD to two loops*. In: *Phys. Lett. B* 447 (1999), pp. 321–326. arXiv: hep-ph/9812205.

[69] Y. Schröder. *The Static potential in QCD*. PhD thesis. Hamburg U., 1999.

[70] C. Anzai, Y. Kiyo and Y. Sumino. *Static QCD potential at three-loop order*. In: *Phys. Rev. Lett.* 104 (2010), p. 112003. arXiv: 0911.4335 [hep-ph].

[71] A. V. Smirnov, V. A. Smirnov and M. Steinhauser. *Three-loop static potential*. In: *Phys. Rev. Lett.* 104 (2010), p. 112002. arXiv: 0911.4742 [hep-ph].

[72] B. A. Kniehl, A. A. Penin, M. Steinhauser and V. A. Smirnov. *Nonabelian $\alpha_s^3/(m_q r^2)$ heavy quark anti-quark potential*. In: *Phys. Rev. D* 65 (2002), p. 091503. arXiv: hep-ph/0106135.

[73] S. Wüster. *Heavy quark potential at order α_s^2/m^2 [in German]*. Diploma Thesis. RWTH Aachen University, 2003.

[74] M. Beneke, J. Piclum and T. Rauh. *P-wave contribution to third-order top-quark pair production near threshold*. In: *Nucl. Phys. B* 880 (2014), pp. 414–434. arXiv: 1312.4792 [hep-ph].

[75] M. Beneke, A. Signer and V. A. Smirnov. *Two loop correction to the leptonic decay of quarkonium*. In: *Phys. Rev. Lett.* 80 (1998), pp. 2535–2538. arXiv: hep-ph/9712302.

[76] P. Marquard, J. H. Piclum, D. Seidel and M. Steinhauser. *Three-loop matching of the vector current*. In: *Phys. Rev. D* 89.3 (2014), p. 034027. arXiv: 1401.3004 [hep-ph].

[77] M.Beneke and Y. Kiyo. *Third-order correction to top-quark pair production near threshold II . Potential contributions*. To appear.

[78] M. Beneke, Y. Kiyo and K. Schuller. *Third-order Coulomb corrections to the S-wave Green function, energy levels and wave functions at the origin*. In: *Nucl. Phys. B* 714 (2005), pp. 67–90. arXiv: hep-ph/0501289.

[79] M. Beneke, Y. Kiyo and K. Schuller. *Third-order non-Coulomb correction to the S-wave quarkonium wave functions at the origin*. In: *Phys. Lett. B* 658 (2008), pp. 222–229. arXiv: 0705.4518 [hep-ph].

[80] N. Brambilla, X. Garcia i Tormo, J. Soto and A. Vairo. *The Logarithmic contribution to the QCD static energy at N^4LO*. In: *Phys. Lett. B* 647 (2007), pp. 185–193. arXiv: hep-ph/0610143.

[81] N. Brambilla, A. Vairo, X. Garcia i Tormo and J. Soto. *The QCD static energy at NNNLL*. In: *Phys. Rev. D* 80 (2009), p. 034016. arXiv: 0906.1390 [hep-ph].

[82] A. Pineda. *Next-to-leading ultrasoft running of the heavy quarkonium potentials and spectrum: Spin-independent case*. In: *Phys. Rev. D* 84 (2011), p. 014012. arXiv: 1101.3269 [hep-ph].

[83] C. Peset, A. Pineda and M. Stahlhofen. *Potential NRQCD for unequal masses and the B_c spectrum at N^3LO*. In: *JHEP* 05 (2016), p. 017. arXiv: 1511.08210 [hep-ph].

[84] N. Brambilla, D. Eiras, A. Pineda, J. Soto et al. *Inclusive decays of heavy quarkonium to light particles*. In: *Phys. Rev. D* 67 (2003), p. 034018. arXiv: hep-ph/0208019.

[85] A. Pineda and M. Stahlhofen. *The static hybrid potential in D dimensions at short distances*. In: *Phys. Rev. D* 84 (2011), p. 034016. arXiv: 1105.4356 [hep-ph].

[86] C. Peset. *Effective field theories for heavy quarkonia and hydrogen-like bound states*. PhD thesis. Barcelona, Autonoma U., 2016.

[87] M. Beneke and M. Steinhauser. *Non-relativistic high-energy physics: top production and dark matter annihilation*. In: *Nucl. Part. Phys. Proc.* 261-262 (2015), pp. 378–413. arXiv: 1506.07962 [hep-ph].

[88] M. Beneke. *A Quark mass definition adequate for threshold problems*. In: *Phys. Lett. B* 434 (1998), pp. 115–125. arXiv: hep-ph/9804241.

[89] A. Pineda and A. Vairo. *The QCD potential at O (1 / m^2) : Complete spin dependent and spin independent result*. In: *Phys. Rev. D* 63 (2001). [Erratum: Phys.Rev.D 64, 039902 (2001)], p. 054007. arXiv: `hep-ph/0009145`.

[90] M. Eidemuller and M. Jamin. *QCD field strength correlator at the next-to-leading order*. In: *Phys. Lett. B* 416 (1998), pp. 415–420. arXiv: `hep-ph/9709419`.

Acknowledgements

I would like to thank Prof. Martin Beneke for his guidance and mentorship throughout this past year. Your support, through numerous meetings and insightful discussions, has guided me to the successful completion of this project and a much deeper understanding of physics.

Thank you to Prof. Clara Peset for all your support, for answering my never-ending questions, and, above all, for welcoming me so warmly to Madrid. My months in Spain were truly amazing, and I am very grateful for this opportunity.

Thank you to the whole group of T31 – Javier, Lorenzo, Andrea, Gael, Simon, Matthias, ... – thanks for all the discussions, for waiting for me at lunch, and for just making normal working days really enjoyable. Thanks to Julian for all your advice and for many great conversations.

Special thanks also to Javier, Mar, and Kai (I just ignore that you moved) – I got the best office I could imagine; thanks for helping me with everything I could ask for.

Thanks to all my friends from the Master's programme. Katrina, Javier, Antonia, David, Daniel, and Pascal – you made the past years a truly great experience.

Thanks also to all the students of the theory department I got to know in Madrid – you made me feel welcome from day one, and I really loved my time in your group.

Special thanks to everyone who helped proofread my thesis: Javier, Moritz, David, and Simon.

Thanks to Anne for all the hour-long phone calls and for just being able to talk about absolutely everything.

To my family, thank you for your unwavering support and for always believing in me – you make all of this possible.

Moritz, thank you for always being there for me, for listening through all the ups and downs, and for just helping me at every possible step.